学位論文

Characteristics and Environments of Mesoscale Vortices that Develop over the Sea of Japan in Cold Seasons

（冬季日本海のメソスケール渦状擾乱の特性と環境場）

平成 27 年 12 月博士（理学）申請

東京大学大学院理学系研究科

地球惑星科学専攻

渡邉　俊一

Abstract

Mesoscale vortices (MVs) called polar mesocyclones or polar lows are frequently observed over high-latitude oceans including the Sea of Japan in cold seasons. This thesis studies the general characteristics of the structures and environments of the MVs over the Sea of Japan by statistical analyses and numerical simulations. To this end, a new objective tracking method for the MVs including meso-β-scale MVs is developed using Meso-scale Analysis (MANAL) provided by Japan Meteorological Agency.

Using the tracking method, the climatology of the MVs over the Sea of Japan is analyzed. The tracks of MVs are concentrated in the western part and the northeastern part of the Sea of Japan. This result agrees well with previous studies based on satellite images. The characteristics of MVs including their direction of movement, size, and intensity are found to vary according to the locations of the MVs.

General characteristics of the environments and structures of the MVs are examined by composite analyses of MANAL and Global Analysis (GANAL). The MVs are classified into several groups according to their locations and moving directions. Common environments of the MVs are a cold air outbreak at the low-level and an upper-level trough accompanied by cold air. The former provides a large baroclinicity and/or a horizontal shear at the low-level, while the latter provides a less stable stratification and dynamic forcing. These environments are favorable for the development of the MVs. However, the configuration of these large-scale features for the MVs as well as meso-scale structures of the MVs varies among the groups. These differences are related to the developing mechanisms of the MVs in each group.

Numerical simulations, in which the composite fields of GANAL are used for the initial and boundary conditions, successfully reproduce the characteristics of the MV in

each group. This result confirms that the composite fields of GANAL represent general characteristics of the large-scale environment for the corresponding MVs. The development mechanisms of southward-moving MVs generated in the northeastern part of the Sea of Japan (NE_s), eastward moving and southeastward-moving MVs generated in the northwestern part of the Sea of Japan (NW_e and NW_se), and the MVs generated in the southwestern part of the Sea of Japan (SW_W) are examined in more detail by the sensitivity experiments.

As for the MV in NE_s, cumulus convection is crucial for the generation and development, while it also exhibits characteristics of baroclinic development. The warm SST in the Strat of Tartary and the Sea of Japan, and the blocking of a cold air by mountains along the eastern coast of the Asian Continent provides a favorable environment for the development of the MV.

The MVs in NW_se, NW_e and SW_W form within a low-level convergence zone (JPCZ). Both the interaction between the upper-level trough and the low-level JPCZ, and condensational heating contribute significantly to the genesis and development of these MVs. The blocking of the cold air by the mountains at the north of the Korean Peninsula turns out to be essential for the formation of the JPCZ and the MVs.

Contents

1 Introduction

1.1 Mesoscale vortices over high-latitude ocean in winter

Mesoscale vortices (MVs) called polar mesocyclones (PMCs) or polar lows (PLs) are often observed over high-latitude oceans in winter. PMCs are cyclonic vortices that develop poleward of the main polar front and have a horizontal size of meso-α (200–2000 km) to meso-β (20–200 km) scale according to the definition by Orlanski (1975). PMCs include PLs, which are intense maritime cyclones with horizontal scales between 200 and 1000 km and with surface wind near or above gale force (Rasmussen and Turner 2003). They are observed over high-latitude oceans in both hemispheres including Northern Atlantic Ocean (e.g. Harold et al. 1999), Northern Pacific Ocean (e.g. Yarnal and Henderson 1989), and Southern Ocean (e.g. Carlton and Carpenter 1990). All of these regions are characterized by marine cold air outbreak from land or sea ice over relatively warm open oceans.

MVs are often accompanied by strong wind and heavy snow/rain fall that cause hazards to coastal regions and marine traffic. However, their accurate prediction remains difficult due to their small horizontal scale (less than 1000 km) and short lifetime (few hours to few days). Thus, genesis, structures, generation and development mechanisms, frequency, and favorable conditions of MVs are important subjects to be clarified.

1.2 MVs over the Sea of Japan

The Sea of Japan (Fig. 1.1) is one of the regions where MVs frequently occur (Asai 1988, hereafter A88; Ninomiya 1989). The Sea of Japan is unique in that it is located in relatively low latitudes (around 40N) compared with other regions where MVs

frequently occur. In winter, the Sea of Japan is located in one of the main streams of polar cold airmass (Iwasaki et al. 2014). In addition, the sea surface temperature (SST) of the Sea of Japan is relatively warm due to the Tsushima Current which is a branch of the Kuroshio Current. These factors provide favorable condition for the genesis and development of MVs.

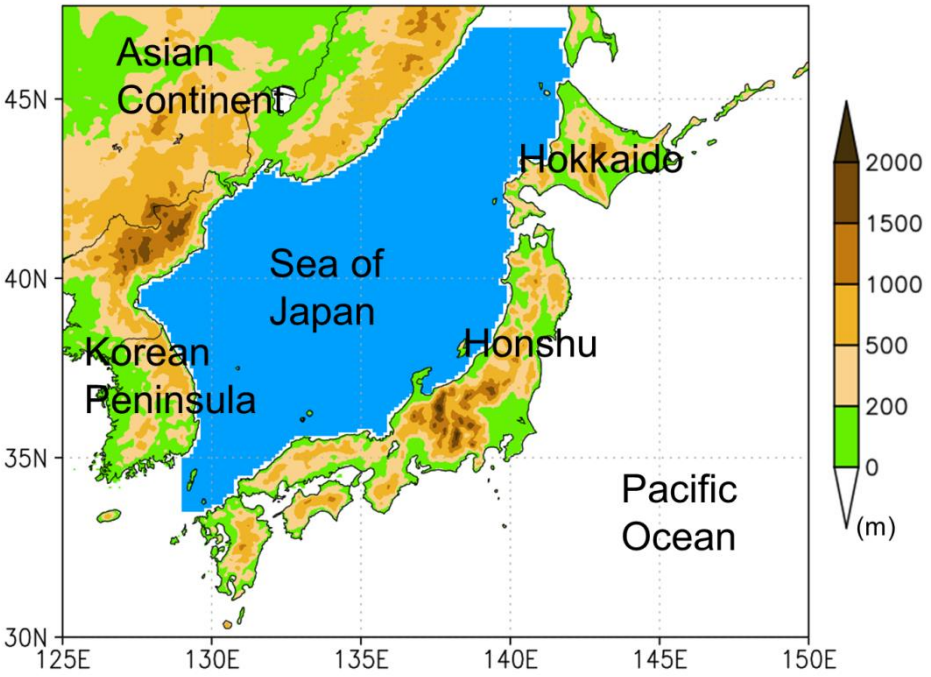

Fig. 1.1 Geography and topography around the Sea of Japan. Tracking of MVs was performed in the blue area.

The MVs over the Sea of Japan are associated with heavy snow/rain fall (e.g., Miyazawa 1967; A88) and strong winds (e.g., Kuroda 1992; Yamagishi et al. 1992), which cause disasters to coastal regions and maritime traffic. For example, a train fell from the Amarube Bridge in the western Honshu Island due to strong winds on 28 December 1986 causing six deaths and six injuries; and three vessels including two vessels of 7000 ton were shipwrecked off the central part of Honshu Island due to a gale force wind and high waves on 24 January 1990 (Kuroda 1992).

Since the 1960s when imagery from meteorological radars and satellites became available, Japanese meteorologists have paid considerable attention to MVs and have performed a number of observational studies (Miyazawa 1967; Okabayashi and Satomi 1971; Shimizu and Uchida 1974; Asai and Miura 1981). Using satellite images, A88 analyzed the locations of MV genesis over the Sea of Japan during the winter of 1983–84 and found that MVs with horizontal scales of less than 300 km are concentrated in two regions (Fig. 1.2): one between the northeastern base of the Korean Peninsula and the central part of Honshu Island, and the other to the west of Hokkaido Island. A cloud band known as the Japan Sea polar air mass convergence zones (JPCZs; A88) are typically present over these two regions. Several studies indicated a link between MVs and the JPCZ (Okabayashi and Satomi 1971; A88; Nagata 1993; Tsuboki and Asai 2004; Kato 2005; Watanabe and Niino 2014).

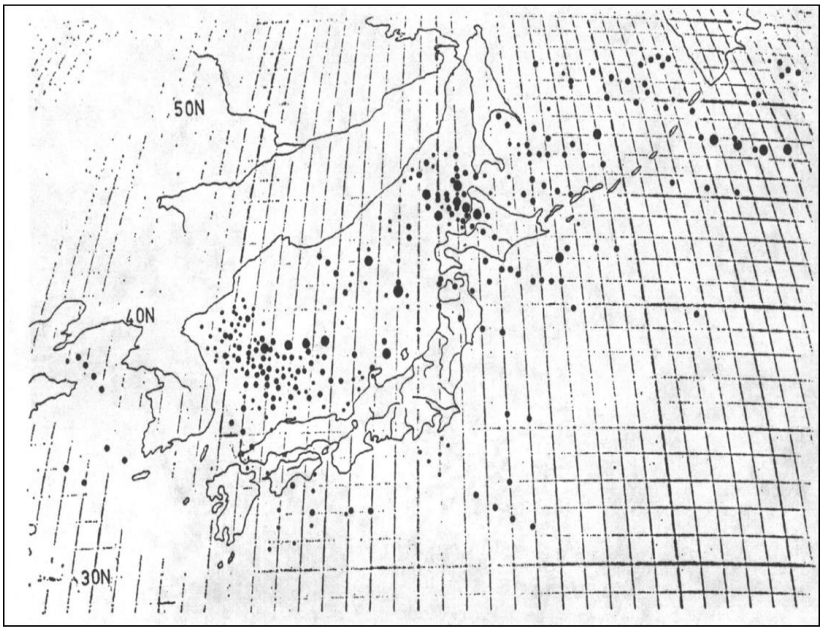

Fig. 1.2 Geographical distribution of the locations of individual MVs observed in satellite images over the Sea of Japan and its vicinity during the winter of 1983–1984. Larger dots denote larger mesoscale cyclones (adapted from A88).

MVs over the Sea of Japan have a wide spectrum of horizontal scales and a variety of cloud pattern. Meso-α-scale MVs are accompanied by comma-shaped (Fig. 1.3a) or spiralform cloud (Fig. 1.3b) (e.g. Shimada et al. 2014). Meso-β-scale MVs are also observed, and occasionally, several mesoβ-scale MVs appear simultaneously within a cloud band (Fig. 1.4) (Kuroda 1992; Fu et al. 2004b). In addition, multiscale MVs which consist of meso-β-scale MVs embedded in meso-α-scale MV or a large-scale system are also observed (Ninomiya et al. 1990; Ninomiya and Hoshino 1990; Ninomiya 1994). These various MVs are likely to originate from different development mechanisms.

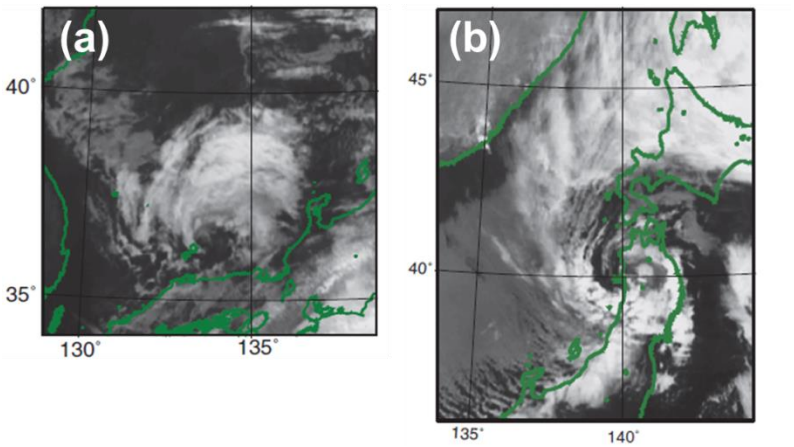

Fig. 1.3 Satellite images of meso-α-scale MVs: (a) a comma-shaped MV and (b) a spiralform MV (Fig. 5c and 3c in Shimada et al. 2014).

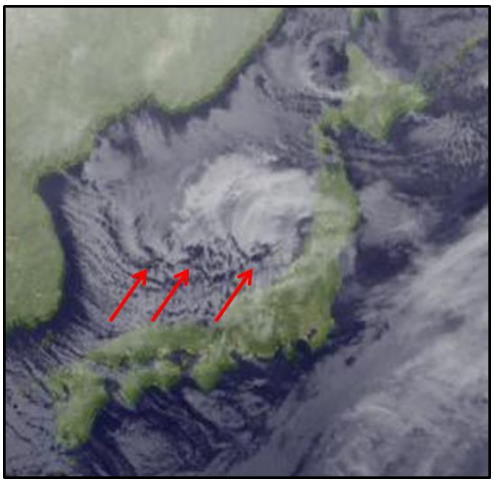

Fig. 1.4 Satellite image of meso-β-scale MVs. The MVs are indicated by arrows.

As for the meso-β-scale MVs, a number of researchers emphasize the importance of horizontal shear of the JPCZ (Asai and Miura 1981; Nagata 1993; Tsuboki and Asai 2004; Kato 2005; Watanabe and Niino 2014). Nagata (1993) succeeded in reproducing realistic MVs embedded in a JPCZ with spiral cloud bands and a cloud-free eye structure by a numerical simulation, and showed that their main energy source was horizontal shear of the JPCZ. Note that mountains at the northern part of the Korean Peninsula play a crucial role in the formation of JPCZ (Yagi et al. 1986; Nagata 1991; Tsuboki and Asai 2004). The effect of thermal contrast between the Korean Peninsula and the Sea of Japan, and SST gradient in the Sea of Japan were also suggested to be important for the JPCZ (Nagata et al. 1986; Nagata 1991).

Condensational heating and associated cumulus convection are also considered to be indispensable for the development of meso-β-scale MVs. While horizontal shear of the JPCZ is prominent only at low levels, cumulus convection contributes to the vertical development of MVs (Kato 2005). Watanabe and Niino (2014) showed that the structure of a mature MV resembled a tropical cyclone, which indicates that the MV developed through a cooperative interaction between the vortex flow and diabatic processes.

For the development of meso-α-scale MVs, baroclinicity plays an important role: Yamagishi et al. (1992) showed that a MV had characteristics of a baroclinic disturbance including frontal structure. Tsuboki and Wakahama (1992) analyzed radiosonde data and found two unstable modes associated with vertical shear of meridional and zonal wind. They suggested that these unstable modes may correspond to observed two kinds of MVs observed off the Hokkaido Island.

Diabatic process also plays an important role in the development of meso-α-scale MVs. (Yanase et al. 2004; Wu et al. 2011). By several sensitivity experiments, Yanase et

al. (2004) showed that condensational heating is important for a short-term development of a MV and that latent and sensible heat fluxes from sea surface indirectly contributed to the development of the MV by maintaining unstable stratification. Wu et al. (2011) applied a piecewise potential vorticity (PV) inversion method to a MV case and showed that condensational heating produced a positive PV anomaly and intensified the MV. In addition, it increased the influence of upper-level PV anomaly on the low-level MV by reducing static stability.

A common characteristic of synoptic fields for the development of both meso-α- and meso-β-scale MVs is an upper-level vortex or trough accompanied by cold airs (Ninomiya 1989; Nagata 1993; Lee et al. 1998; Fu et al. 2004a; Wu et al. 2011; Shimada et al 2014). It brings less stable stratification which is favorable for convection and a dynamic forcing which spins-up a low-level vortex. Shimada et al. (2014) found that a meso-α-scale PV anomaly within a synoptic scale PV anomaly intrudes to around 700-600 hPa level during the development stage of MVs.

Several studies using idealized numerical simulations were performed to understand the diversity of MVs. Yanase and Niino (2007) demonstrated that the cloud patterns and development mechanisms of MVs change significantly when environmental baroclinicity changes. Maejima and Iga (2012) analyzed MVs associated with a frontal structure modeled on a JPCZ. They showed that static stability and the depth of the horizontal shear layer determine the size and development mechanism of the MVs. These findings indicate that strong connection between the features of the MVs and environmental conditions.

As reviewed above, the development mechanism of MVs varies from case to case and several individual processes can operate at the same time in a complex manner.

Moreover, dominant process can change even during the development of a MV (Watanabe and Niino 2014; Shimada et al. 2014). These different development mechanisms are considered to result in different characteristics of MVs. Therefore, it is difficult to acquire comprehensive understanding of the characteristics of MVs only from case studies. The results of idealized numerical simulations indicate that environmental conditions are a key for understanding the characteristics of MVs. However, the general environment for the MV has not been fully clarified.

1.3 Climatological studies of MVs

One way to analyze the general environment of the MVs is to perform a climatological study. A number of studies have investigated the climatology of MVs over various oceans (e.g. Wilhelmsen 1985; Businger 1987; Yarnal and Henderson 1989; Carlton and Carpenter 1990). As for the Sea of Japan, several climatological studies have been performed using satellite images, weather chart, and reanalysis dataset (A88; Ninomiya 1989; Ookubo 1995; Yanase et al. 2015, hereafter Y15).

Ninomiya (1989) analyzed MVs using “nephanalysis” (analysis chart focusing on the types and amounts of clouds) and weather charts, and described their characteristic environments including the low-level cyclonic flow of a polar air and the upper-level cold vortex. Using serial satellite images, Ookubo (1995) demonstrated that there are two types of MVs in the western part of the Sea of Japan: one moves east-northeastward and the other moves southeastward. However, as these studies relied on the subjective detection of MVs, they were unable to deal with a large amount of data. For example, A88 and Ninomiya (1989) analyzed MVs only during one winter, and Ookubo (1995) analyzed only nine MVs.

Recently, a number of objective tracking algorithms have been developed and applied to objective analysis datasets and dynamic downscale datasets (Zahn and von Storch 2008; Xia et al. 2012; Chen and von Storch 2013; Zappa et al. 2014; Y15). Tracking algorithms are useful in obtaining reliable climatological data for MVs because they can objectively and automatically detect a large number of MVs. As for the climatology of PLs over the Sea of Japan, Chen and von Storch (2013) analyzed the entire North Pacific using a regional climate model with a horizontal resolution of 0.4°, and Y15 examined the Sea of Japan in detail using the Japanese 55-year Reanalysis (JRA-55; Kobayashi et al. 2015) with a horizontal resolution of about 60 km. These studies, however, examined only meso-α-scale MVs because of the limited horizontal resolution of the data.

Climatological studies of MVs using satellite images suggest that many MVs smaller than 200 km develop over the Sea of Japan (A88) and over the northeastern Atlantic (Harold et al. 1999; Condron et al. 2006; Blechschmidt 2008). Small MVs have also been observed over the Great Lakes (Hjelmfelt 1990; Laird et al. 2001). The ability to objectively detect MVs is strongly influenced by the resolution of the data, and a large number of MVs smaller than 200 km are missed due to the cause resolution of the dataset (Condron et al. 2006). In addition, the automatic detection of MVs which are embedded in a larger disturbance such as a synoptic-scale low is also difficult (Laffineur et al. 2014).

Figure 1.5a presents a visible image of MVs taken by the Japanese Multifunctional Transport Satellite 2 (MTSAT-2), which shows three meso-β-scale vortices existing simultaneously in the JPCZ. Although JRA-55 marginally resolves the JPCZ, its vorticity spreads over a wide band-shaped region and the vortices are not resolved

clearly (Fig. 1.5b). On the other hand, Fig. 1.5c shows a corresponding plot based on Meso-Scale Analysis (MANAL) data provided by the Japan Meteorological Agency (JMA). This demonstrates that MANAL has a potential to resolve meso-β scale MVs embedded in the JPCZ.

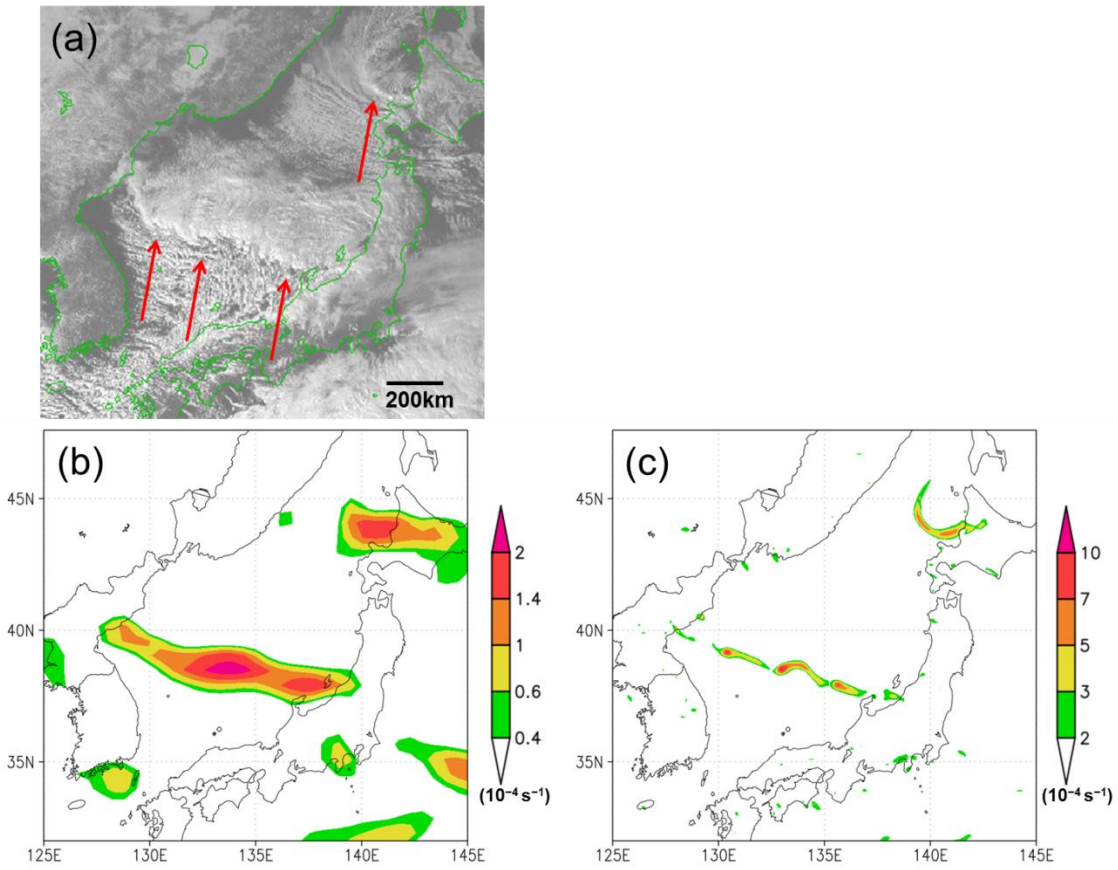

Fig. 1.5 (a) Visible image from MTSAT-2, and (b) and (c) vorticity distributions at 950 hPa at 0600 UTC 29 Jan 2011 (color; 10^{-4} s^{-1}) obtained from JRA-55 and MANAL, respectively. Arrows in (a) indicate the locations of MVs. Note that the color scales in (b) and (c) are different.

1.4 Objective of the present study

In this study, we conduct a climatological study to understand the general characteristics and environment of MVs over the Sea of Japan. To this end, we first develop a new algorithm for the detection and tracking of MVs including meso-β scale

vortices, based on MANAL. The algorithm enables us to examine the statistical characteristics of the MVs including their location, size, intensity, frequency, and moving direction. We also classify the MVs according to their locations and direction of motions and analyze the general environment and the development mechanism by composite analyses and numerical simulations.

This thesis is organized as follows: In chapter 2, we describe the detail of the algorithm for the detection and tracking of MVs. In chapter 3, we show statistical characteristic of MVs. We present the results of the composite analyses in chapter 4 and those of numerical simulations in chapter 5. Finally, we give conclusions and future perspectives in chapter 6.

2 Data and an algorithm for detection and tracking of MVs

In this chapter, we describe a new algorithm for detection and tracking of MVs the horizontal scale of which is between about 50 km and 300 - 400 km. The algorithm consists of three parts: identification of vortices at each time step, connection of vortices in consecutive time steps, and exclusion of synoptic-scale disturbances (SDs). The MVs detected by the algorithm are validated against those detected subjectively based on MANAL and satellite images.

2.1 Data

We use MANAL data (Japan Meteorological Agency 2013) in the tracking analysis of the MVs. MANAL is a product of objective analysis using the JMA Meso-Scale Model, which is based on the JMA nonhydrostatic model (JMA-NHM; Saito et al. 2006), as a forecasting model. For the data assimilation, MANAL uses the four-dimensional variational scheme, JNoVA (JMA-NHM-based Variational Analysis Data Assimilation; Honda et al. 2005). The domain of MANAL is a rectangular area of 3600 × 2880 km in Lambert conformal conic map projection covering Japan and its surroundings. The original MANAL dataset has a horizontal resolution of 5 km with 50 vertical levels, and a temporal resolution of 3 h. In the present analysis, we use a dataset prepared by interpolating the original MANAL data into geographic coordinates with a horizontal grid spacing of 0.1° in latitude, 0.125° in longitude, and 16 pressure levels. This resolution is sufficient to examine the characteristics of meso-β-scale MVs. As most MVs occur during the cold season, we analyze six cold seasons from November 2009 to March 2015 (note that JNoVA was introduced in April 2009). Hourly infrared

(IR) satellite images from MTSAT-2 are used to validate the detected MVs. The NOAA 0.25° daily Optimum Interpolation Sea Surface Temperature (OISST; Reynolds et al. 2007) data are used to examine environments of the MVs.

2.2 Algorithm for tracking MVs

2.2.1 Identification of vortices at each time step

Previous methods for detecting MVs identified only locations of MVs based on vorticity maxima or pressure minima. In addition to this, our method is able to define sizes and shapes of MVs by using high-resolution datasets. They are used for discriminating MVs and SDs.

In the present study, relative vorticity at the 950-hPa level is used to track the MVs. The vorticity field is smoothed using a running mean over 0.4° in latitude and 0.5° in longitude to focus on MVs with horizontal scales larger than, or equal to, meso-β scale. The algorithm used to detect vortices is similar to that developed by Shimizu and Uyeda (2012) to detect convective cells in PPI scans of radar reflectivity. Their algorithm is based on an adaptive threshold scheme that is able to identify a convective cell that includes a single local maximum of reflectivity from the cell groups and is suitable for identifying MVs embedded in a larger system such as the JPCZ.

Figure 2.1 shows a schematic diagram of the algorithm used to identify the vortices. First, the location of the maximum vorticity is detected. A "vortex area" is defined as a continuous area of vorticity $\geq \zeta_{min0}$ (1.5×10^{-4} s^{-1}) surrounding the maximum (the red area in Fig. 2.1a). Similarly, the maximum of vorticity in the rest of the area is again detected and a corresponding vortex area is defined (the green area in Fig. 2.1a). This process is repeated until all peaks having vorticity $\geq \zeta_{max0}$ (2.0×10^{-4} s^{-1}) have been

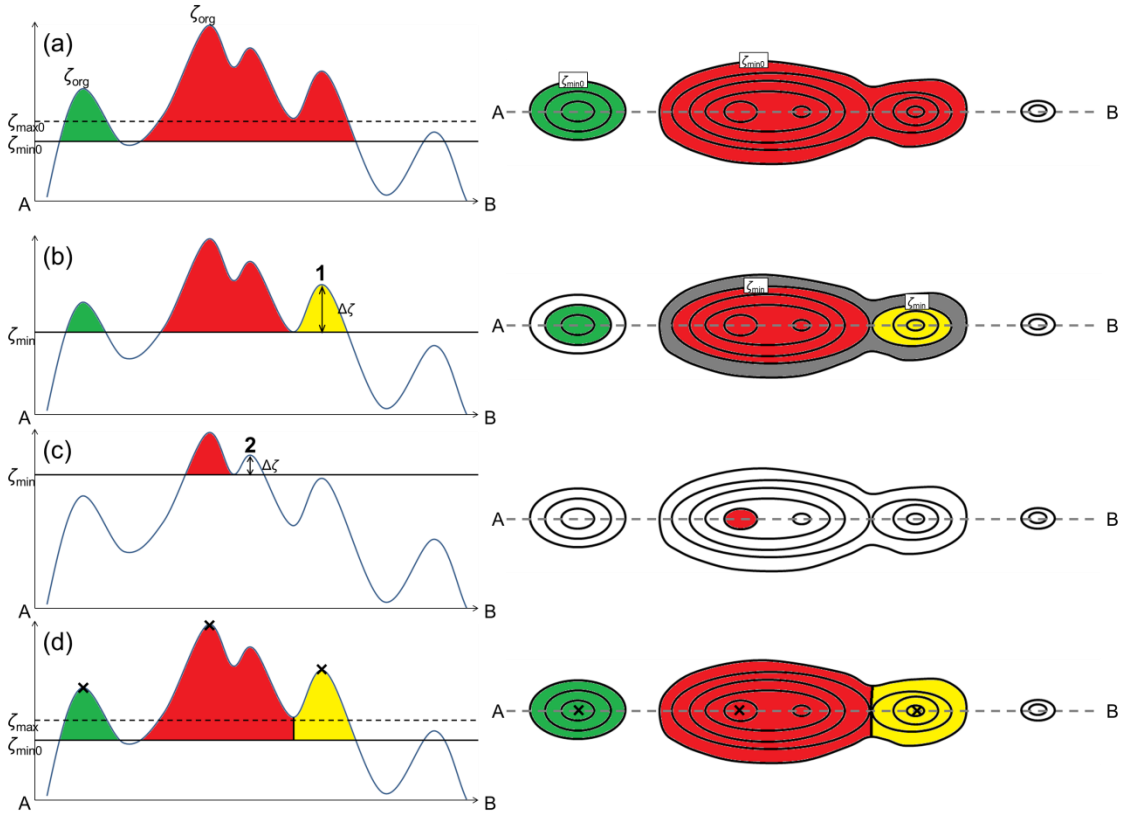

Fig. 2.1. Schematic diagram of the algorithm used to identify vortices. The right panels show the horizontal distribution of the vorticity field and the left panels show vorticity along line A–B in the right panels. (a) shows the original vortex areas, which are defined as the green and red areas. (b) shows an example of a peak (peak 1) identified as a vortex. The gray area in (b) is where vorticity is lower than the temporary threshold ζ_{min} and will be distributed to either the yellow or red vortex area in the last step. (c) shows an example of a peak (peak 2) identified as a part of the neighboring vortex. (d) shows the final result of the identification process. The isolated vortex areas are defined as the green, red, and yellow areas in (d). The center of each vortex is shown by cross marks in (d). See text for details.

detected (Fig. 2.1a). The vortex area defined here is referred to as an "original vortex area", and the peak vorticity in each original vortex area is referred to as ζ_{org}. There are two kinds of original vortex area: one with a single peak (green area in Fig. 2.1a) and one with multiple peaks (red area in Fig. 2.1a). A vortex area with a single peak is referred to as an "isolated-vortex area" and that with multiple peaks as a "multiple-vortex area". The former is identified as a vortex at this point.

Table 2.1 Thresholds used to identify vortices.

Threshold	Value
ζ_{min0}	1.5×10^{-4} s^{-1}
ζ_{max0}	2.0×10^{-4} s^{-1}
$\Delta\zeta_{min}$	0.6×10^{-4} s^{-1} ($\zeta_{org} \geq 5.0 \times 10^{-4}$ s^{-1}) 0.3×10^{-4} s^{-1} (4.0×10^{-4} s$^{-1} \leq \zeta_{org} < 5.0 \times 10^{-4}$ s^{-1}) 0.24×10^{-4} s^{-1} (3.0×10^{-4} s$^{-1} \leq \zeta_{org} < 4.0 \times 10^{-4}$ s^{-1}) 0.2×10^{-4} s^{-1} (2.0×10^{-4} s$^{-1} \leq \zeta_{org} < 3.0 \times 10^{-4}$ s^{-1})
ζ_{max}	3.0×10^{-4} s^{-1} ($\zeta_{org} \geq 5.0 \times 10^{-4}$ s^{-1}) 2.7×10^{-4} s^{-1} (4.0×10^{-4} s$^{-1} \leq \zeta_{org} < 5.0 \times 10^{-4}$ s^{-1}) 2.5×10^{-4} s^{-1} (3.0×10^{-4} s$^{-1} \leq \zeta_{org} < 4.0 \times 10^{-4}$ s^{-1}) 2.0×10^{-4} s^{-1} (2.0×10^{-4} s$^{-1} \leq \zeta_{org} < 3.0 \times 10^{-4}$ s^{-1})

Table 2.2 Criteria for excluding one of two vortices in close proximity. If the ratio of the vorticity of the weaker peak to the stronger peak is less than these values, the weaker peak is excluded.

Distance (d)	Ratio of two peaks
d ≤ 50 km	1.0
50 < d ≤ 100 km	0.9
100 < d ≤ 150 km	0.8

To identify vortices in a multiple-vortex area, the threshold ζ_{min} used to define a vortex area is increased until a single peak exists within a vortex area (Fig. 2.1b and 2.1c). If the difference $\Delta\zeta$ between the vorticity of the peak and the threshold ζ_{min} is more than $\Delta\zeta_{min}$, and if the vorticity of the peak is larger than ζ_{max}, then the peak and

corresponding vortex area are identified as a vortex (peak 1 and the yellow area in Fig. 2.1b; for the values of $\Delta\zeta_{min}$ and ζ_{max}, see Table 2.1). If $\Delta\zeta$ is less than $\Delta\zeta_{min}$, or if the vorticity of the peak is less than ζ_{max}, the peak is regarded as part of a neighboring vortex (peak 2 in Fig. 2.1c). Note that $\Delta\zeta_{min}$ and ζ_{max} depend on ζ_{org} (Table 2.1). This procedure is continued until all peaks in multiple-vortex areas are identified. Then, the distances between the peaks are examined. If two peaks in the same multiple-vortex area are close to each other, then the weaker peak is not selected as an isolated vortex, based on criteria related to the distance between the two peaks and the ratio of vorticity between the peaks (Table 2.2). There are two kinds of areas in a multiple-vortex area: the first belongs to a vortex area defined by the threshold ζ_{min} that separates two peaks (e.g., red and yellow areas in Fig. 2.1b), and the other is the rest of the multiple-vortex area (gray area in Fig. 2.1b). For a grid point within the latter area, the distances between the grid point and the edge of the vortex areas are calculated. The grid point is assigned to the vortex area whose edge is closest to it. In this way, each vortex and its vortex area are determined as in Fig. 2.1d. The center and intensity of each vortex are defined by the location and magnitude of the vorticity peak. The size of each vortex is defined by the area of the isolated vortex area.

2.2.2 Connection of vortices at consecutive time steps

To connect vortices at consecutive time steps, a steering wind for each vortex is calculated to estimate the movement of the vortex. This steering wind is defined as a wind averaged over a box that encloses an area of 4° in latitude by 5° in longitude between 1000 and 700 hPa, where the center of the box is chosen to coincide with the vortex center. The position of a vortex at the next time step is estimated by assuming

that the vortex is advected by the steering wind. For this estimated position, two requirements are imposed. First, the vortex at the next time step must be located within 1° in longitude and 0.8° in latitude of the estimated position (i.e., the estimated area; Fig. 2.2a). If there are more than two vortices in the estimated area, the vortex closest to the estimated position is linked to the previous vortex. If there is no vortex that satisfies the first requirement, the second requirement is considered, which is that a part of an isolated vortex area at the next time step overlaps with the estimated area (Fig. 2.2b). If there are more than two isolated vortex areas a part of which overlaps with the estimated area, the vortex at the previous time step is linked to the vortex with an isolated vortex area having the largest amount of overlap with the estimated area.

If a vortex does not have a corresponding vortex at the previous (next) time step, that time step is defined as the genesis (dissipation) time. If more than two previous vortices are connected to a single vortex at the next time step, they are recognized as being merged. In this study, Vortices with a lifetime exceeding 6 h (three time steps) are defined as MVs.

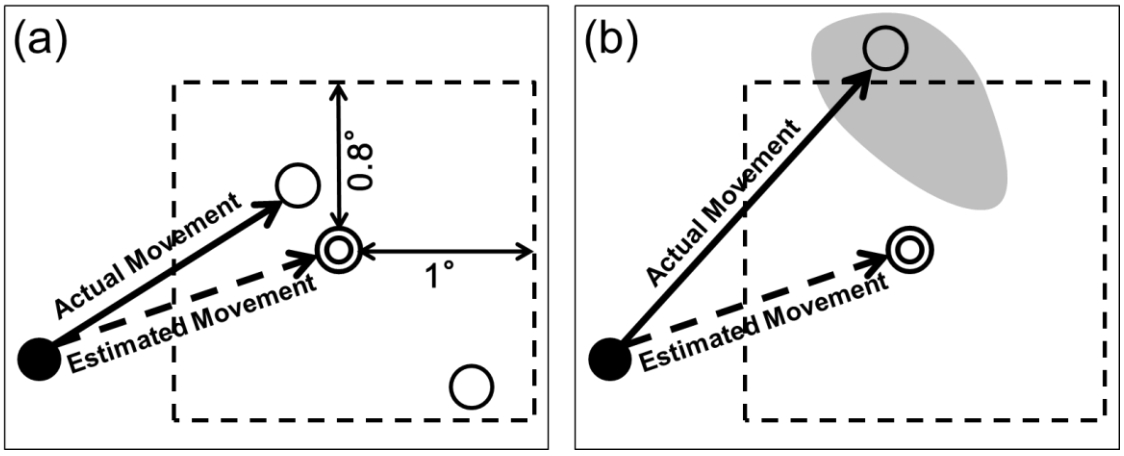

Fig. 2.2. Schematic diagram of the requirements for connecting vortices at consecutive time steps. Closed circle is the center of a vortex at the previous time step. The double circle is the estimated position of the vortex at the next time step. Open circles are centers of vortices at the next time step. The gray area in (b) is an isolated vortex area of a vortex at the next time step. See text for details.

2.2.3 Exclusion of SDs

As we do not use a spatial high-pass filter, the present tracking method also picks up SDs such as synoptic-scale lows and cold fronts. Previous tracking method used additional criteria for discriminating MVs and SDs: The most commonly used criterion is based on stability of stratification, where MVs occur in less stable environment (Zahn and von Storch 2008; Xia et al. 2012; Chen and von Storch 2013; Zappa et al. 2014; Y15). Another commonly used criteria is based on moving direction of a MV,which has a southward component (Zahn and von Storch 2008; Xia et al. 2012; Chen and von Storch 2013). However, these criteria are not suitable for studying the environment of MVs, since they use information of the environment beforehand. Therefore, we introduce a scheme that discriminate SDs from MVs without information of the environmental condition.

In the present study, the size of the vortex area and sea level pressure (SLP) are used to identify synoptic-scale lows (Fig. 2.3). First, the sizes of the original vortex areas are examined and SLP minima that are at least 0.5 hPa less than the surroundings are detected. Then, a vortex that is located in an original vortex area larger than 40,000 km^2 and is within 300 km of an SLP minimum is considered as a synoptic-scale low (black cross in Fig. 2.3). Although some large MVs can be erroneously classified as synoptic-scale lows using these thresholds, almost all synoptic-scale lows are properly classified here. If a vortex is in an original vortex area larger than 40,000 km^2 but is located farther than 300 km from an SLP minimum, the vortex is not considered as a synoptic-scale low (white cross in Fig. 2.3). The present scheme is able to distinguish between a synoptic-scale low and a vortex embedded within it. Such multi-scale structures are sometimes observed over the Sea of Japan (e.g. Ninomiya 1994).

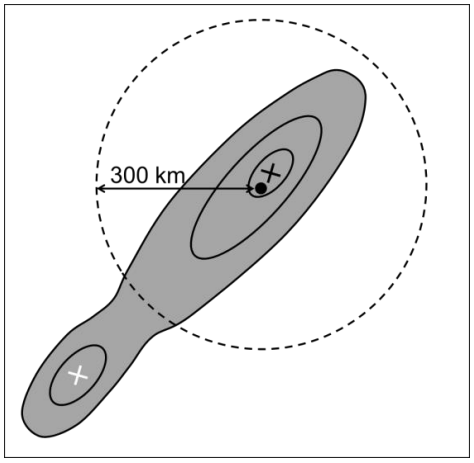

Fig. 2.3. Schematic diagram for identifying synoptic-scale lows. Gray area is an original vortex area. Crosses denote centers of vortices and a black dot denotes a minimum of SLP. In this case, the black cross is considered to be a synoptic-scale low but the white cross is not. Note that there is no minimum of SLP within 300 km of the white cross. See text for details.

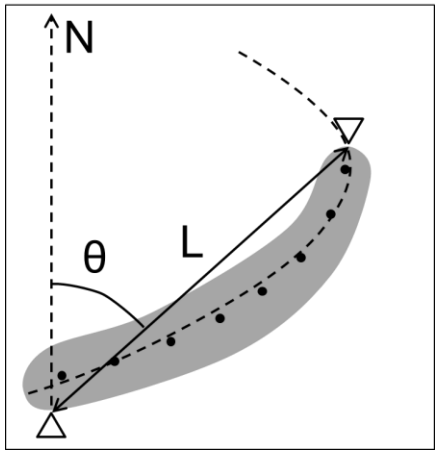

Fig. 2.4. Schematic diagram of the procedure used to identify cold fronts. Gray area is an original vortex area. Triangles indicate the northern and southern edges of the original vortex area, L is the distance between the two edges, and θ is the clockwise angle between the line connecting the two edges and north. Black dots are grid points determined to be ridges of vorticity field. Dashed curve is a fitting curve. See text for details.

Next, the shape of the original vortex area is used to identify cold fronts (Fig. 2.4). Typical cold fronts extend linearly in northeast-southwest direction. First, the southern and northern edges of each original vortex area are detected. The distance between the two edges (L in Fig. 2.4) and the clockwise angle between the line connecting the two

edges and north (θ in Fig. 2.4) are calculated. If the distance is greater than 400 km and the angle is between −20° and +60°, the original vortex area is further examined. First, the ridge of the vorticity field in the original vortex area is detected in the following way. A grid point on the ridge is determined by choosing the point where the vorticity is one of the three largest of the nine neighboring grid points. Then, the grid points chosen in this way are fitted by a smooth quadratic curve. If the average curvature of the quadratic curve is less than 0.1 (the curvature is positive when the quadratic curve is convex westward) and the coefficient of determination (R^2) is greater than 0.8, the vortices in the original vortex area are considered part of a cold front.

Finally, all time steps from the lifetime of the MV are examined according to the above two schemes. If the number of time steps when the vortex is considered a synoptic-scale low or a cold front is more than one-seventh of the whole lifetime of the MV, then the MV is excluded as a SD.

2.3 Validation of the tracking algorithm

When the present tracking method was applied to the MANAL data, 644 MVs were detected over the six cold seasons. To evaluate the validity of the tracking algorithm, we subjectively examined all of the detected MVs by using the vorticity and the SLP field from MANAL and satellite IR images. We first checked whether a detected MV was subjectively judged to be a MV using the MANAL data, and then checked whether the MV was evident in the IR images. MVs were then classified into one of three groups (Table 2.3): those that were judged to be MVs using the MANAL data and were also found in the satellite images (class-A), those that were judged to be MVs from the MANAL data but were not found in the satellite images (class-B), and those that were

not judged to be MVs (class-C). It is found that 379 MVs (59%) belong to class-A and 80 MVs (12%) to class-B. Thus, 71% of the MVs detected by the present method are judged to be MVs by subjective detection using the vorticity and SLP field. Some of the class-B MVs are covered by upper-level clouds in the satellite image, but others were so weak that they were not accompanied by obvious cloud features. Class-C contains 185 MVs (29%) that were either part of a cold front or a weak vorticity peak in a synoptic-scale low. There are also vortices which are classified into SDs by our discrimination scheme but are judged to be MVs by subjective analyses. 18 of such MVs were found among 216 SDs in 6 cold seasons.

In order to reduce false detections, we introduced thresholds for the intensity and lifetime of the MVs. We selected MVs that satisfied either of the following criteria (hereafter referred to as strong-criteria): 1) the lifetime exceeded 9 h and the vorticity exceeded 3.0×10^{-4} s^{-1} for at least two successive time steps, or 2) the lifetime exceeded 6 h and the vorticity exceeded 4.5×10^{-4} s^{-1} at least once during the lifetime. 290 MVs are found to satisfy strong-criteria (Table 2.3). The numbers of MVs classified into classes -A, -B, and -C were 225 (78%), 25 (8.6%), and 40 (14%), respectively, and 86% of the MVs agreed with the subjective detection using the vorticity and SLP field. Thus, the strong-criteria reduce the number of false detections. Note that the strong-criteria also reduce the number of class-A MVs. Moreover, some MVs found in satellite images had only a weak surface vorticity signature or none. Thus, our method missed some MVs. In the following section, however, we focus on the MVs that satisfied strong-criteria to obtain more robust results.

In the tracking algorithm, we use several thresholds, which are empirically determined based on subjective analyses on MANAL and satellite images. The results

of the tracking depend on these thresholds. In general, more (less) MVs are detected with moderate (strict) thresholds, while more (less) false detections are found. As the number of false detections is reduced by the strong-criteria, the threshold for the intensity of a vortex ζ_{max0} has large influence on the result. We checked the sensitivity to ζ_{max0} by setting ζ_{max0} to 3.0×10^{-4} s^{-1} and 1.5×10^{-4} s^{-1}. With ζ_{max0} of 3.0×10^{-4} s^{-1}, 171 MVs which satisfy the strong-criteria were detected. The numbers of classes -A, -B, and -C MVs were 141 (82%), 13 (7.6%), and 17 (10%), respectively. Although the larger ζ_{max0} reduces the proportion of false detection, it also reduces the number of class-A MVs. With ζ_{max0} of 1.5×10^{-4} s^{-1}, more MVs were detected. However, most of them are class-C MVs. The number of MVs which satisfy the strong-criteria is 326 and the numbers of classes -A, -B, and -C MVs were 241 (74%), 35 (9.2%), and 55 (17%), respectively. The number of class-A MVs is slightly larger than that for ζ_{max0} of 2.0×10^{-4} s^{-1}, while the number of class-C MVs is also increased. Since the thresholds depend on the characteristics of the data set including horizontal resolutions and physical processes incorporated in the parent model, we need to set appropriate thresholds first for each dataset based on subjective analyses. Once appropriate thresholds are set, the present method is very effective for obtaining the climatology of the MVs.

Table 2.3 Numbers of MVs classified by subjective analysis of MANAL and satellite images.

	Without strong-criteria	With strong-criteria
Class-A	379 (59%)	225 (78%)
Class-B	80 (12%)	25 (8.6%)
Class-C	185 (29%))	40 (14%)
Total	644	290

3 Statistical characteristics of the MVs

3.1 Introduction

Although a number of statistical analyses have been performed for MVs over various high-latitude oceans, most of these studies have investigated only meso-α-scale PLs. Few studies have examined the statistical characteristics of meso-β-scale MVs. As for the Sea of Japan, recently, Y15 analyzed statistical characteristics of the MVs using JRA-55. Because of the coarse resolution of JRA-55, a majority of meso-β-scale MVs, which are frequently observed over the Sea of Japan, have not been included in their study. Thus, statistical characteristics of MVs including meso-β-scale MVs remain to be clarified.

In this chapter, we examine the general characteristics of MVs identified by our tracking algorithm. First, we examine the climatology of MVs including their frequency and geographical distribution. Next, MVs are classified into groups according to their location, and the characteristics of each group of MVs including their intensity, size, and movement are investigated. The criteria for discriminating MVs and SDs are also discussed.

3.2 Climatology of MVs

3.2.1 Frequency of MVs

MVs form most frequently during midwinter from December to January (Fig. 3.1). This result is similar to Y15. The average number of MVs per cold season is 48.3 and year-to-year standard deviation is 8.5 (not shown). Since the period of this analysis is only 6 cold seasons, however, analysis over a longer time period may be required to obtain more robust results. Figure 3.1 also shows monthly frequencies of Classes-A, -B

and –C MVs. We find that the proportion of class-C MVs is large in November and March when synoptic-scale lows are common over the Sea of Japan. Vorticity peaks associated with these synoptic-scale lows are sometimes erroneously classified as MVs.

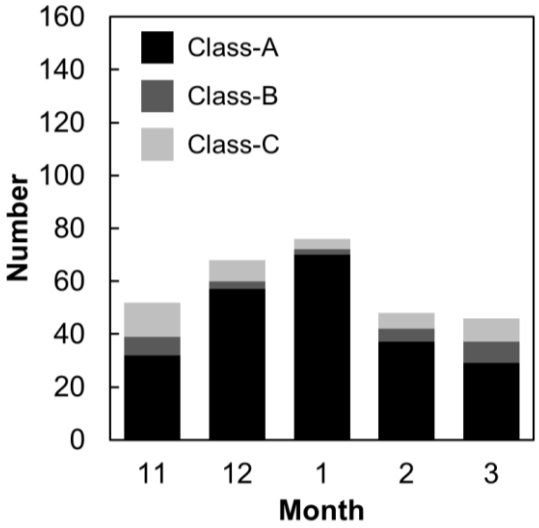

Fig. 3.1. Total monthly number of detected MVs over the six cold seasons between November 2009 and March 2015. Black, dark-gray, and light-gray bars indicate the numbers of class A, B, and C MVs, respectively.

3.2.2 Geographical distribution of the MVs

Figure 3.2 shows the tracks and locations at maximum intensity of the MVs (Fig. 3.2a) and the average number found within a 1° × 1° grid in the cold season (Fig. 3.2b). The tracks of the MVs are concentrated mainly in two regions: the western part of the Sea of Japan from the base of the Korean Peninsula to the center of Honshu Island (the WJ-region), and the western part of the northern Sea of Japan to the west of Hokkaido Island (the NJ-region). Several MVs are also found in the central part of the Sea of Japan around 138°E, 40°N (the CJ-region). The MVs are classified into three groups according to the location where they reached their maximum intensity (Fig. 3.2b). The numbers of the MVs in the WJ-, NJ-, and CJ-regions were 146, 98, and 46, respectively.

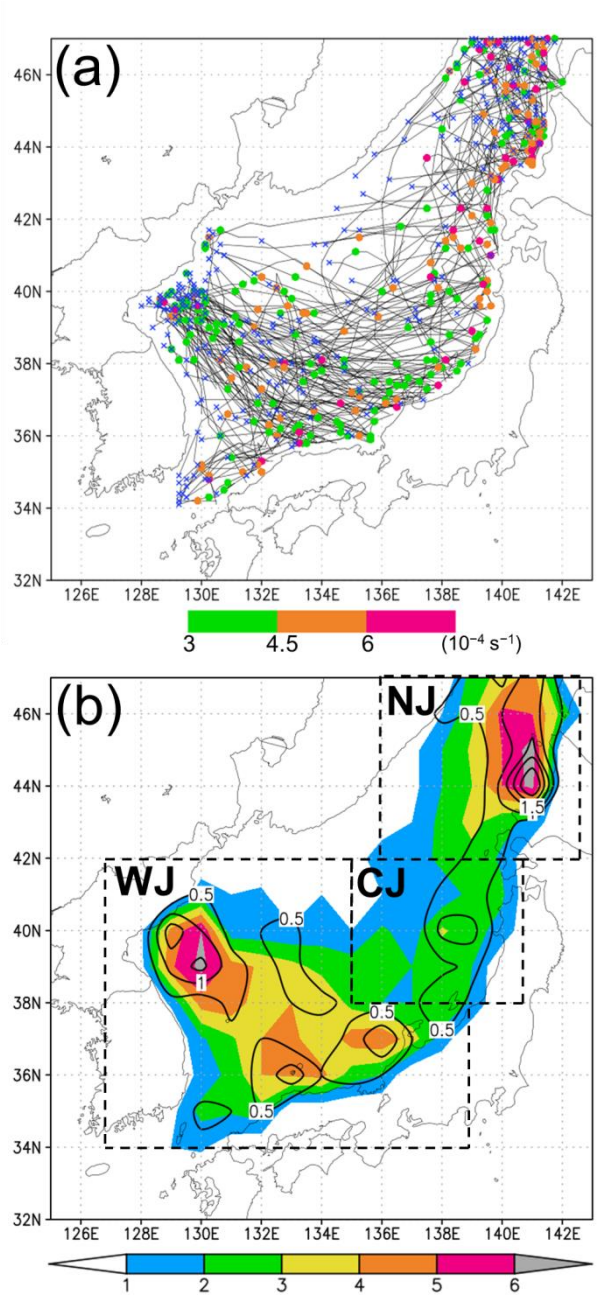

Fig. 3.2. (a) Tracks of MVs over the six cold seasons. Blue crosses are the locations of the genesis of the MVs. Dots are the locations of the maximum intensity of MVs and their colors indicate the maximum vorticity (10^{-4} s^{-1}). (b) Average number of tracks (color) and the locations at the maximum intensity (contours) found within a 1° × 1° grid in a cold season. The geographical locations of the WJ-, CJ-, and NJ-regions are indicated by dashed lines.

3.3 Characteristics of classified MVs

We examine typical characteristics of the MVs in each region, such as their direction of movement (Fig. 3.3), maximum intensity (Fig. 3.4), and size (Fig. 3.5).

In the WJ-region, most of the MVs are generated leeward of the mountains to the north of the Korean Peninsula (see also Fig. 1.1) and move southeastward (Fig. 3.3). There are also MVs that move eastward or east-northeastward along the coast of Honshu Island (Fig. 3.3). A considerable number of MVs attain their maximum intensity at the beginning of their lifespan, whereas the rest of MVs intensify during their lifetime and reach peak intensity near Honshu Island (Fig. 3.2). The maximum vorticity of MVs in this region is small in comparison with other regions (Fig. 3.4), although a few intense MVs (e.g., maximum vorticity > 8.0×10^{-4} s^{-1}) are occasionally observed. The average size of MVs in this region is intermediate among the three regions (Fig. 3.5), although large MVs (> 30,000 km^2) are also observed occasionally.

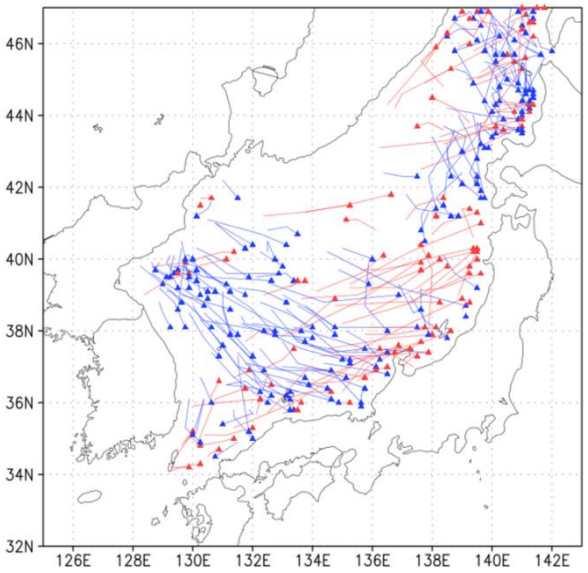

Fig. 3.3. Tracks of MVs for 6 h prior to the time of maximum intensity. Triangles show the location of maximum intensity. Tracks of MVs that have their maximum intensity at their initial time step are excluded from this plot and those of MVs whose lifetime is shorter than 6 h prior to the time of maximum intensity are plotted only for their lifetime. Red and blue lines indicate that the meridional movement of MVs is northward and southward, respectively.

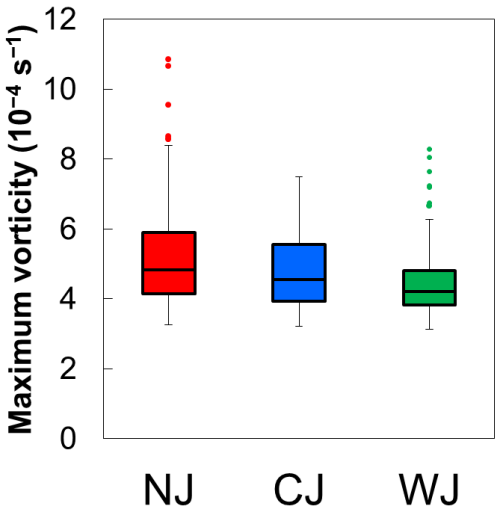

Fig. 3.4. Boxplot of the maximum vorticity of MVs in each region. The box shows the interquartile range (IQR) extending from the lower quartile to the upper quartile. The median value is shown by the horizontal line in the box. The vertical lines ("whiskers") extending upwards and downwards from the box reach the maximum and minimum within 1.5 × IQR from the upper and lower quartile, respectively. Outlying points are plotted individually as colored dots.

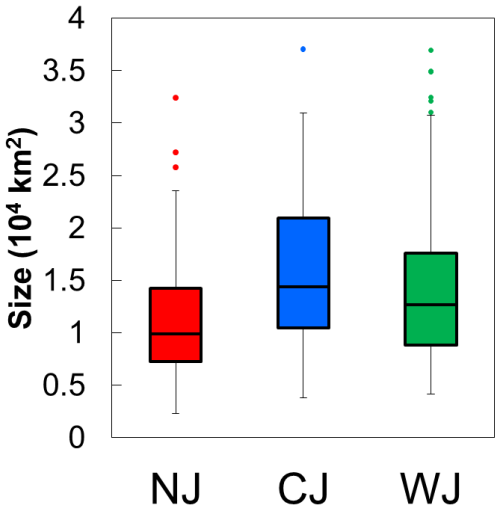

Fig. 3.5. As for Fig. 3.4 except for the size of MVs at their maximum intensity.

MVs in the NJ-region reach their maximum intensity near Hokkaido Island (Fig. 3.2) and have two major directions of movement: southward and eastward (Fig. 3.3). Most MVs in this group make landfall on Hokkaido Island, although some of the

southward-moving MVs move into the CJ-region along the western coast of northern Honshu Island (Fig. 3.2a). The maximum vorticity of MVs in this region is the largest and sometimes exceeds 8.0×10^{-4} s^{-1} (Fig. 3.4). The average size of MVs is smaller than that in the other regions, and most MVs are smaller than 20,000 km^2 (Fig. 3.5).

MVs in the CJ-region tend to move eastward or northeastward and reached their maximum intensity off the northwest coast of Honshu Island (Fig. 3.3). Their average maximum vorticity is intermediate among the three regions, and MVs with maximum vorticity exceeding 8.0×10^{-4} s^{-1} are not observed in this region (Fig. 3.4). These MVs are relatively large and more than 25% of MVs are larger than 20,000 km^2 (Fig. 3.5).

3.4 Discussion

3.4.1 Comparison with previous works

We now compare the results obtained by our tracking method with previous studies on MVs over the Sea of Japan, where the latter are based mainly on the subjective analysis of satellite images. The geographical distribution of the detected MVs (Fig. 3.2) agrees well with the results of A88 (Fig. 1.2). The two major directions of movement of MVs around the center of Honshu Island, which are southeastward and east-northeastward (Fig. 3.3), also agree well with the results of Ookubo (1995). Thus, the tracking algorithm accurately reproduces the characteristics of the MVs that were derived from the subjective analysis of satellite images.

Previous objective tracking methods for PLs used the difference between SST and temperature at 500 hPa (T500; hereafter SST − T500 is referred to as T_{diff}) to discriminate between PLs and SDs (Zahn and von Storch 2008; Xia et al. 2012; Chen and von Storch 2012; Zappa et al. 2014; Y15). For example, Y15 used $T_{diff} > 43$ K as a

criterion for PLs. Figure 3.6 shows histograms of T_{diff} averaged over a 1° × 1° box around the center of a vortex at the time of its maximum intensity. In the plot, the MVs and SDs are identified using our algorithm. The SDs occur even if T_{diff} is small, whereas MVs tends to develop for large T_{diff}. Eighty percent of SDs develop for a T_{diff} less than 43 K, whereas more than half of the MVs occur when T_{diff} is greater than 43 K. Although our algorithm for identifying MVs is based solely on vorticity and SLP (and some of the large MVs can be categorized as synoptic-scale lows), the results are consistent with those obtained by previous methods that used the T_{diff} as the discriminating criterion. Moreover, since our method is independent of thermal stratification, it can deal with MVs that develop mainly as a result of dynamic instability including barotropic instability.

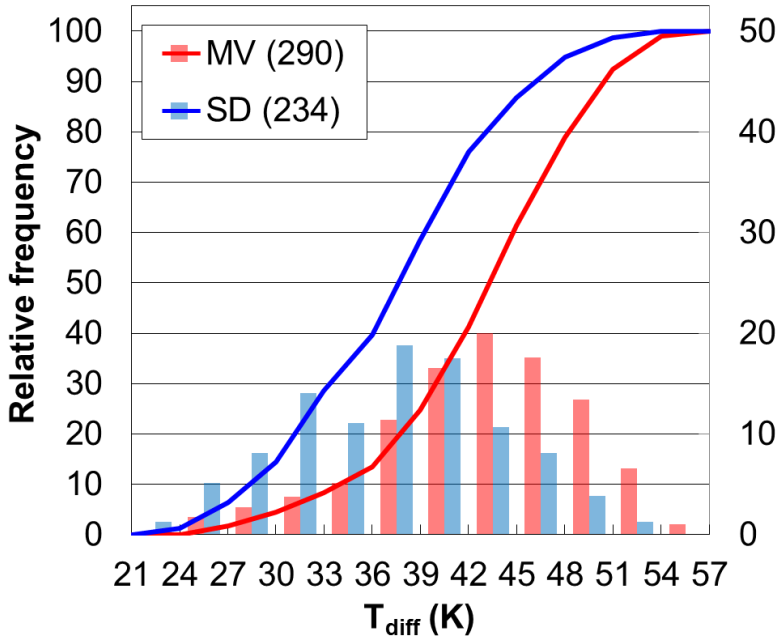

Fig. 3.6. Relative frequency (bars) and cumulative relative frequency (lines) of MVs and SDs for T_{diff}. The scales for the relative frequency and cumulative relative frequency are shown on the right and left axes, respectively.

Y15 studied PLs over the Sea of Japan. Since we analyzed MVs including meso-β-scale MVs and weaker MVs, several differences exist between our results and those of Y15. The number of MVs identified in this study is seven times (twice) as large as those for strong (weak) threshold identified in Y15. This is because our result includes meso-β-scale MVs. Moreover, our algorithm can identify and count individual MVs appearing simultaneously in a larger system. Note also that our algorithm identifies MVs in an environment with small T_{diff}, such as those developing through barotropic instability.

The geographical distribution and direction of movement of MVs are also different from Y15 with respect to several points. In the present study, a peak in the location of the maximum intensity is found near the base of the Korean Peninsula (Fig. 3.2b), which is indistinct in Y15 (see Fig. 8 in Y15). The MVs that develop in this region are so weak that most of them do not satisfy the intensity criterion in Y15. In the WJ-region, PLs in Y15 tend to move eastward (see fig. 7 in Y15), whereas we found that MVs tend to move southeastward (Fig. 3.3). Most of these MVs are at the meso-β-scale and are associated with the JPCZ. In the NJ-region, although both eastward-moving and southward-moving MVs were detected in the present study, the proportion of eastward-moving MVs in the present study (Fig. 3.3) is smaller than that in Y15. As southward-moving MVs are relatively small, some are likely to be excluded in Y15, while some of the eastward-moving MVs may be excluded as a synoptic-scale low by our algorithm.

3.4.2 Environment of MVs

The characteristics of MVs depend on environmental factors such as the

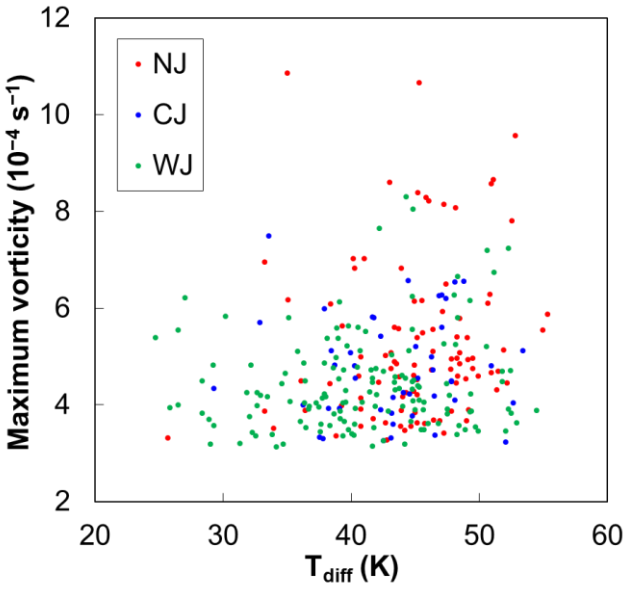

Fig. 3.7. Scatter plot of maximum vorticity and T_{diff} for MVs in each region.

baroclinicity and vertical stability of the atmosphere (Yanase and Niino 2007). Here, we examine the vertical stability of the atmosphere in which the MVs developed. Figure 3.7 shows a scatter plot of the maximum intensity represented by vorticity and T_{diff} averaged in a 1° × 1° box around the center of the MV for WJ, CJ and NJ. Although weak MVs are distributed across a wide range of T_{diff} values, the more intense MVs tend to occur in environments with a large T_{diff}. MVs in the WJ-region sometimes occur under less unstable conditions (T_{diff} < 35 K) although most of them are weak. Such MVs are formed by the horizontal shear in the JPCZ, but do not intensify further because the environment is not favorable to their development. In the NJ-region, intense MVs (i.e., maximum vorticity > 8.0×10^{-4} s^{-1}) tend to occur under highly unstable conditions (T_{diff} > 45 K). Very cold air (T500 < −40°C) frequently intrudes into this region, and this is favorable for the development of MVs. In the CJ-region, there is no obvious relationship between MV intensity and the vertical stability of the atmosphere, which

indicates that the diabatic contribution is likely to be less important for the development of the MVs in this region. This result, and the relatively large size of the MVs in this region, suggests that baroclinicity is likely to be important for the development of MVs in the CJ-region. Detailed mechanisms of development of MVs in each region will be discussed in chapter 4 and 5.

3.5 Conclusions

Statistical characteristics of MVs identified by the new tracking algorithm are examined. The average monthly frequency of MVs is largest in January. The tracks of MVs are concentrated in the western part of the Sea of Japan and to the west of Hokkaido Island. The geographical distribution of the MVs agrees well with previous studies based on satellite images during a relatively short period.

Our method for discriminating between MVs and SDs is solely based on the vorticity and pressure fields and is independent of the environmental condition such as stratification. Therefore, it is possible to deal with MVs that develop mainly through horizontal shear instability. Moreover, our results show that MVs tend to occur in more unstable environment, but SDs do not necessarily require unstable stratification. This gives a credit to the criteria based on T_{diff}, which was used by previous studies.

MVs are classified into three groups (NJ, CJ, and WJ) according to the region where they attained their maximum intensity. MVs in each region have different characteristics with regard to their direction of movement, size, and intensity. These characteristics are likely to be related to the environmental conditions at the time of formation and the developmental mechanism. In the following chapters, we will examine these points in more detail by composite analyses and numerical simulations.

4. Composite analysis on environments and structures of MVs

4.1 Introduction

A number of case studies have been made on the structures and development mechanisms of MVs over the Sea of Japan. Their results showed that the characteristics of the MVs widely vary from case to case. However, it is not easy to obtain a comprehensive understanding of the general characteristics of MVs only from these case studies. One of the important approaches to understand diversity and generality of MVs is to clarify the environments in which they are embedded and develop. Using a composite analysis, Yanase et al. (2015; hereafter Y15) showed typical environmental fields for the development of meso-α-scale PLs: e.g., an upper-level cold trough and a synoptic-scale low to the east of the MVs. However, they did not examine meso-β-scale MVs nor their environments in detail.

In this chapter, we perform composite analyses to examine the general characteristics of MVs including meso-β-scale vortices. First, MVs are classified into groups according to their location and direction of movement. Next, composite analyses are made for several groups of MVs that are often observed. Two kinds of composite are made for the synoptic-scale environment and the mesoscale structure, respectively. Using the composite, general characteristics of MVs and their environment are discussed.

4.2 Classification of MVs

As shown in chapter 3, the tracks of MVs are concentrated in several area of the Sea of Japan. MVs in each area have several typical directions of movement. Therefore, MVs are classified according to their location and direction of movement. First, MVs

are classified by the geographical distribution of their tracks: north eastern part of the Sea of Japan (NE), central part of the Sea of Japan (C), northwestern part of the Sea of Japan (NW), and southwestern part of the Sea of Japan (SW) (Fig. 4.1). MVs in each region are further classified according to the typical direction of movement. In NE area, MVs are classified into three groups (Fig. 4.2a-c): those moving southward and landing on Honshu Island (NE_s), those moving southward to the Ishikari Bay and landing on Hokkaido Island (NEI_s) and those moving eastward (NE_e). In C area, MVs dominantly move eastward (C_e) (Fig. 4.2f). In NW area, there are southeastward moving MVs (NW_se) and eastward moving MVs (NW_e) (Fig. 4.2d-e). In SW area, MVs reach their maximum intensity to the west of 134E (SW_W) (Fig. 4.2g) and east of 134E (SW_E) (not shown).

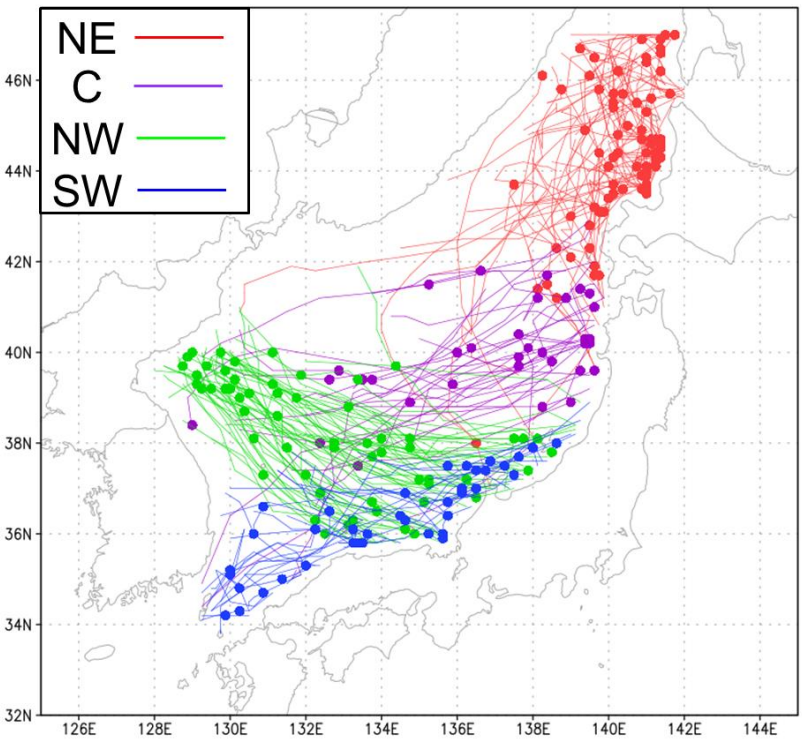

Fig. 4.1 Tracks of MVs classified by their geographical distribution. Red, purple green and blue lines indicate the tracks of NE, C, NW, and SW MVs, respectively. Dots indicate the location where MVs reach their maximum intensity.

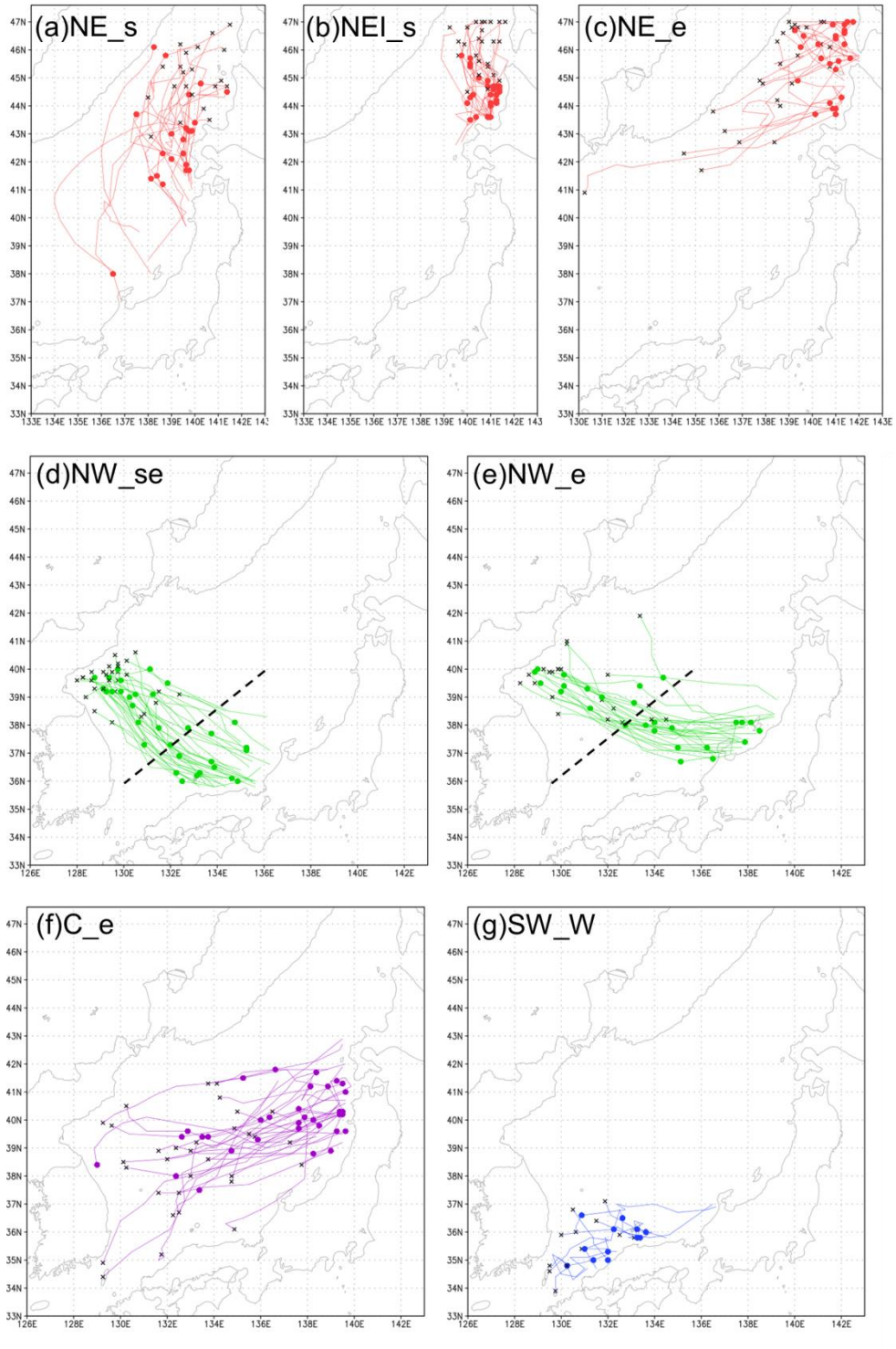

Fig. 4.2 Tracks of (a) NE_s, (b) NEI_s, (c) NE_e, (d) NW_se, (e) NW_e, (f) C_e, and (g) SW_W MVs. Dots indicate the locations where MVs reach their maximum intensity and black crosses indicate the locations of generation of MV. The KTs for NW_se and NW_e are is defined by the time when MVs are closest to dashed line in (d) and (e), respectively.

4.3 Data and methodology

MANAL and Global Analysis (GANAL) provided by JMA are used (Japan Meteorological Agency 2013) for the composite analyses. Note that GANAL and MANAL are made by data assimilation using Global Spectral Model (GSM) and Meso-Scale Model (MSM) of JMA, respectively, where GANAL is used as an outer boundary conditions for MANAL. The composite of GANAL and MANAL represent the synoptic-scale environment and the mesoscale structure of MVs, respectively.

A key time (KT) for each MV is defined by the time when it is closest to a particular location or when it reaches its maximum intensity. Lag composite fields at t=+x (−x) hour are calculated by superposing meteorological elements x hour prior to (after) the KT in a geographically fixed coordinate for each group of MVs. Following Y15, we separate the total composite field into a mean field and an anomaly field. The mean field is defined by an average between −7 day and + 7 day, and the anomaly field by deviation of the composite field from the mean field. We also define a climatological winter mean by an average between November and March for six years.

4.4 MVs in NE area

It has been shown in section 4.2 that the MVs in NE area are classified into three groups: NE_s, NEI_s and NE_e. Figure 4.3 shows examples of MVs in NE_s (Fig. 4.3a), NEI_s (Fig. 4.3b), and NE_e (4.3c). During the six cold seasons, 22, 28 and 27 MVs are categorized into NE_s, NEI_s and NE_e, respectively. The environments and structures of MVs in each group are studied in detail in this subsection.

4.4.1 MVs moving southward (NE_s)

MVs in NE_s (Fig. 4.2a) were generated to the west and northwest of Hokkaido Island, moved southwestward at the beginning and then they changed their direction of motion to southeastward. Finally they landed on Honshu Island and dissipated. Most of them reached their maximum intensity at around 43°N. Therefore the reference time KT for NE_s is defined by the time when MVs are closest to 43°N.

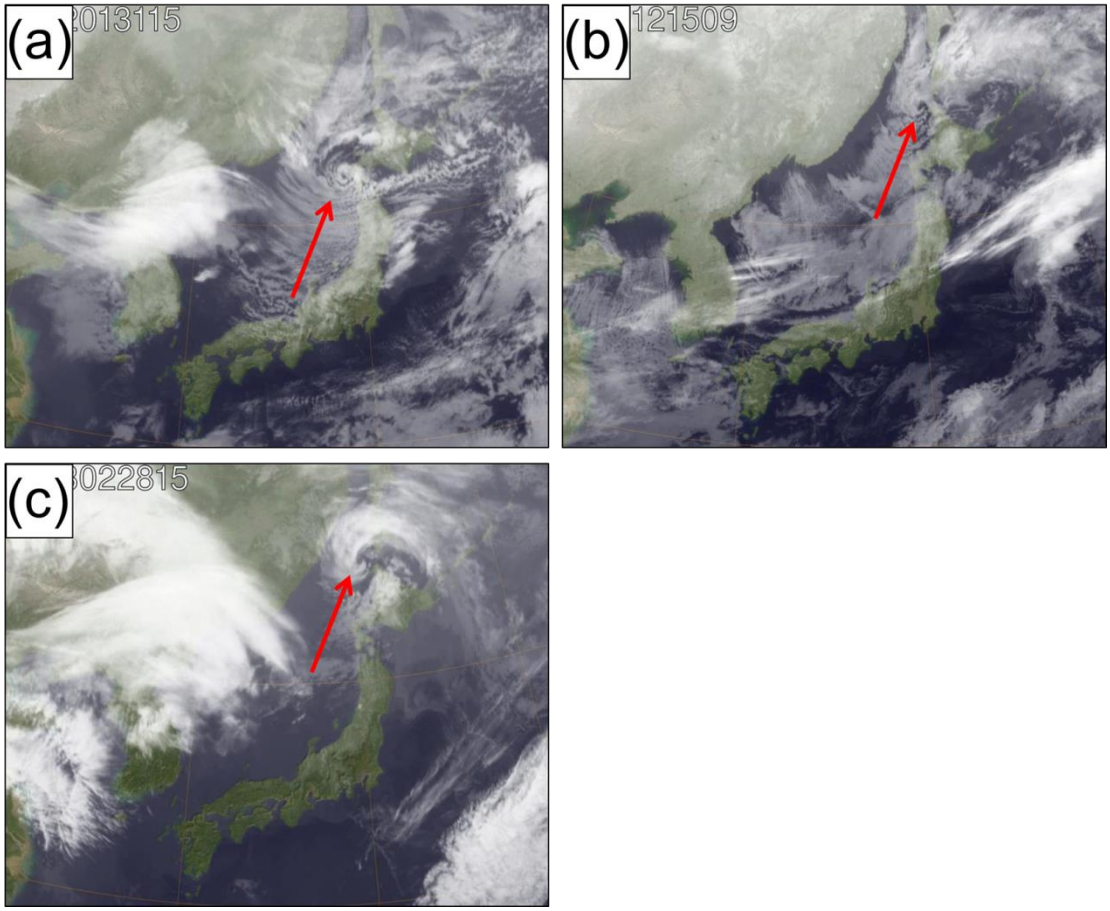

Fig. 4.3 Satellite images of the MVs. (a) NE_s, (b) NEI_s, and (c) NE_e. An arrow in each panel indicates the MV.

We first examine synoptic-scale environment of the MVs using a composite of GANAL. Figure 4.4 shows the total and anomaly fields of sea level pressure (SLP) and

the total field of horizontal wind at 850 hPa from −48 hour to +24 hour. Throughout this period, a high pressure system over the Siberia (the Siberian High) and a low pressure system over the North Pacific Ocean (the Aleutian Low) are distinct. This pressure pattern is typical when the East Asian winter monsoon prevails over the Sea of Japan, and is also seen in the climatological mean field (not shown). However, the Aleutian Low at −48 and −24 hour is located further south than that in the climatological mean (Fig. 4.4a and 4.4b).

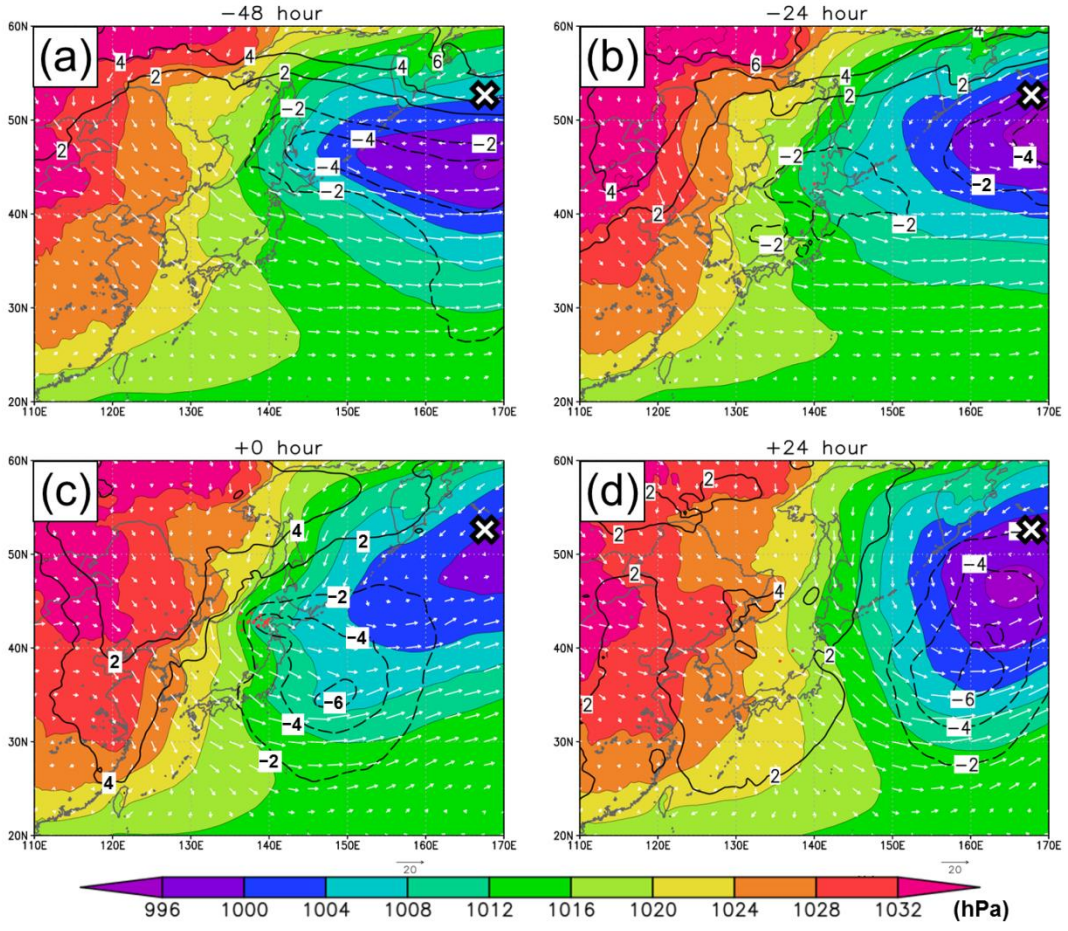

Fig. 4.4 GANAL composite of the total fields of SLP (color; hPa) and horizontal wind at 850 hPa (vector; m s^{-1}) and the anomaly field of SLP (contour; the contour interval is 2 hPa and the contours for negative values are depicted by dashed lines.) for NE_s: (a) −48 hour, (b) −24 hour, (c) 0 hour, and (d) +24 hour. The white cross the location of the center of the Aleutian Low in the climatological mean. Red dots indicate the location of MVs.

In the anomaly field, the synoptic-scale environment is more obvious. At −48 hour a negative SLP anomaly extends from the Aleutian Low to the northeast of Hokkaido Island (Fig. 4.4a). The western part of this anomaly corresponds to the preceding extratropical cyclone and it advances to further east at −24 hour (Fig. 4.4b). A positive SLP anomaly is seen to the north of the negative SLP anomaly. Since this pattern causes easterly component of wind between negative and positive SLP anomalies, northeasterly wind exists to the northwest of Hokkaido Island in the total field (Fig. 4.4a-b). Note that the wind direction at the west of Hokkaido Island changes from northeasterly to northwesterly as the latitude decreases (Fig. 4.4a-c). MVs appear and develop in this cyclonic flow by 0 hour (Fig. 4.4b-c). At the same time, a new synoptic-scale low gradually develops over the Pacific Ocean to the east of Japan and the MVs are located in the northwest quadrant of the synoptic-scale low (Fig. 4.4c). The synoptic-scale low continues to develop over the Pacific Ocean after the MVs land on Honshu Island and dissipate (Fig. 4.4d).

The synoptic-scale SLP pattern causes a typical temperature pattern in the lower atmosphere. Figure 4.5 shows the total and anomaly fields of temperature and the total field of horizontal wind at 850 hPa from −48 hour to +24 hour. Before the MVs appear, the easterly associated with the preceding synoptic-scale low advects warm air to the Sea of Okhotsk and a warm anomaly forms there, while the northwesterly advects cold air from Asian Continent over the Sea of Japan and a cold anomaly exist to the southwest of Hokkaido Island (Fig. 4.5a-b). This results in a zonal temperature gradient between the west of Hokkaido Island and Kuril Island, where the temperature increases eastward. The cold air intrudes further to the east and the MVs appear and develop at the boundary between the warm and cold anomalies (Fig. 4.5b-c). By + 24 hour, the

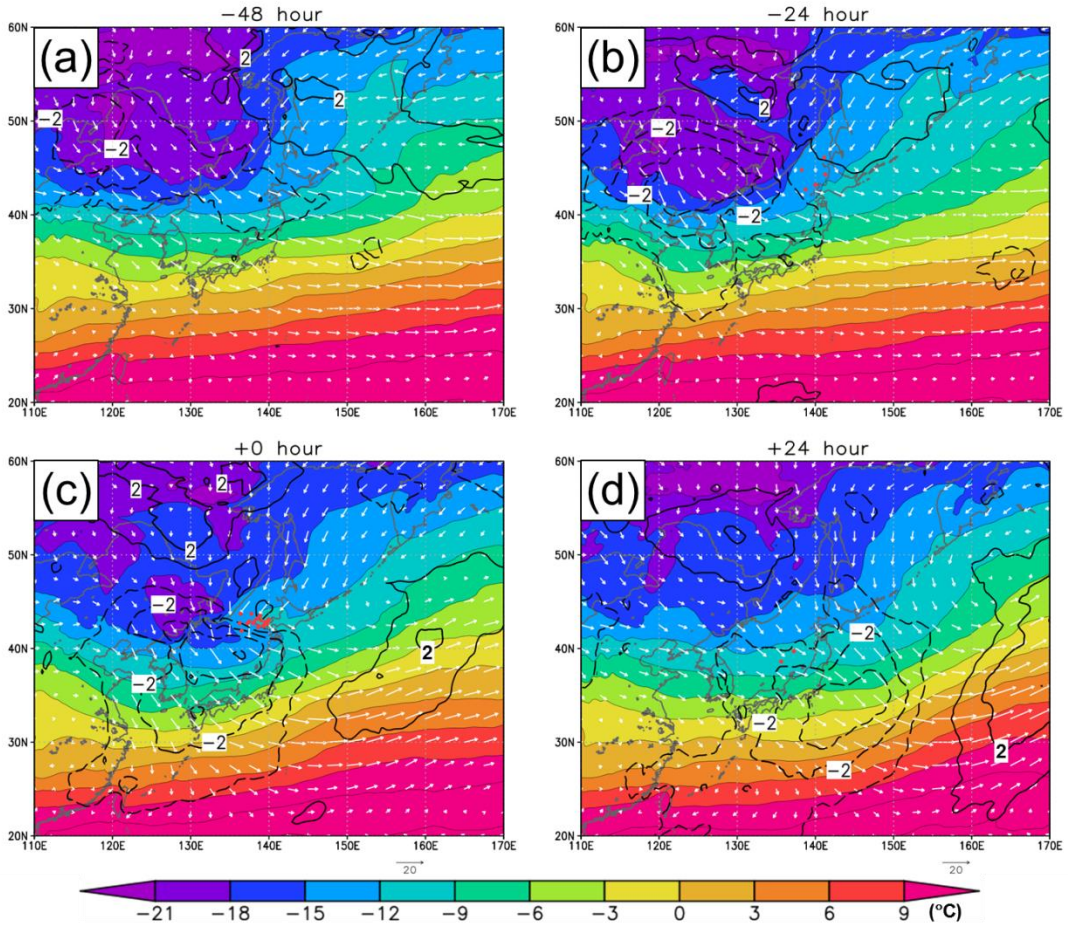

Fig. 4.5 GANAL composite of the total field of temperature (color; °C) and horizontal wind at 850 hPa (vector; m s^{-1}) and the anomaly field of temperature (contour; the contour interval is 1 °C and the contours for negative values are depicted by dashed lines.) at 850 hPa for NE_s. (a) −48 hour, (b) −24 hour, (c) 0 hour, and (d) +24 hour. Red dots indicate the location of MVs.

center of the cold anomaly moves over the Pacific Ocean (Fig. 4.5d).

The upper-level environment is characterized by a cold vortex moving eastward (Fig. 4.6). At −48 hour, a negative height anomaly and positive vorticity at 500hPa exist above the northern part of the Japanese Islands (Fig. 4.6a and 4.6b). They are related to the preceding extratropical cyclone. At −24 hour, another cold vortex appears over the eastern part of the Asian continent (Fig. 4.6c and 4.6d) and moves eastward. As the cold vortex approaches the northeastern part of the Sea of Japan, the MVs are generated and

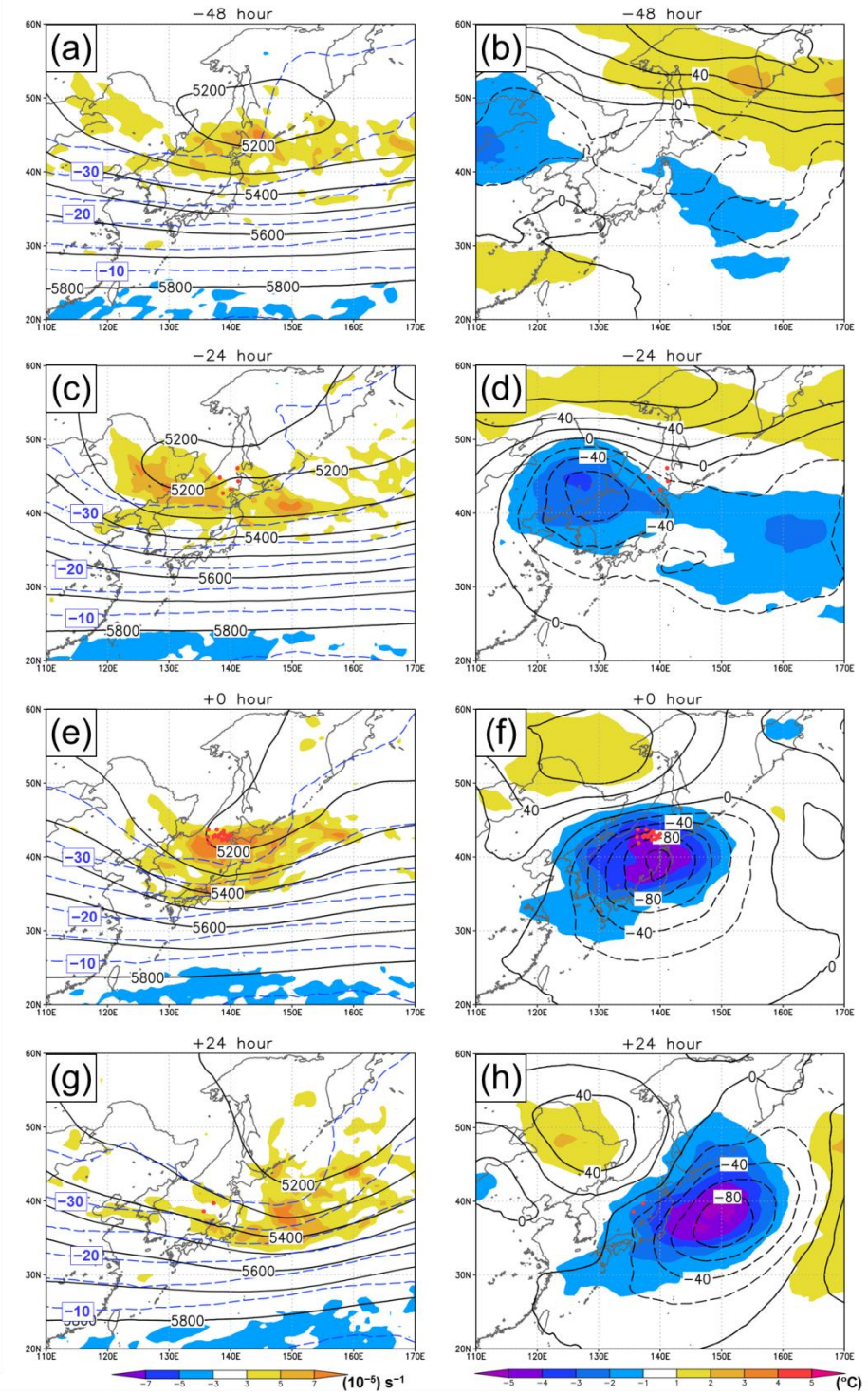

Fig. 4.6 GANAL composite of total fields of vorticity (color; 10^{-5} s^{-1}), geopotential height (black solid contour; the contour interval is 100 m), and temperature (blue contour; the contour interval is 5 °C) at 500 hPa (left column) and anomaly fields of temperature (color; °C) and geopotential height at 500 hPa (contour; the contour interval is 20m) (right column) for NE_s: (a), (b) −48 hour, (c), (d) −24 hour, (e), (f) 0 hour, and (g), (h) +24 hour. Red dots indicate the location of MVs.

develop beneath the cold vortex (Fig. 4.6e and 4.6f). Note that the MVs are located slightly north of the center of the upper-level positive vorticity. The cold vortex continues to march eastward and finally moves over the Pacific Ocean (Fig. 4.6g and 4.6 h).

Next, we examine the mesoscale environment and structure of NE_s using the composite of MANAL. Figure 4.7 shows the total field of SLP, temperature and horizontal wind at 850 hPa. A surface trough extending westward from east and a zonal temperature gradient are evident to the west of Hokkaido Island at −24 hour (Fig. 4.7a). A region of warm air gradually develops to the west of Hokkaido Island in the following 24 hours. At 0 hour (Fig.4.7b), a low pressure area associated with the MVs is collocated with the warm region. At the same time, cold advection intensifies to the south of the warm region. Consequently, the contours of the temperature show marked westward protuberance.

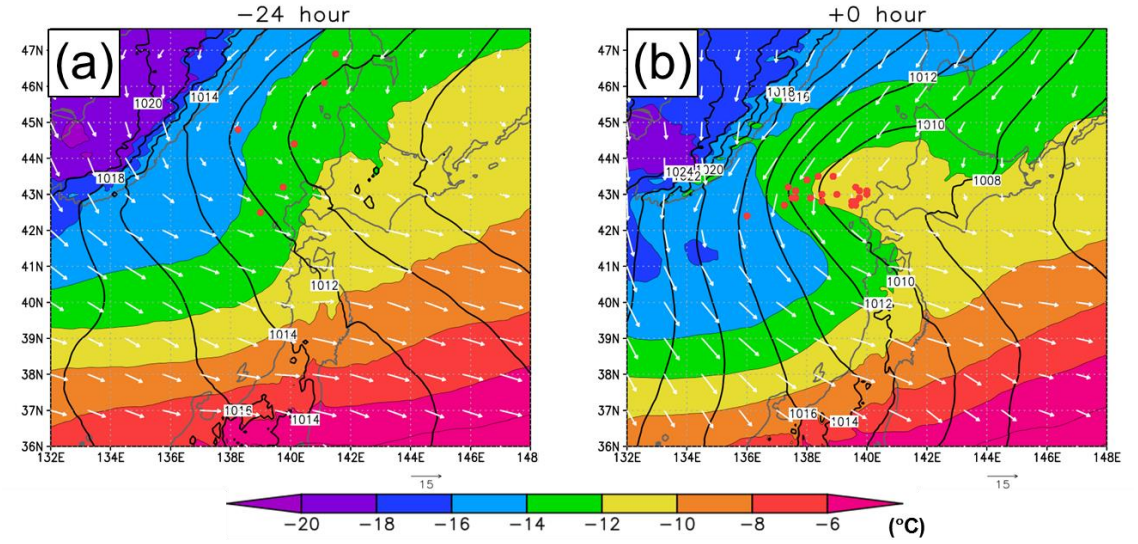

Fig. 4.7 MANAL composite of total field of temperature (color; °C), horizontal wind at 850 hPa (vector; m s^{-1}), and SLP (contour; the contour interval is 2 hPa) for NE_s. (a) −24 hour and (b) 0 hour. Red dots indicate the location of MVs.

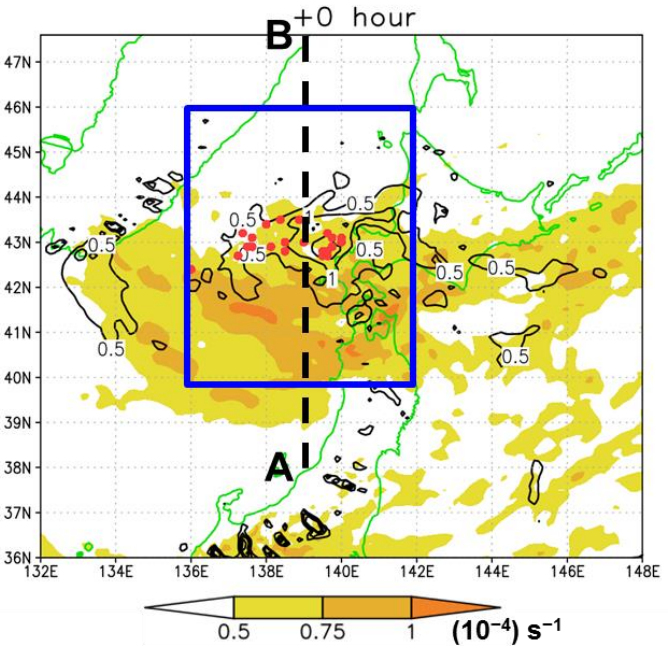

Fig. 4.8 MANAL composite of total fields of vorticity at 500 hPa (color; 10^{-4} s^{-1}) and 850 hPa (contour; the contour interval is 0.5×10^{-4} s^{-1}), respectively, for NE_s at 0 hour.v Red dots indicate the location of MVs.

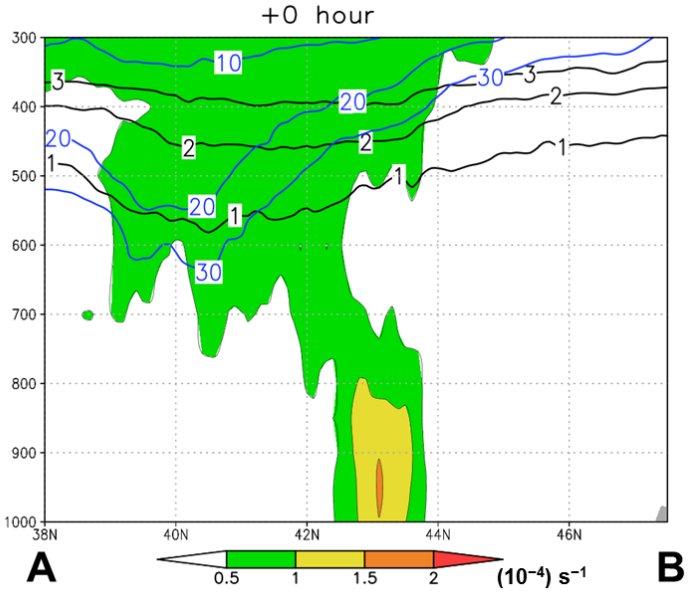

Fig. 4.9 MANAL composite of total field of potential vorticity (black contour; PVU), vorticity (color; 10^{-4} s^{-1}) and relative humidity (blue contour; %) along AB line in Fig. 4.8. Only the contours of relative humidity less than 30 % are drawn.

At the upper-level, a meso-α-scale region of positive vorticity passes slightly south of the MVs (Fig. 4.8). In the meridional-vertical cross section along A-B line in Fig. 4.8, a positive PV anomaly accompanied by dry air intrudes into 600 hPa to the south of the low-level MVs, and the region with vorticity exceeding 0.5×10^{-4} s^{-1} tilts southward with height from the surface to the upper-level (Fig. 4.9). The hodograph of the wind surrounding the MVs (Fig. 4.10) shows a meridional shear, where the northerly wind decreases with height. This is a reverse shear condition, which is often found when MVs develop (e.g. Kolstad 2006). These structures of MVs and their environments imply a baroclinic development of the MVs.

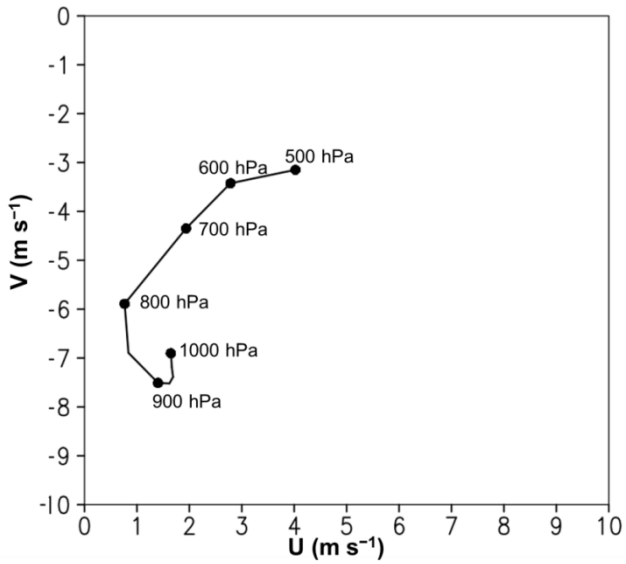

Fig. 4.10 MANAL composite of hodograph of the total wind field averaged in the blue box in Fig. 4.8.

A cold air at the upper-level is also a characteristic feature associated with the MVs development. Since the core of the cold air passes right above the developing MVs (Fig. 4.11a) and there is a warm region around MVs at the low-level (Fig. 4.7c), the stability of the atmosphere decreases around the MVs (Fig. 4.11b). The less stable stratification

makes the effect of the upper-level forcing larger at the low-level. In this less stable atmosphere, updrafts are also evident around the MVs. The updrafts are strongest at the low-level around 850 hPa (not shown), which implies that these updrafts are associated with cumulus heating. Thus, the development of MVs is likely to be also related to cumulus convection.

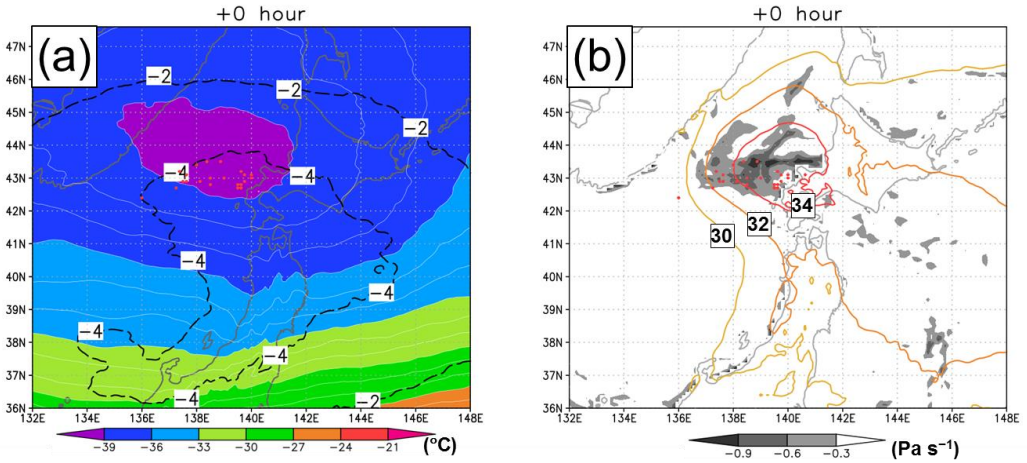

Fig. 4.11 (a) MANAL composite of the total field of temperature (color; °C) at 500 hPa and the anomaly field of temperature (contour; °C) at 500 hPa at 0 hour for NE_s. (b) MANAL composite of the total field of the temperature difference between 950 hPa and 500 hPa (contour; °C) and vertical p-velocity at 850 hPa (shaded; Pa s^{-1}). The vertical p-velocity is drawn only over the sea. Red dots indicate the location of MVs.

The characteristics of NE_s are summarized as follows: Prior to the generation of the MVs, the synoptic-scale systems provide favorable conditions including zonal temperature gradient and a cyclonic flow at the low-level to the west of Hokkaido Island. The MVs are generated and develop when an upper-level trough accompanied by a cold air approaches this area. The MVs have a southward-tilting structure in a reverse shear and are suggested to develop through baroclinicity. The MVs are also accompanied by cumulus convection.

4.4.2 MVs moving southward and approaching Ishikari Bay (NEI_s)

MVs in NEI_s (Fig. 4.2b) are generated to the west and northwest of Hokkaido Island and move southward or southeastward toward the Ishikari Bay. They eventually land on Hokkaido Island and dissipate. The locations where they reach their maximum intensity are concentrated in the Ishikari Bay. Therefore the KT for NEI_s is defined as the time when the MVs reach their maximum intensity.

The overall synoptic-scale and mesoscale environment and structure of NEI_s are similar to those of NE_s. Therefore the development mechanism is considered to be also similar, and we will not repeat similar figures to Figs. 4-11. However, there exist several differences in the synoptic environment that cause the difference of the location and path of the MVs: The location of the Aleutian Low and the paths of the upper-level cold trough and surface synoptic-scale low in the composite of NEI_s differ from those of NE_s (Fig. 4.12). The Aleutian Low in the total field for the NEI_s are located almost at the same position as climatological mean, so that the horizontal wind to the west of Hokkaido Island has more eastward component than that of NE_s. The path of the upper-level trough in NEI_s is located further north than that of NE_s, so that the locations of the MVs shift northward. The surface cyclone in NEI_s is also located to the north of that in NE_s. Note that the MVs of NEI_s are located to the west of the synoptic-scale low, whereas the MVs of NE_s to the northwest of the surface synoptic-scale low.

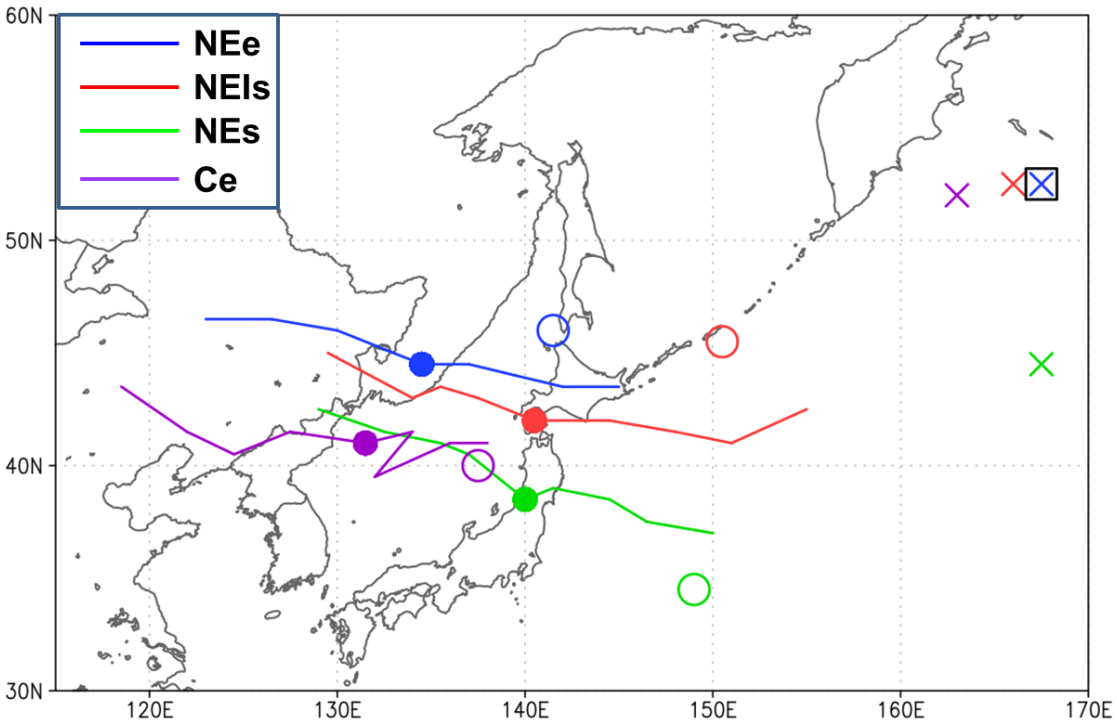

Fig. 4.12 Tracks of minimum of geopotential height anomaly at 500 hPa from −24 hour to + 24 hour for the GANAL composite of NE_e (blue), NEI_s (red), NE_s (green), and C_e (purple). The closed circles are locations of the minimum of geopotential height anomaly at 500 hPa at 0 hour. The open circles are locations of the minimum of SLP anomaly at 0 hour. The crosses are the locations of the Aleutian Low at −48 hour. The open square is the location of the Aleutian Low in the climatological mean field.

4.4.3 MVs moving eastward (NE_e)

MVs in NE_e (Fig. 4.2c) are initiated at the northern part of the Sea of Japan and move eastward. Although the area of analysis in the present study is restricted within the Sea of Japan, some of the MVs continue to move over the Pacific Ocean. The KT for NE_e is defined by the time when the MVs reach their maximum intensity.

In the synoptic-scale anomaly field of the SLP, weak negative and positive anomalies are seen at the west and east of Japan, respectively, at −48 hour (Fig. 4.13a) This anomaly pattern weakens zonal gradient of SLP and also the northwesterly winter

Asian monsoon. The two anomalies of SLP move eastward during the following 48 hours (Fig. 4.13b-c). At 0 hour, the MVs are located in the low pressure area to the northwest of Hokkaido Island (Fig. 4.13c). In contrast to NE_s, the MVs are almost collocated with the center of the negative SLP anomaly. Unfortunately, the tracks of the MVs over the Pacific Ocean are not examined. However, the negative SLP anomaly to the northeast of Hokkaido Island at +24 hours indicates that the MVs continue to move eastward and develop further over the Pacific Ocean (Fig. 4.13d).

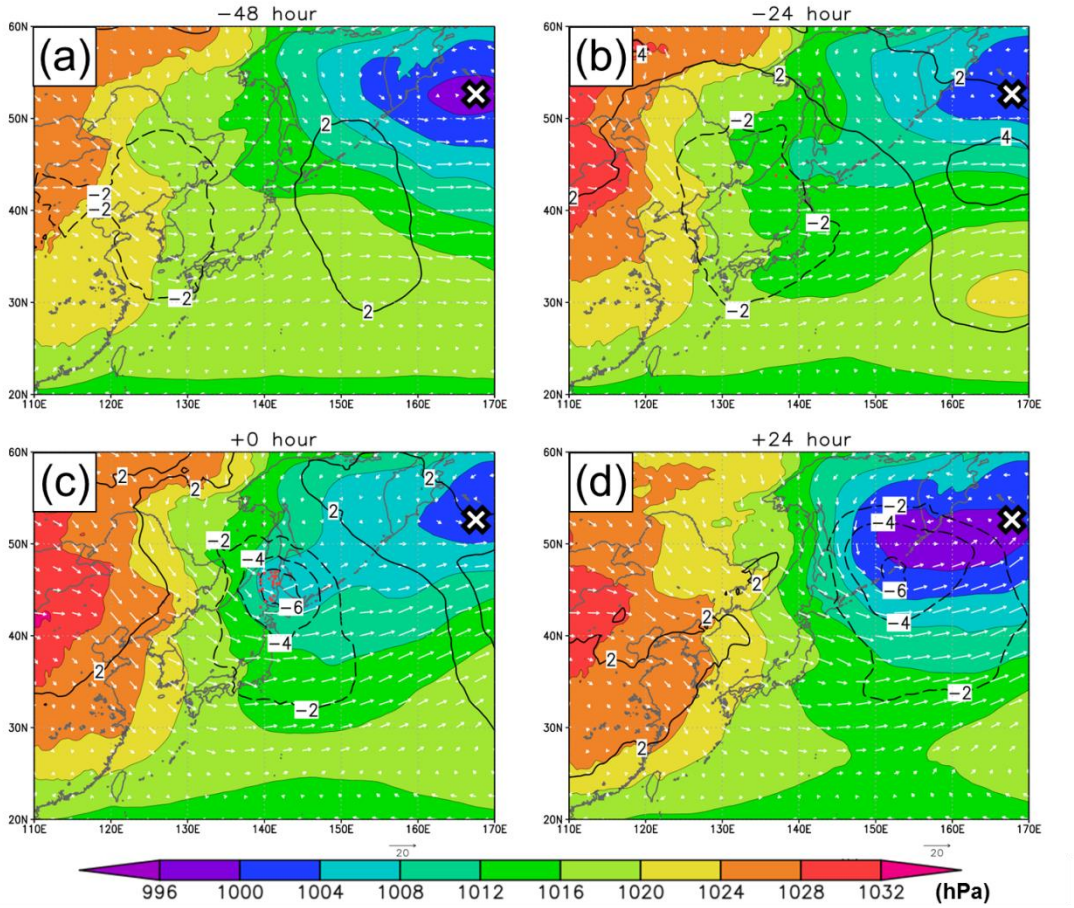

Fig. 4.13 As for Fig. 4.4 except for NE_e.

In the large-scale temperature field, a broad baroclinic zone with meridional temperature gradient is evident over the Japanese Islands (Fig. 4.14a). Since the cold air

outbreak has not started before −24 hour, the low-level atmosphere over the Sea of Japan is warmer than mean field and the cold airmass remains over the Asian Continent (Fig. 4.14a-b). Consequently, the contours of temperature at 850 hPa in the total field extend in almost zonal direction around Hokkaido Island before the MVs are generated (Fig. 4.14a-b). Thus, the structure of temperature at the low-level before the MVs of NE_e appear is quite different from those of NE_s and NEI_s. At 0 hour, synoptic-scale cold and warm anomalies form to the west and east of the Japanese Island, respectively, due to horizontal temperature advection (Fig. 4.14c). The MVs are located in between the cold and warm anomalies. These systems continue to move eastward at +24 hour (Fig. 4.14d).

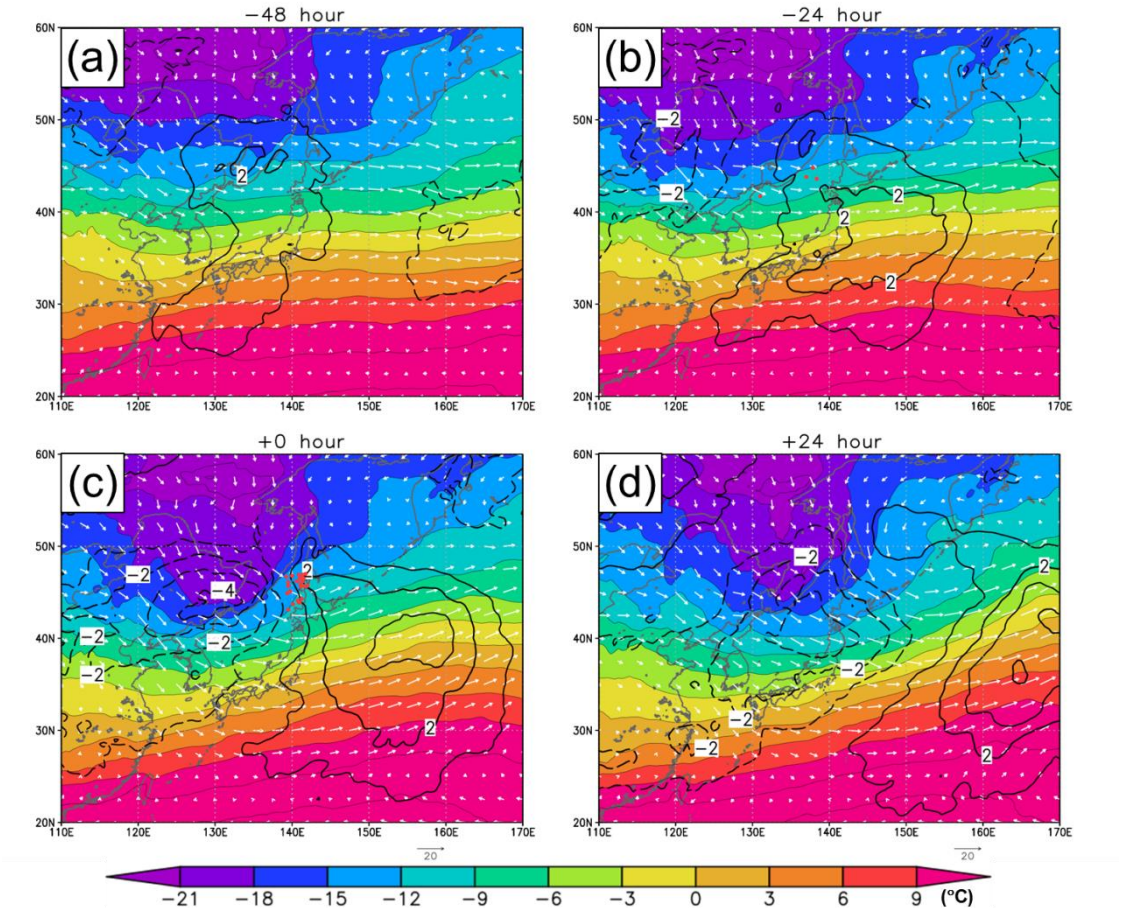

Fig. 4.14 As for Fig. 4.5 except for NE_e.

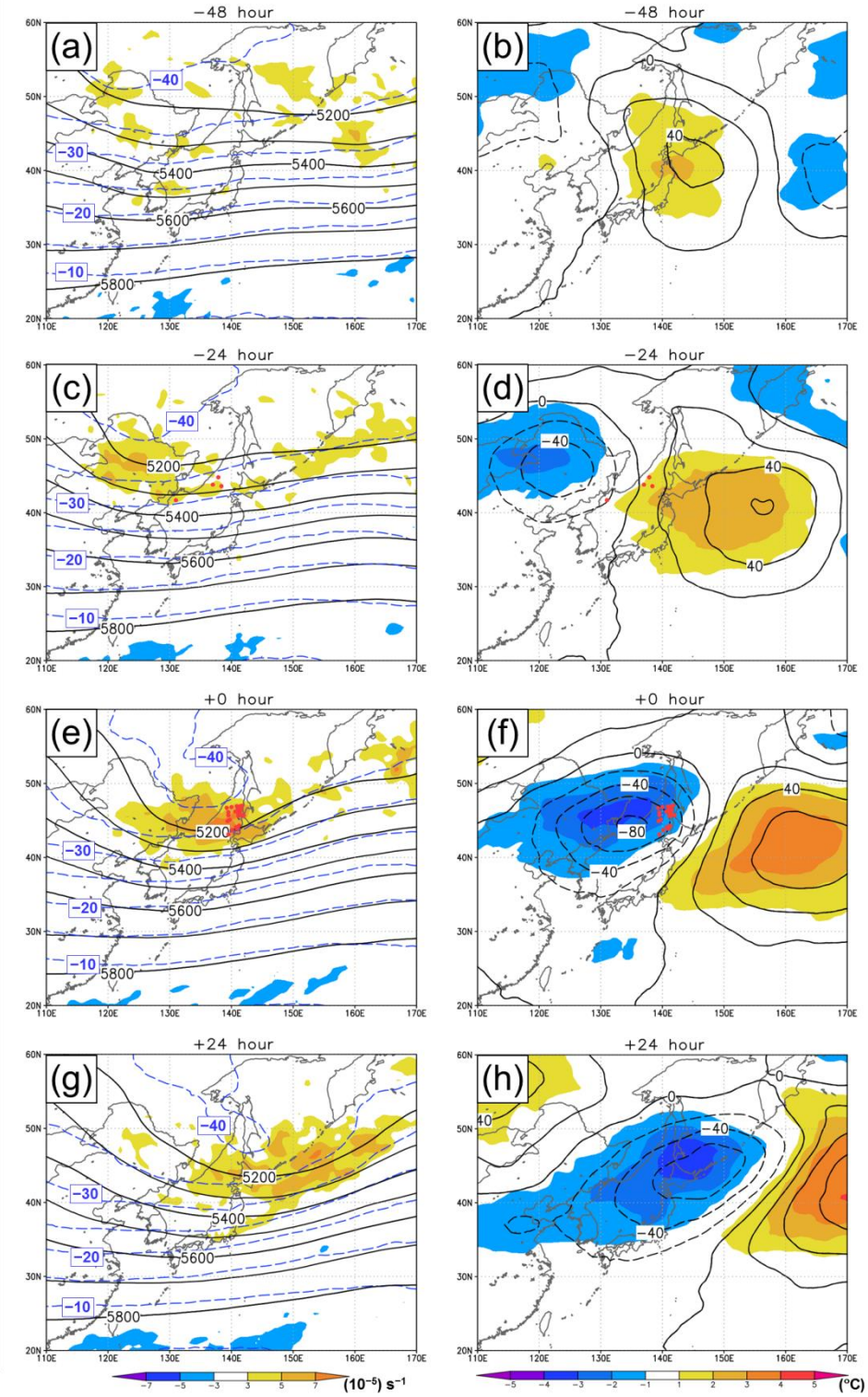

Fig. 4.15 As for Fig. 4.6 except for NE_e.

A pressure pattern associated with mid-latitude baroclinic wave is evident in the upper-level (Fig. 4.15). A ridge is located above Japan, whereas a trough accompanied by a region of positive vorticity exists over the Asian Continent at −48 hour (Fig. 4.15a). A cold air follows the west side of the trough (Fig. 4.15b). The trough and ridge move eastward as they become more developed (Fig. 4.15c and 4.15d). The center of the negative height anomaly passes over Hokkaido Island (Fig. 4.12). At 0 hour, the center of the negative height anomaly is located to the west of the SLP anomaly (Fig. 4.12 and 4.13c). Thus, the MVs develop to the east of the upper-level cold trough (Fig. 4.15e and 4.15f). Finally, the trough moves over the Pacific Ocean (Fig. 4.15g and 4.15h).

Next, we examine the mesoscale environment and structure of NE_e. Figure 4.16 shows the total fields of SLP, and temperature and horizontal wind at 850 hPa. As seen in the composite of GANAL, meridional temperature gradient is evident to the west of Hokkaido Island at −24 hour (Fig. 4.16a). The MVs gradually develop during the following 24 hours. At 0 hour, the MVs are collocated with the SLP minimum (Fig. 4.16b). The zonal pressure gradient increases and cold advection intensifies to the west of the MVs, whereas southwesterly advects warm air to the east of the MVs. This temperature structure is similar to extratropical cyclones.

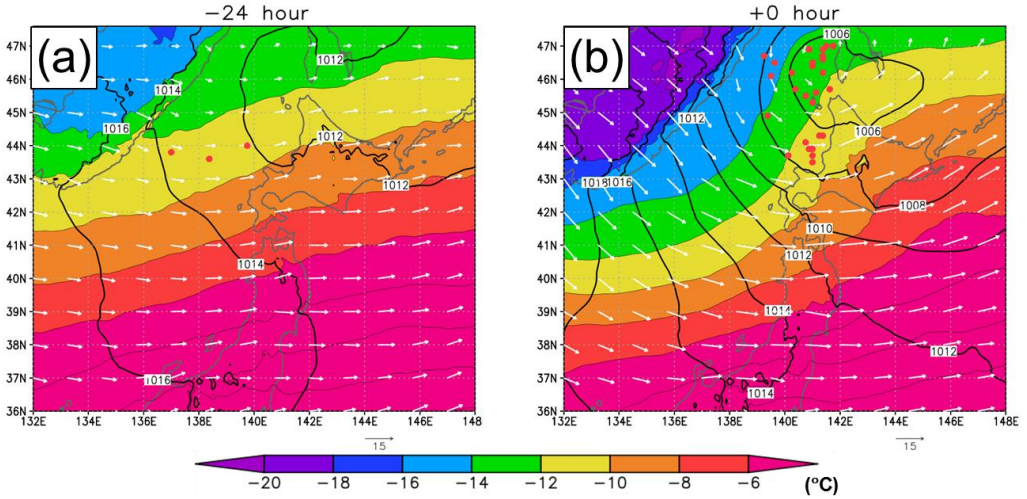

Fig. 4.16 As for Fig. 4.7 except for NE_e.

At the upper-level, positive vorticity anomaly exists to the west of the MVs (Fig. 4.17). In the zonal-vertical cross section along A-B line in Fig. 4.17, a positive PV anomaly accompanied by dry air intrudes into 550 hPa to the west of the low-level MVs (Fig. 4.18). The hodograph of the wind surrounding the MVs show a strong zonal shear, where the westerly wind increases with height (Fig.4.19). This is a forward shear condition where the direction of thermal wind is parallel to the wind at the steering level. The configuration of vorticity disturbances at the upper- and lower-levels is favorable for a baroclinic development associated with the zonal shear.

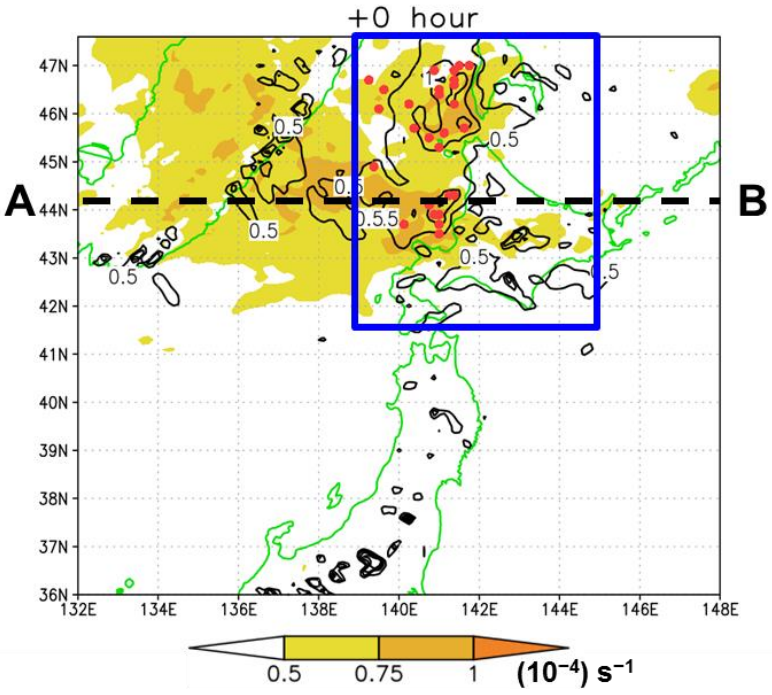

Fig. 4.17 As for Fig. 4.8 except for NE_e.

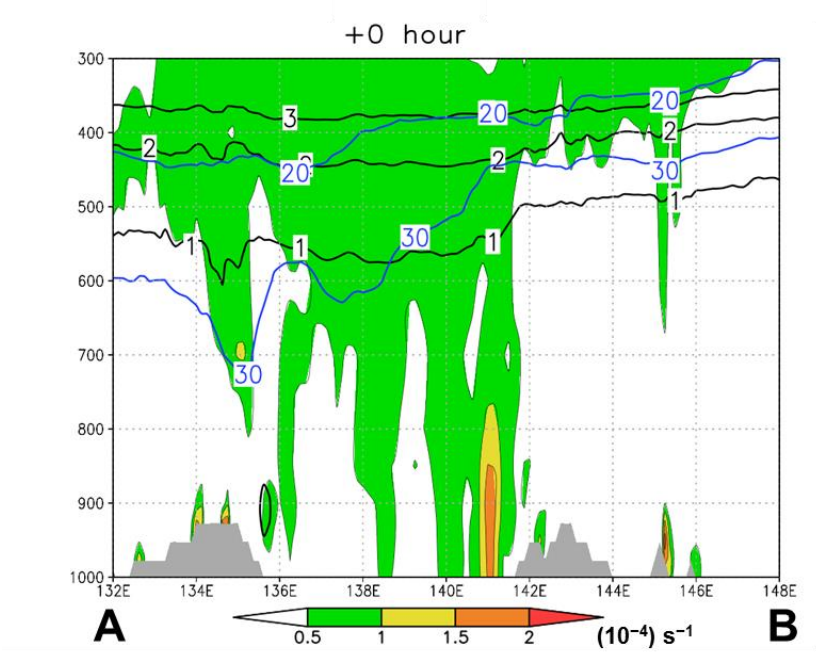

Fig. 4.18 As for Fig. 4.9 except for the vertical cross section along the AB line in Fig. 4.17. The gray shade near the surface indicates the topography.

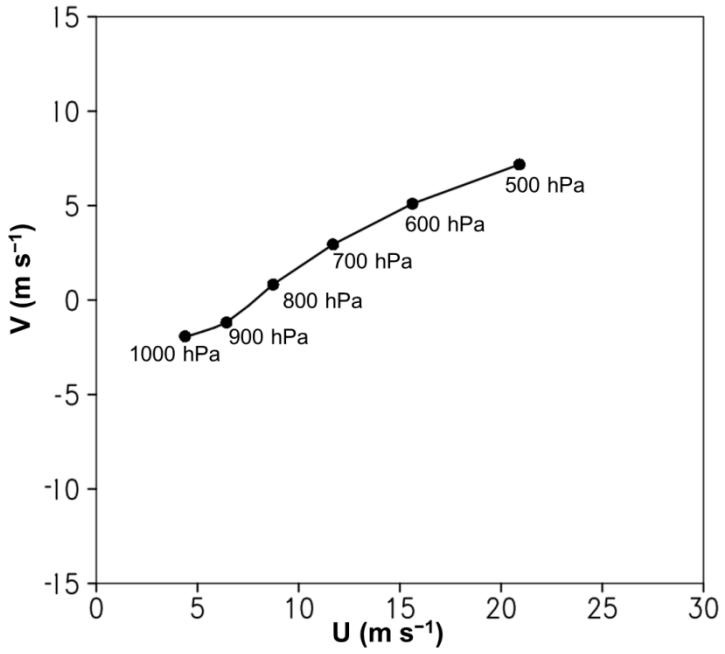

Fig. 4.19 MANAL composite of hodograph of the total wind field averaged in the blue box in Fig. 4.17.

In contrast to NE_s, the core of the upper-level cold air in NE_e passes north of the MVs (Fig. 4.20a) and consequently the stratification is more stable than NE_s (Fig. 4.20b). Although the updraft in the composite field is indistinct because of rather scattered distribution of the MVs (Fig. 4.20b), most of the MVs in NE_e are also accompanied by cumulus convection. The dynamic updrafts induced at the forward side of an advancing upper-level positive vorticity are considered to provide a favorable condition for cumulus convection.

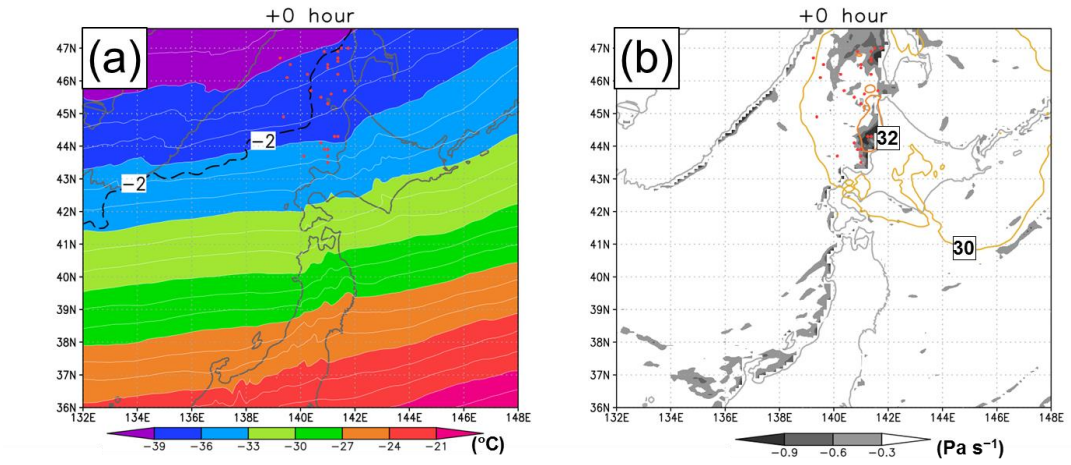

Fig. 4.20 As for Fig. 4.11 except for NE_e.

The characteristics of NE_e are summarized as follows. Prior to the generation of the MVs, a broad baroclinic zone with meridional temperature gradient exists around the Japanese Islands including the northern part of the Sea of Japan. The MVs are generated and develop to the east of an upper-level trough accompanied by a cold air that passes over Hokkaido Island. While the structure and environment of NE_e implies a baroclinic development, the MVs are also accompanied by cumulus convection. The MVs in NE_e resemble ordinary extratropical cyclones except that their horizontal scale is smaller.

4.4.4 Discussion

The MVs in NE area have two dominant direction of movement: southward and eastward. Y15 showed that the PLs moving southward appear in a reverse shear condition, whereas PLs moving eastward appear in a forward shear condition. Our results confirm that this feature is unchanged even if meso-β-scale MVs are included. Note that Terpstra (2014) showed PLs over the Nordic Sea in forward and reverse shear conditions have similar characteristics.

Tsuboki and Wakahama (1992) showed that there are two kinds of southward-moving MVs to the west of Hokkaido Island: Type I that has a horizontal scale of 200-300 km and Type II that has a horizontal scale of 500-700 km. Type I moves southward, whereas Type II moves south-southwestward at first and then changes its moving direction to south-southeastward. The movements of the MVs in the present study suggest that Type I and Type II correspond to NEI_s and NE_s, respectively. By a linear stability analysis of a "quasi-geostrophic" flow for the wind profile observed by rawinsonde at Wakkanai (45.42°N, 141.68°E), they found two kinds of unstable modes (Mode I and Mode II): Mode I is associated with zonal temperature gradient, while Mode II is associated with meridional temperature gradient. They insisted that Mode I and Mode II correspond to Type I and Type II, respectively. In the present study, however, both NEI_s and NE_s are associated with zonal temperature gradient. This difference is likely to be due to the location of the rawinsonde station. They use the rawinsonde data at Wakkanai, which is located at the northern edge of Hokkaido Island. In fact, the zonal temperature gradient is indistinct even in the composite for NE_s (Fig. 4.7a-b). Moreover, Mode II in Tsuboki and Wakahama (1992), which is associated with zonal temperature gradient, may correspond to NE_e.

4.5 MVs in C area

4.5.1 MVs moving eastward (C_e)

In C area, MVs dominantly move eastward (C_e) (Fig. 4.2f). During the six cold seasons, 26 MVs are categorized into C_e. The characteristics of C_e are nearly similar to those of NE_e. Therefore the development mechanism seems to be also similar. The distinct difference from NE_e is that the upper-level trough passes southward compared with that in NE_e (Fig. 4.12). Consequently, the MVs develop over the central part of the Sea of Japan. Note that some MVs in C_e are meso-α-scale extratropical cyclones accompanied by cold and warm fronts.

4.6 MVs in NW area

MVs in NW area are classified into two groups: NW_se and NW_e. Figure 4.21 shows examples of MVs in NW_se (Fig. 4.21a) and NW_e (Fig. 4.21b). During the six cold seasons, 35 and 27 MVs are categorized into NW_se and NW_e, respectively. The environment and structure of the MVs in each group are studied in detail in this subsection.

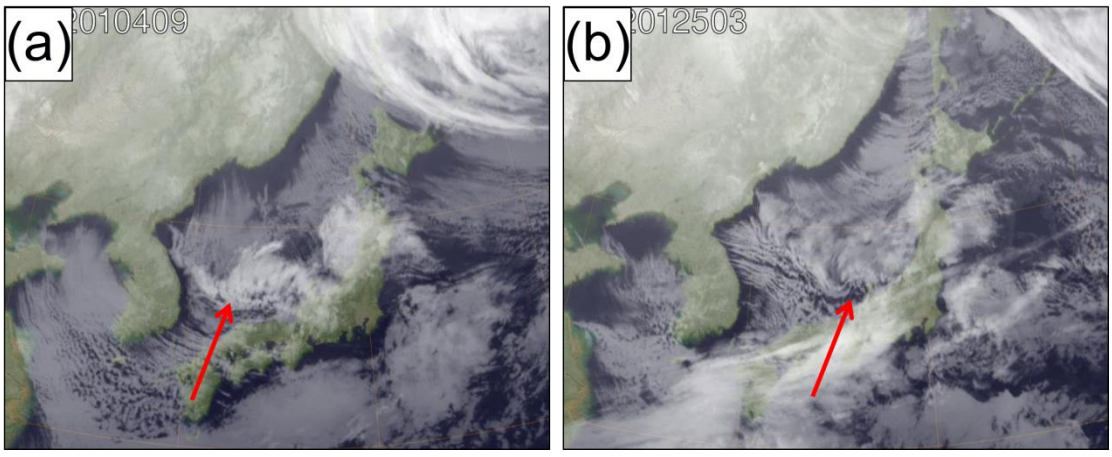

Fig. 4.21 (a) Satellite images of MVs (a) NW_se and (b) NW_e. An arrow in each panel indicates the MV.

4.6.1 MVs moving southeastward (NW_se)

MVs in NW_se (Fig. 4.2d) formed over the northwestern part of the Sea of Japan, moved southeastward and landed on Honshu Island. The KT for NW_se is defined by the time when MVs are closest to dashed line in Fig. 4.2d, which crosses the tracks of the MVs near their intermediate points at almost right angles.

We first examine synoptic-scale environment of the MVs using a composite of GANAL. Before the generation of the MVs, a positive SLP anomaly exists over the Pacific Ocean (Fig. 4.22a). The pressure gradient over the Sea of Japan is moderate (Fig. 4.22a) and the northwesterly winter Asian monsoon is relatively weak compared with mean field (not shown). Since the cold winter monsoon is weak at −48 hour, the low-level atmosphere over the Sea of Japan is warmer than the mean field and the cold airmass remains over the Asian Continent (Fig. 4.23a). As a synoptic-scale low in the western part of Japan (Fig. 4.22b) develops and moves to the east of Japan (Fig. 4.22c), the pressure gradient increases and the northwesterly intensifies. The cold air breaks out over the Sea of Japan and the northwesterly strengthens (Fig. 4.23b-c). The MVs appear at the eastern edge of the cold air (Fig. 4.23c) and are located in a trough extending westward from the synoptic-scale low whose center is located at the eastern coast of Honshu Island at 0 hour (Fig. 4.22c). Then, the MVs land on Honshu Island and dissipate, while the synoptic-scale low continues to develop and move further eastward (Fig. 4.22d). After the MVs have dissipated, the cold northwesterly prevails over the Sea of Japan (Fig. 4.22d and 4.23d).

Synoptic-scale trough and ridge moving eastward are evident at the upper-level (Fig. 4.24). A ridge accompanied by warm air is located above Japan, whereas a trough accompanied by a cold air exists over the Asian Continent at −48 hour (Fig. 4.24a and

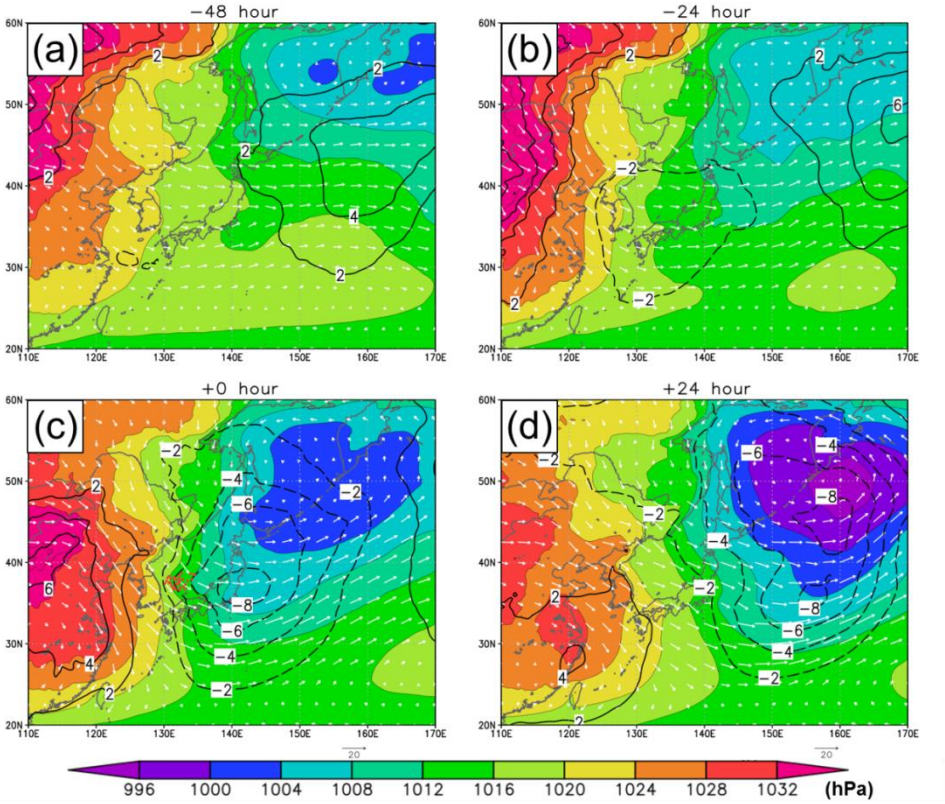

Fig. 4.22 As for Fig. 4.4 except for NW_se.

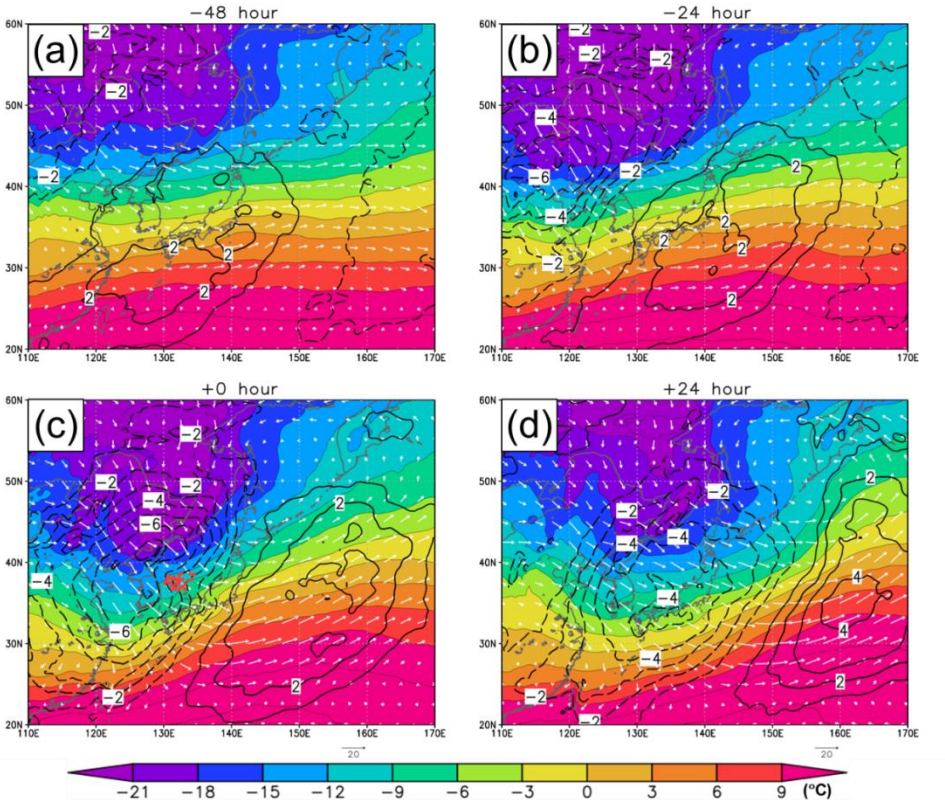

Fig. 4.23 As for Fig. 4.5 except for NW_se.

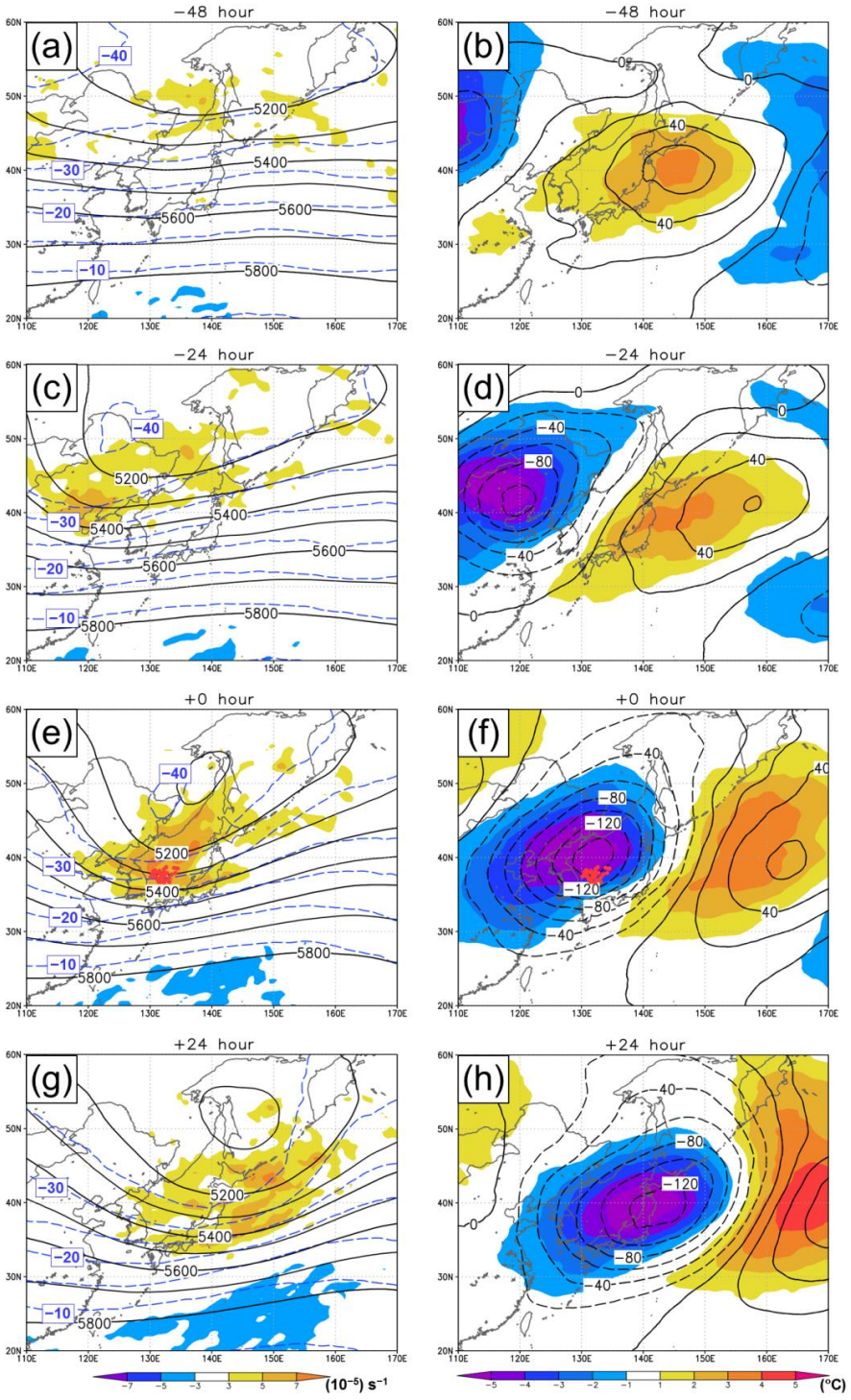

Fig. 4.24 As for Fig. 4.6 except for NW_se.

4.24b). The trough and ridge move eastward while developing (Fig. 4.24c and 4.24d). The center of the negative height anomaly passes over the root of the Korean Peninsula. The MVs develop beneath the upper-level trough and cold air although the MVs are located slightly south of the center of the negative height anomaly (Fig. 4.24e and 4.24f). Finally, the trough moves over the Pacific Ocean (Fig. 4.24g and 4.24h). Note that the synoptic-scale low develops to the east of the upper-level trough (Fig. 4.22c and 4.22d)

Next, we examine the mesoscale environment and structure of NW_se using a composite of MANAL. Figure 4.25 shows the total fields of SLP and horizontal wind at 850 hPa and the anomaly field of temperature at 850 hPa at 0 hour. When cold air breaks out from the Asian Continent to the Sea of Japan, it is blocked by the mountains at the north of the Korean Peninsula and split into two streams: a north-northwesterly at the northern side and a west-northwesterly at the southern side. A thermal ridge which corresponds to a SLP trough forms between the two streams. The MVs are located in the SLP trough.

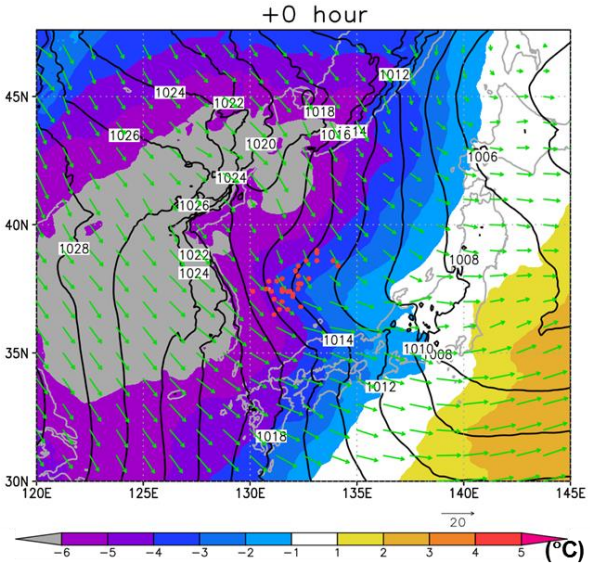

Fig. 4.25. MANAL composite of the total fields of SLP (contour; the contour interval is 2 hPa) and horizontal wind at 850 hPa (vector; m s^{-1}) and the anomaly field of temperature at 850 hPa (color; °C) at 0 hour for NW_se. Red dots indicate the location of MVs.

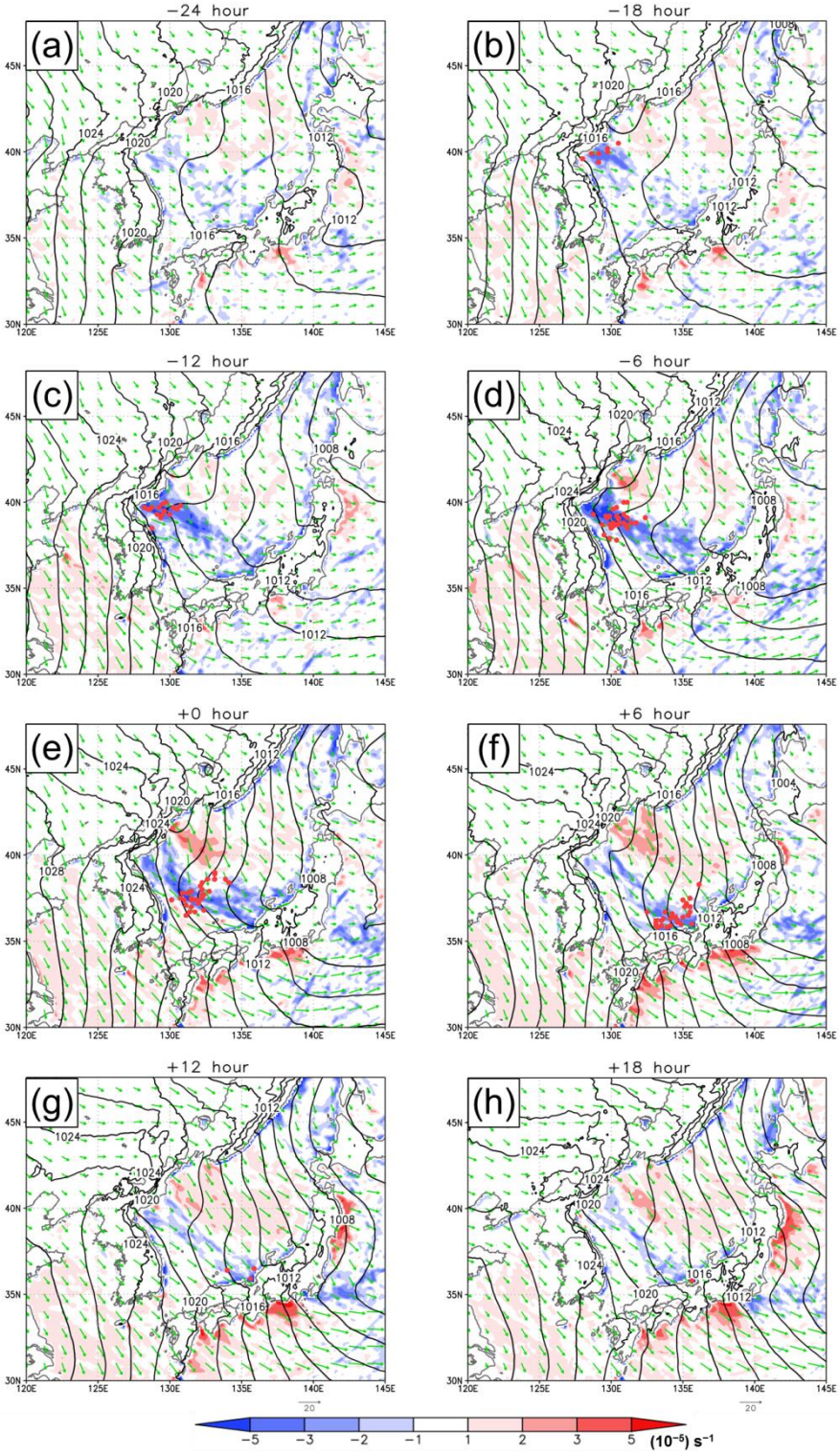

Fig. 4.26. MANAL composite of the total field of SLP (contour; the contour interval is 2 hPa), horizontal wind at 950 hPa (vector; m s^{-1}), and its divergence (color; 10^{-5} s^{-1}) for NW_se. (a) −24 hour, (b) −18 hour, (c) −12 hour, (d) −6 hour, (e) 0 hour, (f) +6 hour, (g) +12 and (h) +18 hour. The divergence is drawn only over the sea. Red dots indicate the location of MVs.

The two streams of cold air cause a convergence zone over the Sea of Japan. This convergence zone is the JPCZ. At −24 hour, a weak convergence zone extends southeastward from the northwestern corner of the Sea of Japan (Fig. 4.26a). As the cold air outbreak intensifies, the convergence zone gradually intensifies from the northwestern corner of the Sea of Japan (Fig. 4.26a-c). At the same time, it somewhat rotates cyclonically and extends in a more zonal direction (Fig. 4.26c-d). The MVs are generated on the convergence zone where strong horizontal wind shear exists (Fig. 4.26b-d). Then, the convergence zone moves southward with the MVs (Fig. 4.26d-f). The convergence zone extends in a more meridional direction in the northwest side of the MVs (Fig.4.26e-f). Consequently, the MVs are located at a bending point where the direction of the convergence zone changes (Fig. 4.26e). After the MVs land on Honshu Island and dissipate, the convergence zone extends in the northwest-southeast direction in a strong northwesterly while gradually becoming indistinct (Fig. 4.26g-h).

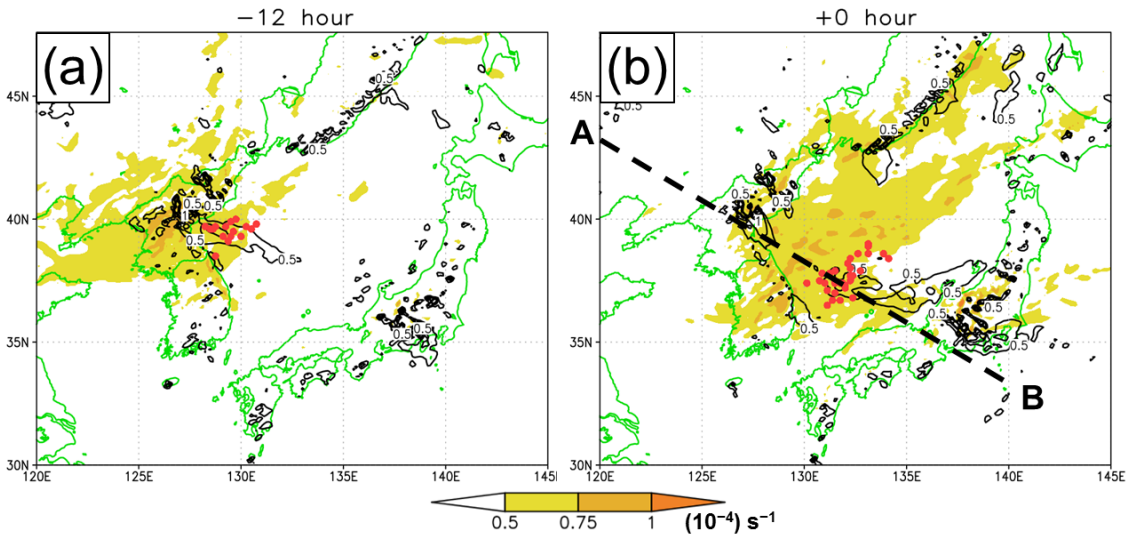

Fig. 4.27. MANAL composite of total field of vorticity at 500 hPa (color; 10^{-4} s^{-1}) and vorticity at 850 hPa (contour; the contour interval is 0.5×10^{-4} s^{-1}) for NW_se at 0 hour. (a) −12 hour and (b) 0 hour. Red dots indicate the location of MVs.

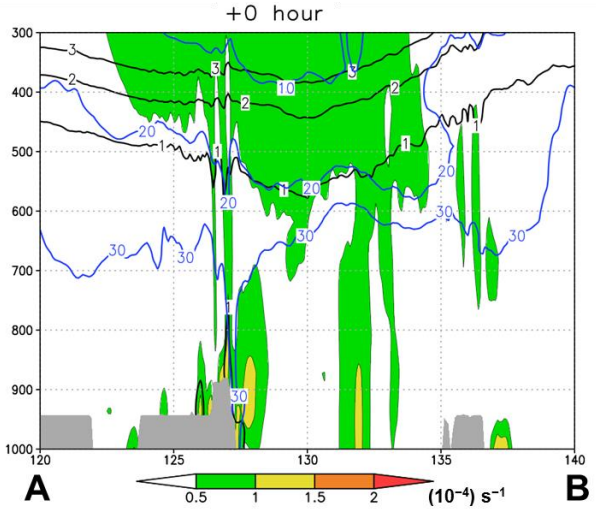

Fig. 4.28 As for Fig. 4.9 except for the vertical cross section along the AB line in Fig. 4.27b. The gray shade near the surface indicates the topography.

As seen in the GANAL composite, a trough moves eastward in the upper-level. When the region of positive vorticity associated with the upper-level trough approaches the northwestern edge of the Sea of Japan, the MVs are generated in the east part of the region (Fig. 4.27a). In the following 12 hours, the upper-level positive vorticity and the MVs move together (Fig. 4.27b). In the vertical cross section along the line A-B in Fig. 4.27b), a positive PV anomaly intrudes into around 600 hPa northwest of the MVs (Fig. 4.28). This configuration implies that upper-level forcing contributes to the generation and development of the MVs.

The cold air accompanying the upper-level trough also contributes to reduce the stability of the atmosphere over the Sea of Japan (Fig. 4.29a). In the low-level, since the warm air remains along the convergence zone due to the blocking of cold air by the mountains (Fig. 4.25), local stability minimum forms along the convergence zone (Fig.4.29b). Moreover, strong dynamical convergence exists at the low-level. As a result, active cumulus convection and associated meso-scale updrafts occur along the convergence zone. The MVs develop in this area of active cumulus convection.

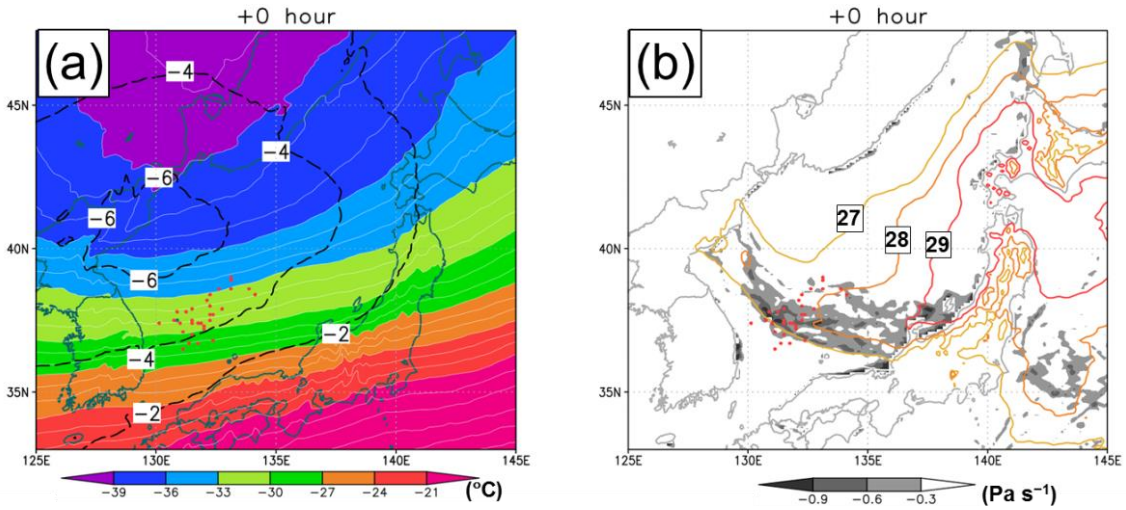

Fig. 4.29 As for Fig. 4.11 except for NW_se.

It is noteworthy that some MVs in NW_se attain their maximum intensity at the beginning of their lifespan, whereas the rest of MVs in this group intensify during their lifetime and reach peak intensity near Honshu Island (Fig. 4.2d). To examine the factor for the development of the MVs, we have classified NW_se into two groups: developing MVs (16 MVs) that reach their peak intensity either at or after the KT and non-developing MVs (19 MVs) that reach their peak intensity before the KT. Then composite analyses are made for each group of MVs.

Figure 4.30 shows MANAL composite of total fields of vorticity at 500 hPa and 850 hPa at 0 hour and the path of the minimum of the geopotential height anomaly at 500 hPa for the developing and non-developing MVs. The location of the minimum of geopotential height anomaly is almost same at −24 hour. However, that for the developing MVs moves southeastward together with the MVs, whereas, that for the non-developing MVs moves eastward and goes away from the MVs. The dynamic forcing associated with upper-level trough directly contributes to the development of the MVs. It also intensifies the cumulus convection by inducing updraft ahead of it.

Moreover, associated with southern path of the upper-level trough, the cold air at the upper-level intrude into further south for developing MVs, which cause less stable stratification (Fig. 4.31a and 4.31c). Consequently, the cumulus convection for

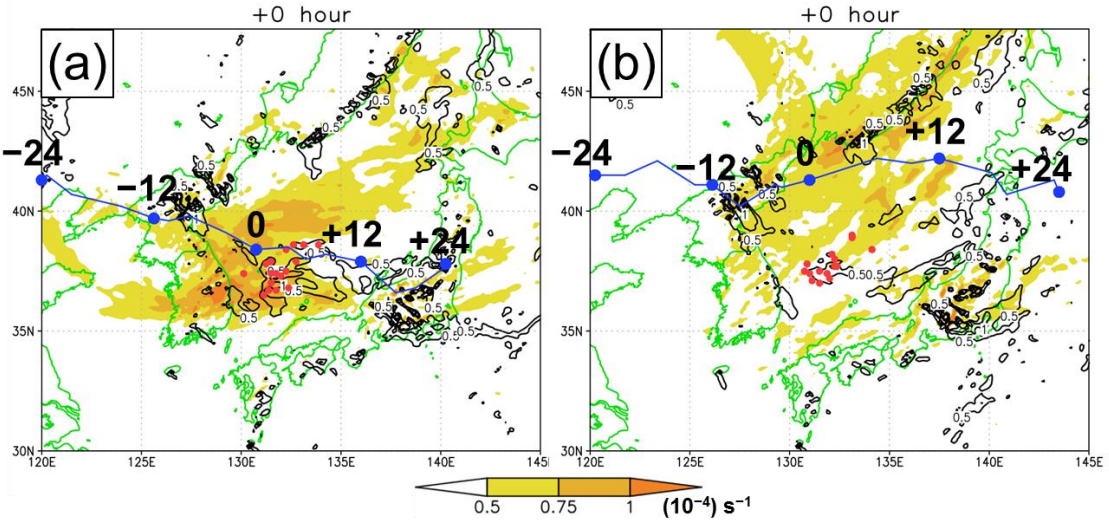

Fig. 4.30 As for Fig. 4.8 except for (a) developing MVs and (b) non-developing MVs. The blue lines show the path of the minimum of the height anomaly at 500 hPa.

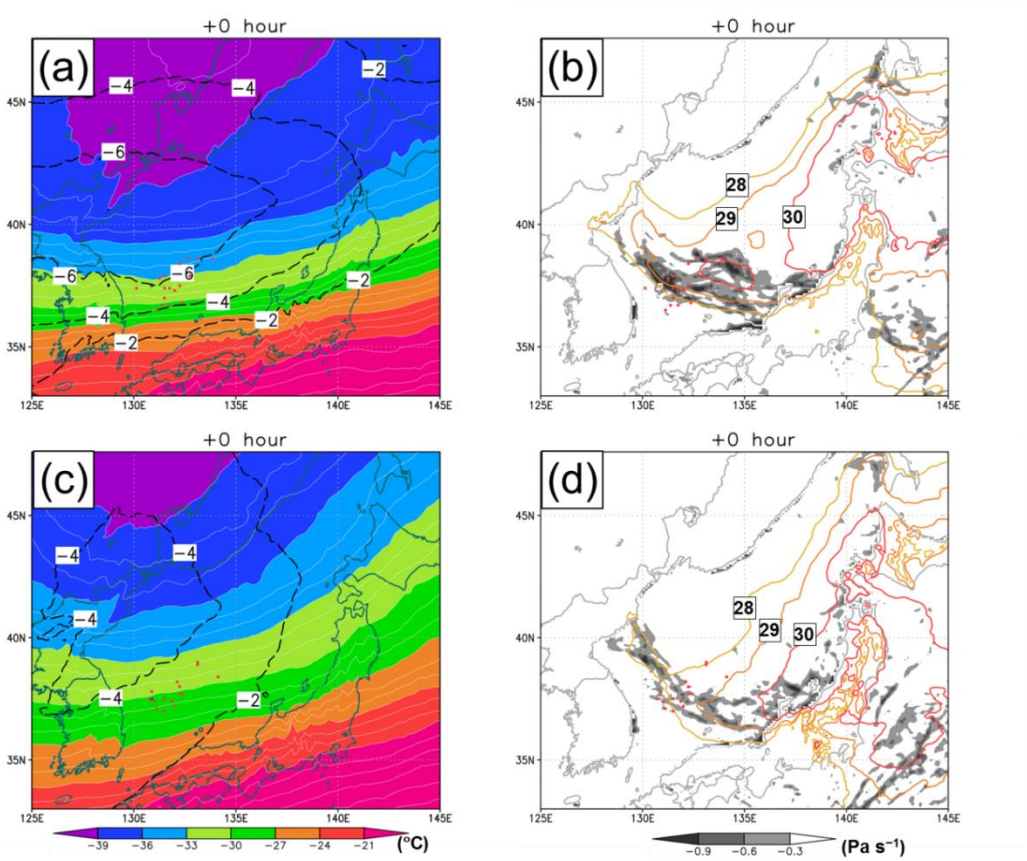

Fig. 4.31 As for Fig. 4.11 except for (a), (b) developing MVs and (c), (d) non-developing MVs.

developing MVs is more active (Fig. 4.31b and 4.31d). Thus, both the upper-level forcing and cumulus convection contribute to the development of the MVs.

The characteristics of NW_se are summarized as follows. When an upper-level trough moves into the Sea of Japan and a synoptic-scale low develops to the east of the upper-level trough, cold air breaks out over the Sea of Japan. The cold air is blocked by the mountains at the north of the Korean Peninsula, and a convergence zone forms in the lee side of the mountain. The convergence zone intensifies from its northwestern edge as the upper-level positive vorticity approaches. The MVs appears in the convergence zone where strong horizontal shear exists. They move southeastward accompanying the convergence zone moving southward. The comparison between developing and non-developing MVs shows that both the upper-level forcing and active cumulus convection play important roles in the development of the MVs.

4.6.2 MVs moving eastward (NE_e)

The movement of the MVs in NW_e (Fig. 4.2e) is initially similar to NW_se, but becomes eastward near Honshu Island. The KT for NW_e is defined by the time when MVs are closest to dashed line in Fig. 4.2e as for NW_se.

The synoptic-scale environment of NE_e is nearly similar to that of NW_se, including the path of the upper-level trough. If we examine it in more detail, however, the relative location of MVs to the synoptic-scale system differs between NW_se and NW_e. At 0 hour, the center of the negative SLP anomaly is over the Sea of Japan (Fig. 4.32), indicating that the MVs in NW_e are closer to or collocated with the synoptic-scale low. The minimum of the negative height anomaly at 500 hPa in NW_e is located northwest of the MVs (Fig. 4.33), while that in NW_se north of the MVs at 0

hour (Fig. 4.26e-f). Thus, the relative position of the MVs to the synoptic-scale system in NW_e are more eastward than that in NW_se.

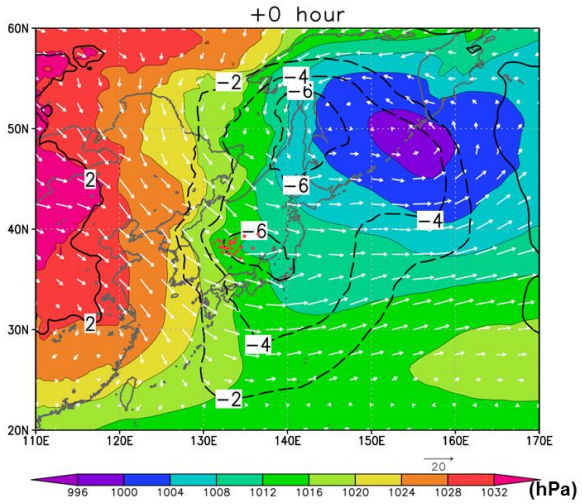

Fig. 4.32 As for Fig. 4.4 except for NW_e at 0 hour.

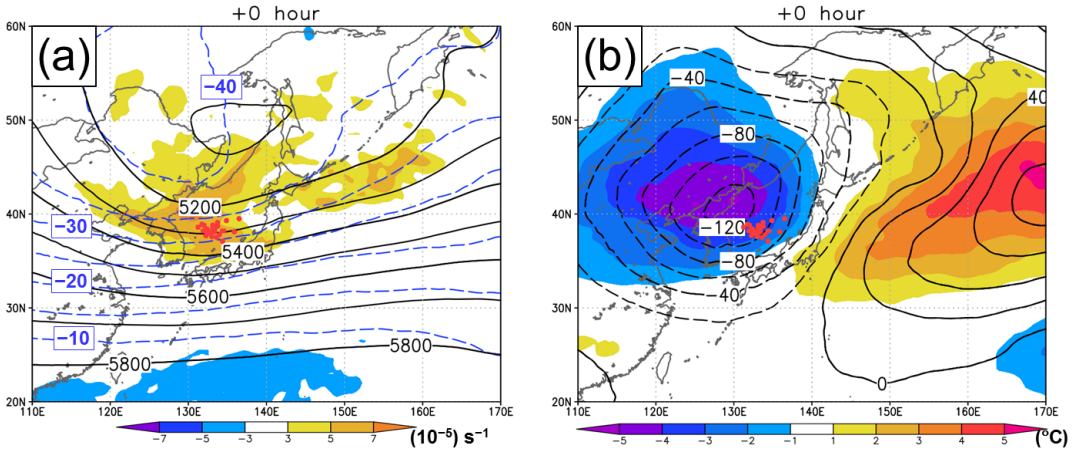

Fig. 4.33 As for Fig. 4.6 for NW_e at 0 hour.

In the mesoscale environment, the behavior of MVs with respect to the convergence zone differs between NW_e and NW_se. The MVs in NW_se moves southeastward together with the convergence zone after the convergence zone have rotated cyclonically and extended in the zonal direction (Fig. 4.26). In contrast, the cyclonic rotation of the convergence zone is more distinct in NW_e (Fig. 4.34b-d), and the MVs in NW_e move eastwardimultaneously with the rotation (Fig. 4.34a-f). Figure 4.35

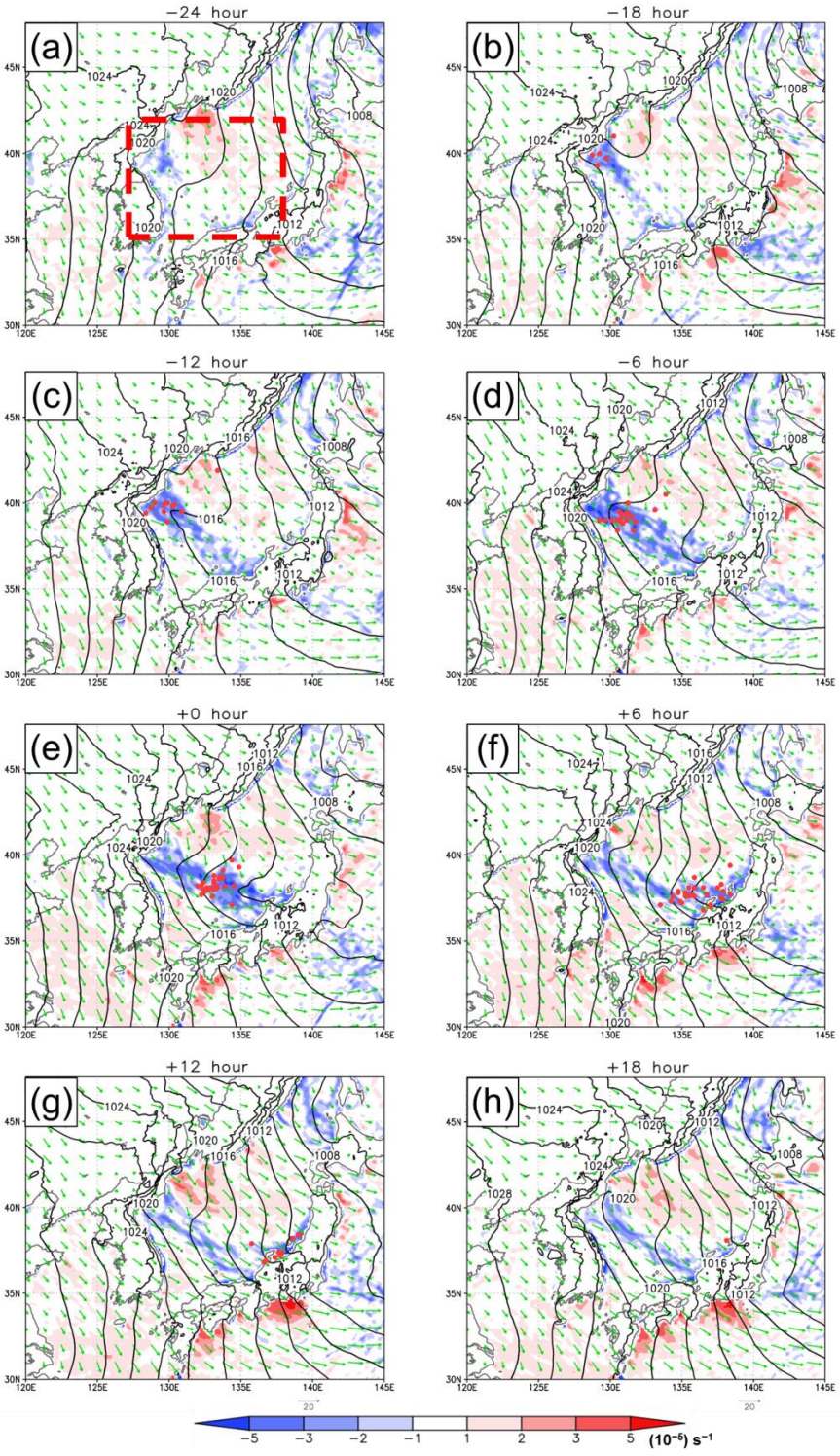

Fig. 4.34 As for Fig. 4.26 except for NW_e.

shows a time series of composite of horizontal wind averaged in a box of 127°E-138°E and 35°N-42°N between 950 and 850 hPa (The area is shown in Fig. 4.34a). The eastward component of the horizontal wind in NW_e increases from −24 hour to 0 hour. This change causes the cyclonical rotation of the convergence zone. On the other hand, although the eastward component of the horizontal wind in NW_e increases from −24 hour to −12 hour an increase of the northerly component between −12 hour and 0 hour is pronounced in NW_se. This causes the southward movement and bend of the convergence zone behind of the MVs in NW_se. Note that the time series of NW_e and NW_se roughly overlap if the former is delayed for 12 hours.

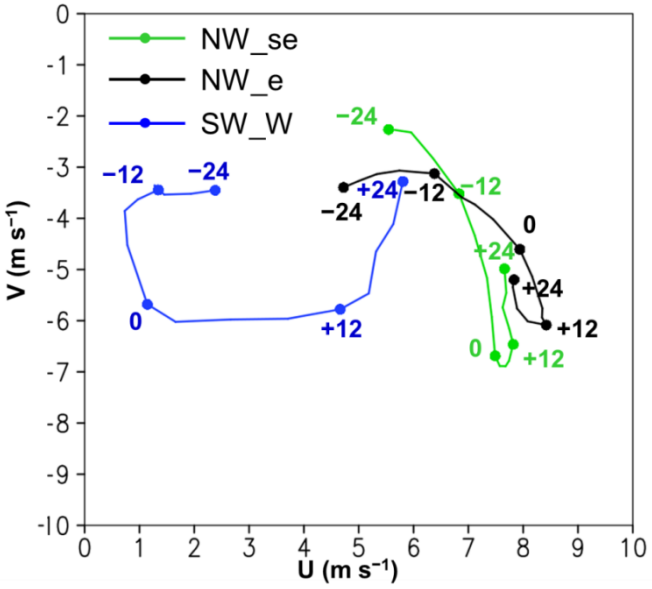

Fig. 4.35 Time series of composite of horizontal wind averaged in a box of 127°E-138°E and 35°N-42°N between 950 and 850 hPa. The area is shown in Fig. 4.34a.

The synoptic-scale and mesoscale environment for NW_e and those for NW_se can form consecutively. Furthermore, these two types of MVs sometime appear simultaneously, in which a MV located in the east moves eastward or east-northeastward, while another one located in the west moves southeastward

(Ookubo 1995; Tsuboki and Asai 2004). In fact, such pairs of MVs were observed 7 times during the six cold seasons.

4.6.3 Discussion

The MVs in NW area are associated with a convergence zone (JPCZ) which is consistent with a number of previous case studies (e.g. Nagata 1993). The convergence zone is likely to be caused by the blocking of the cold air by the mountains at the north of the Korean Peninsula, which is also consistent with the previous studies (e.g. Yagi et al. 1986; Nagata 1991). MVs in NW area are generated in a strong horizontal shear associated with the convergence zone, which indicates that their generation is due to mainly barotropic instability. However, the upper-level vortex and cumulus convection also plays a role for the development of the MVs. Therefore the development mechanism is likely to change during the development of the MVs as revealed by Watanabe and Niino (2014).

The MVs in NW_se is located at the bending point where the convergence zone is convex southward. This is due to the increase of southerly component of low-level wind. On the other hand, the MVs in NW_e develop during the cyclonic rotation of the convergence zone associated with the increase of the easterly component of low-level wind. This feature is consistent with the result by Ookubo (1995) that MVs moving southeastward (east-northeastward) is initiated when the bending point where the convergence cloud band bends toward south (north) was formed.

4.7 MVs in SW area

MVs in SW area are classified according to the location where they reach their

maximum intensity: west of 134°E (SW_W) and east of 134°E (SW_E). Figure 4.36 shows an example of SW_W. During the six cold seasons, 12 and 9 MVs in SW_W and SW_E group, respectively, occurred. Here the environments and structures of the MVs in SW_W are studied in detail in this subsection.

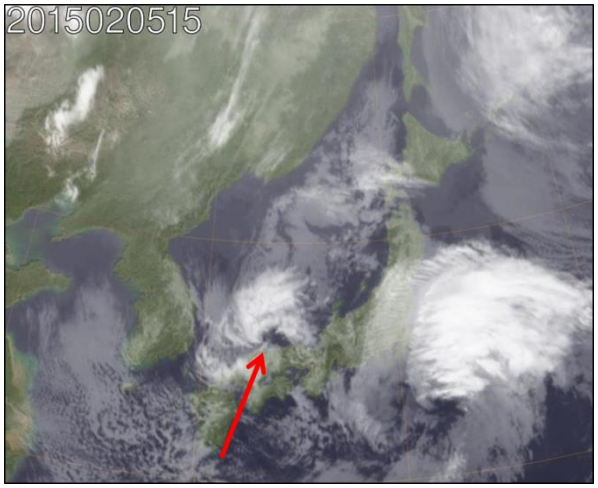

Fig. 4.36 Satellite image of a MV in SW_W

4.7.1 MVs attaining their maximum intensity in the western side (SW_W)

MVs in SW_W (Fig. 4.2f) formed over the southwestern part of the Sea of Japan. Although their movements were generally slow and complicated, they finally landed on Honshu Island and dissipated. The KT for SW_W is defined by the time when the MVs reach their maximum intensity.

As in the previous subsections, we first examine synoptic-scale environment of the MVs using a composite of GANAL. At −24 hour (Fig. 4.37b), the Siberian High extends over the Sea of Japan, while a negative SLP anomaly exists over the East China Sea. This pressure pattern weakens the low-level wind over the western part of the Sea of Japan, whereas it intensifies northwesterly over the Yellow Sea and the East China Sea. The negative SLP anomaly develops into a synoptic-scale low as it moves eastward along the southern coast of Honshu Island (Fig.4.37c), which further intensifies the

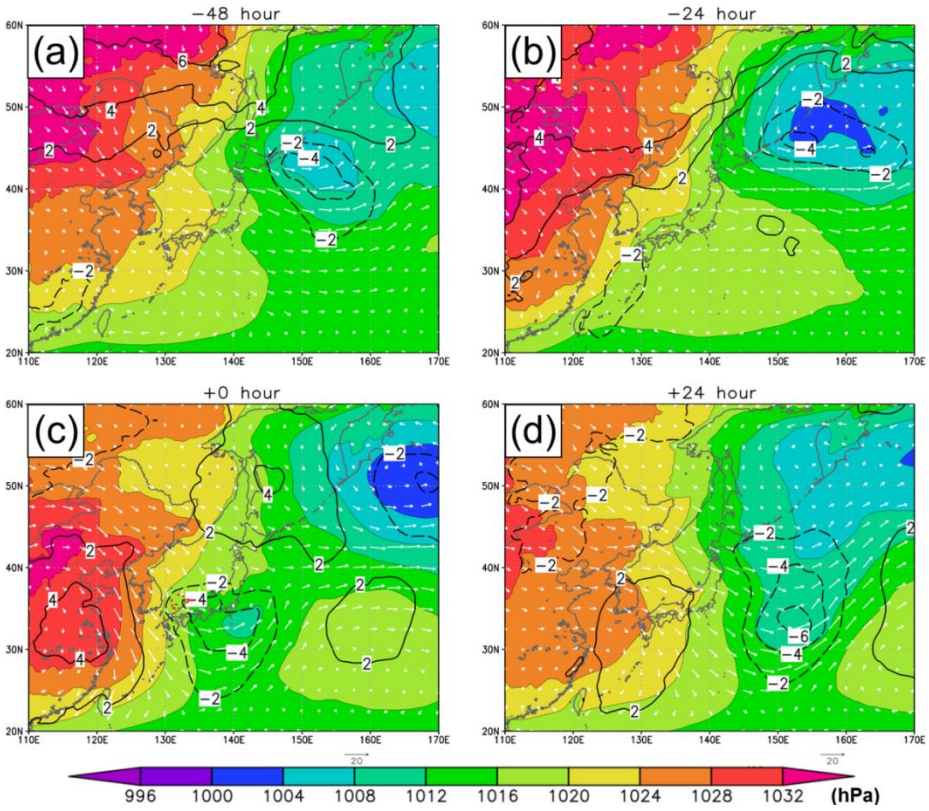

Fig. 4.37 As for Fig. 4.4 except for SW_W.

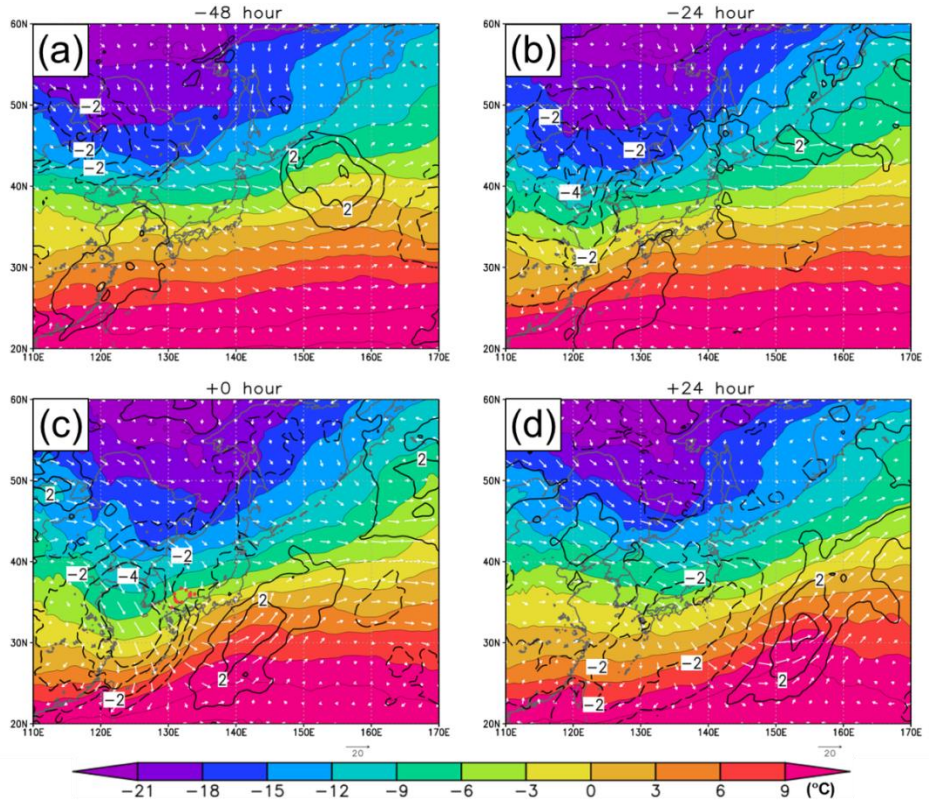

Fig. 4.38 As for Fig. 4.5 except for SW_W.

northwesterly over the Yellow Sea and the East China Sea. Therefore cold air over the Asian Continent breaks out mainly to the Yellow Sea and the East China Sea (Fig. 4.38b-c). The MVs are located at the eastern edge of the cold air (Fig. 4.38c) and at the northwestern quadrant of the synoptic-scale low (Fig. 4.37c). Then, the MVs land on Honshu Island and dissipate, while the synoptic-scale low continues to develop and move eastward (Fig. 4.37d). The center of the cold anomaly moves over the Pacific Ocean by + 24 hour (Fig.4.38d).

Similarly to NW_se and NW_e, a synoptic-scale cold trough moving eastward is evident at the upper-level (Fig. 4.39). However, the center of the negative height anomaly passes over the southern part of the Korean Peninsula (Fig. 4.39b, d, f). The MVs appear to the east of the upper-level negative height anomaly (Fig. 4.39d). Since the movements of the MVs are slow, the negative height anomaly overtakes the MVs and is located right above the MVs at 0 hour (Fig. 4.39e-f). Finally, the trough moves over Pacific Ocean (Fig. 4.39g-h).

Next, we examine the mesoscale environment and structure of SW_W using a composite of MANAL. Figure 4.40 shows the total field of SLP and horizontal wind at 850 hPa and the anomaly field of temperature at 850 hPa at 0 hour. As seen in the GANAL composite, the cold air outbreak is strong over the East China Sea, while it is weak over the Sea of Japan. A low pressure area associated with the MVs is collocated with a relatively warm area in the cold anomaly. To the southwest of the low pressure area, strong cold advection occurs.

A convergence zone is seen in the composite field for SW_W (Fig. 4.41), which is similar to that in NW_se and NW_e. However its movement is quite different. It is stationary along the eastern coast of the Korean Peninsula extending in the meridional

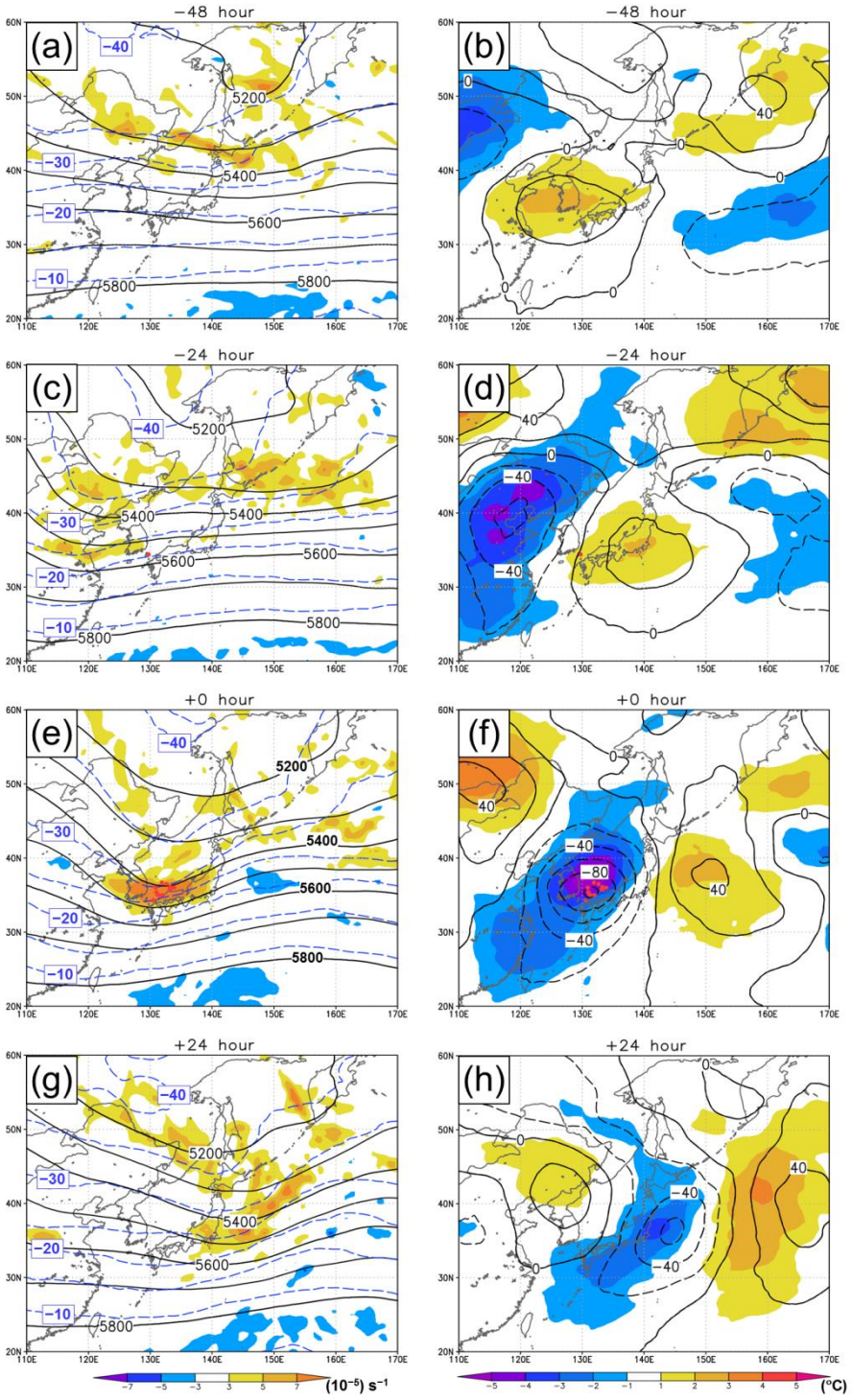

Fig. 4.39 As for Fig. 4.6 except for SW_W.

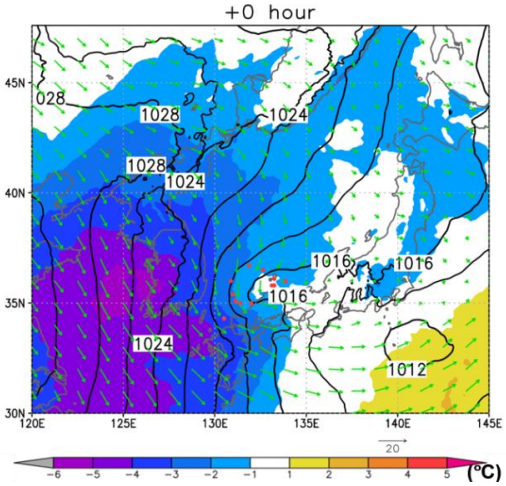

Fig. 4.40. As for Fig. 4.25 except for SW_W.

direction during the development of the MVs (Fig. 4.41a-e). The averaged low-level wind for SW_W before 0 hour is northerly (Fig. 4.35). Thus, the convergence zone is almost parallel to the direction of the low-level wind. The MVs appear and develop at the southern part of the convergence zone. After the MVs land on Honshu Island and dissipate, the convergence zone also disappears (Fig. 4.41f-h).

In Figure 4.42 we have seen the relationship between the upper-level vortex and low-level MVs in SW_W. At −12 hour, a meso-α-scale region of positive vorticity at the upper-level is located to the northwest of the MVs (Fig.4.42a), which is favorable for a baroclinic development of the MVs. On the other hand, the upper-level vortex is located right above the MVs at 0 hour when the MVs reach their maximum intensity (Fig. 4.42b). These two vortices are vertically coupled (Fig. 4.43). However, the upper-level vortex continues to move eastward and goes away from the MVs after 0 hour (Fig. 4.39g), resulting in a separation of the upper- and low-level vortices (not shown).

The upper-level cold air intrudes over the Sea of Japan (Fig. 4.44a), whereas, the low-level cold air outbreak is relatively weak over the Sea of Japan (Fig. 4.40). Therefore the atmosphere over the Sea of Japan becomes less stable (Fig. 4.44b). The

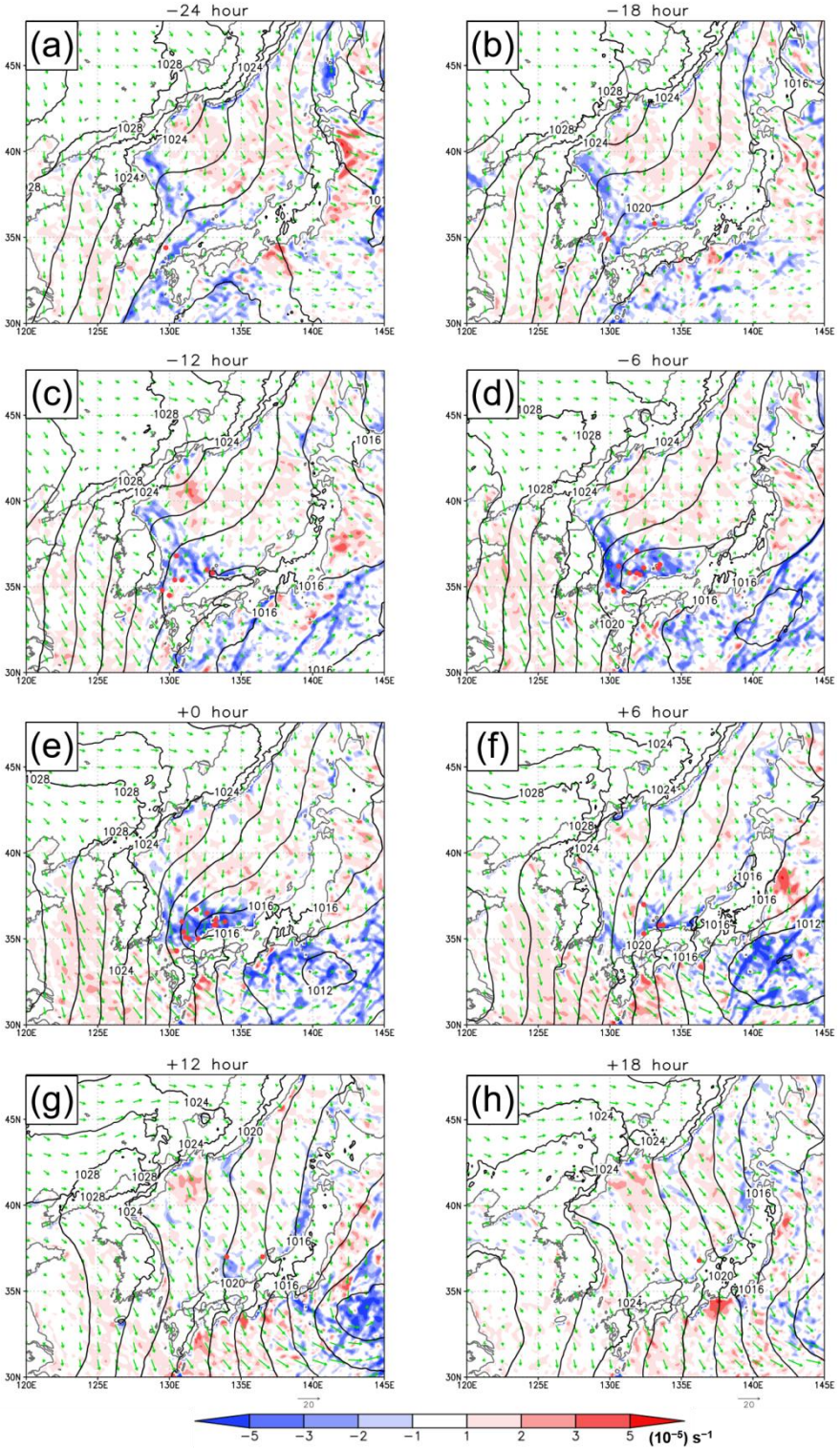

Fig. 4.41. As for Fig. 4.26 except for SW_W.

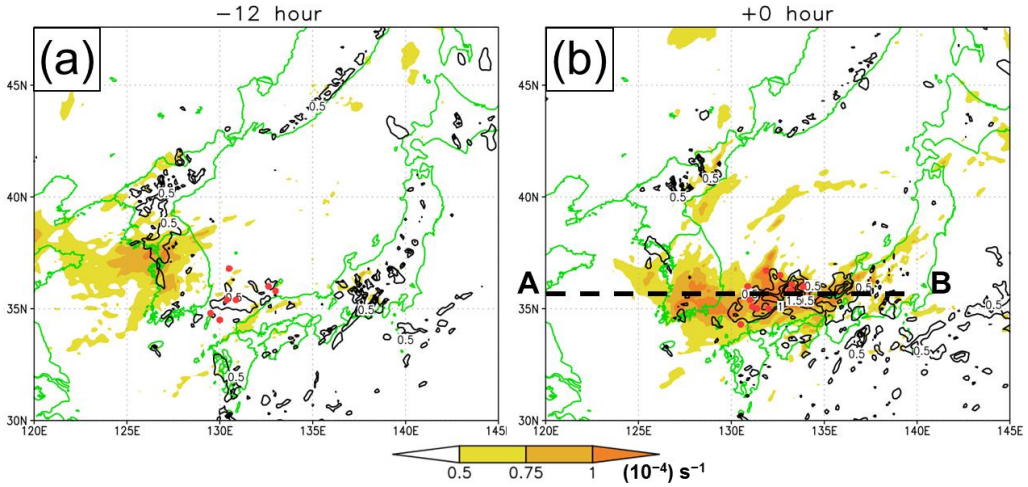

Fig. 4.42. As for Fig. 4.27 except for SW_W.

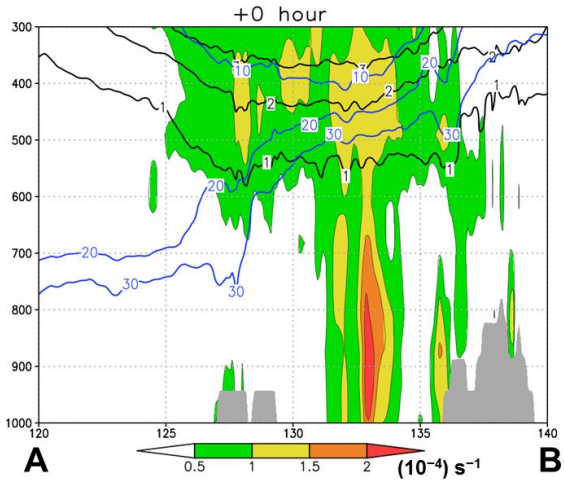

Fig. 4.43 As for Fig. 4.9 except for the vertical cross section along the AB line in Fig. 4.42b. The gray shade near the surface indicates the topography.

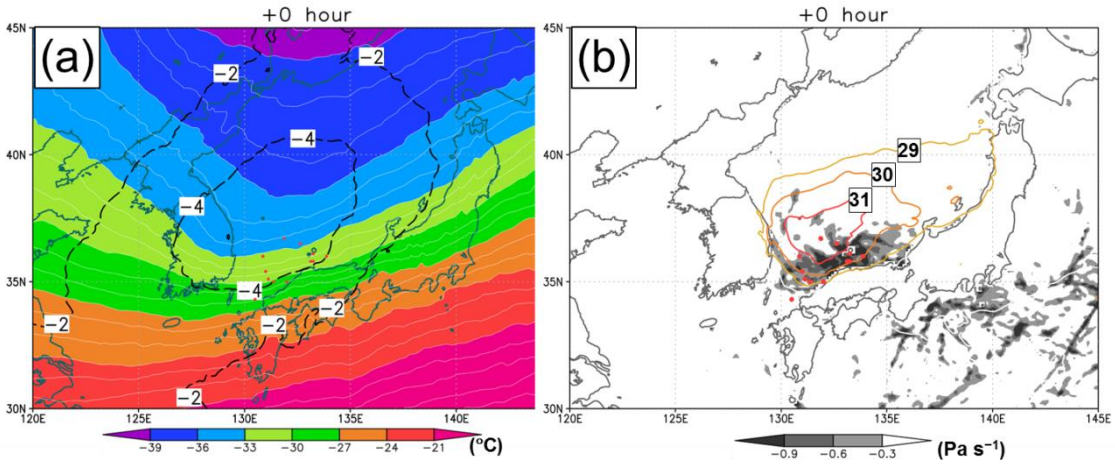

Fig. 4.44 As for Fig. 4.11 except for SW_W.

MVs are accompanied by active cumulus convection in the less stable environment (Fig. 4.44b). In contrast to NW_se, the updraft is evident only around the MVs and the cloud band associated with the convergence zone does not exist.

The characteristics of SW_W are summarized as follows. Before the MVs appear, a convergence zone extends in the meridional direction in the lee side of the mountain at the north of the Korean Peninsula, which is parallel to the low-level northerly wind. When an upper-level trough comes into the Sea of Japan after passing over the southern part of the Korean Peninsula, the MVs develop to the east of the trough. The upper-level trough is collocated with the MVs and they become coupled at 0 hour when the MVs reach their maximum intensity. The MVs develop in a less stable environment and are accompanied active cumulus convection.

4.7.2 Discussion

The significance of an upper-level vortex for the development of the MVs in SW_W is pointed out in several case studies (Yamagishi et al. 1992; Shimada et al. 2014). Shimada et al. (2014) showed that a meso-α-scale upper-level PV anomaly intrudes to 700-600 hPa level to the west of a developing MV. They also showed that in contrast to the low-level MV, the upper-level PV anomaly does not intensify. Our result is consistent with their findings. The MVs develop when the upper-level vortex is located to the west of the low-level MVs and they reach their maximum intensity when the upper-level vortex overlaps with them. However, the phase of the upper-level vortex and MVs is not locked in contrast to a case of extratropical cyclones, and the MVs decay after the upper-level vortex moves away from the MVs.

4.8 Conclusions

We have examined general characteristics of MVs and their environment by composite analyses. We have classified MVs according to their location and direction of movement. The composite analyses show the general characteristics of the environment and structure of the MVs. The results of composite analyses are consistent with previous case studies. Therefore our results provide a universal evidence for the general characteristics of the MVs than previous case studies.

One of the common features of the environment of the MVs in various areas is the cold air outbreak in the low-level. The MVs appear at the edge of the low-level cold air where two different airmasses are adjacent and consequently both large baroclinicity and horizontal shear exist. If we look at meso-scale structure of the MVs in each group, several different characteristics among each group are found in the low-level. The southward-moving MVs in the NE area are associated with zonal temperature gradient and cyclonic shear flow at the low-level, whereas the eastward-moving MVs develop in a meridional temperature gradient. The MVs in NW and SW areas are related to a convergence zone which is formed in the lee side of the mountain at the north of the Korean Peninsula. However, the behavior of the convergence zone and its relationship with the MVs varies according to the location and the direction of movement of the MVs.

The upper-level trough accompanied by cold air is also a characteristic of the environment of the MVs. It intensifies the MVs due to dynamic effect including baroclinic process and updrafts in its front side. The upper-level cold trough also contributes to provide a less stable stratification. The active cumulus convection in a less stable environment is associated with the MVs.

Our composite analyses indicate that the path of the upper-level trough or vortex determines the location where MVs appear. This is consistent with the study by Kolstad (2011), suggesting that the upper-level forcing determines whether or not polar lows will form. While the upper-level trough is likely to pass over the Sea of Japan without geographic preference, the genesis of MVs is concentrated in several particular areas over the Sea of Japan such as NE area and NW area, Therefore some other factors for forming a favorable condition for MVs is likely to exist in these regions. The mechanisms for development of MVs in each region are examined in the following chapter by numerical simulations.

5. Numerical simulations

5.1 Introduction

In the previous chapter, we have examined the general environment and structure of the MVs by composite analyses. The results show several common factors for the development of MVs including a cold air outbreak in the low-level and an upper-level trough accompanied by cold air. There are also mesoscale structures that are characteristic for each area such as the convergence zone or warm area at low-level. Although the composite analyses give average features of the environment in which the MVs develop, they do not assure that the composite environment would generate the corresponding MVs. Furthermore, they do not clarify the formation mechanism of the mesoscale structure.

In this chapter, we perform numerical simulations in which the composite field is used for the initial and boundary conditions in order to confirm that each composite field does certainly generate the corresponding MV. If a MV in a certain group is reproduced from the corresponding composite field, the composite field is considered to have general characteristics of the environment for MVs in that particular group. Moreover, we will examine the structure of the reproduced MV and perform sensitivity experiments for several factors including condensational heating, SST, and topography. Through these numerical simulations, we can acquire more reliable understanding about the development mechanism of the MVs than only a single case study can.

5.2 Model and experimental designs

The JMA nonhydrostatic model (JMA-NHM; Saito et al. 2006) is used for the present numerical simulations and sensitivity experiments. The model domains are

shown in Fig. 5.1. They are chosen so that they contain the center of negative height anomaly at −24 hour. The number of horizontal grid points for the MVs in NE area and in NW and SW areas are 350 × 250 (Fig. 5.1a) and 400 × 320 (Fig. 5.1b), respectively. The horizontal grid resolution is 10 km, and 40 vertical grid points are distributed from the surface to 15540 m, where grid intervals vary from 40 m at the surface to 802 m at the upper boundary.

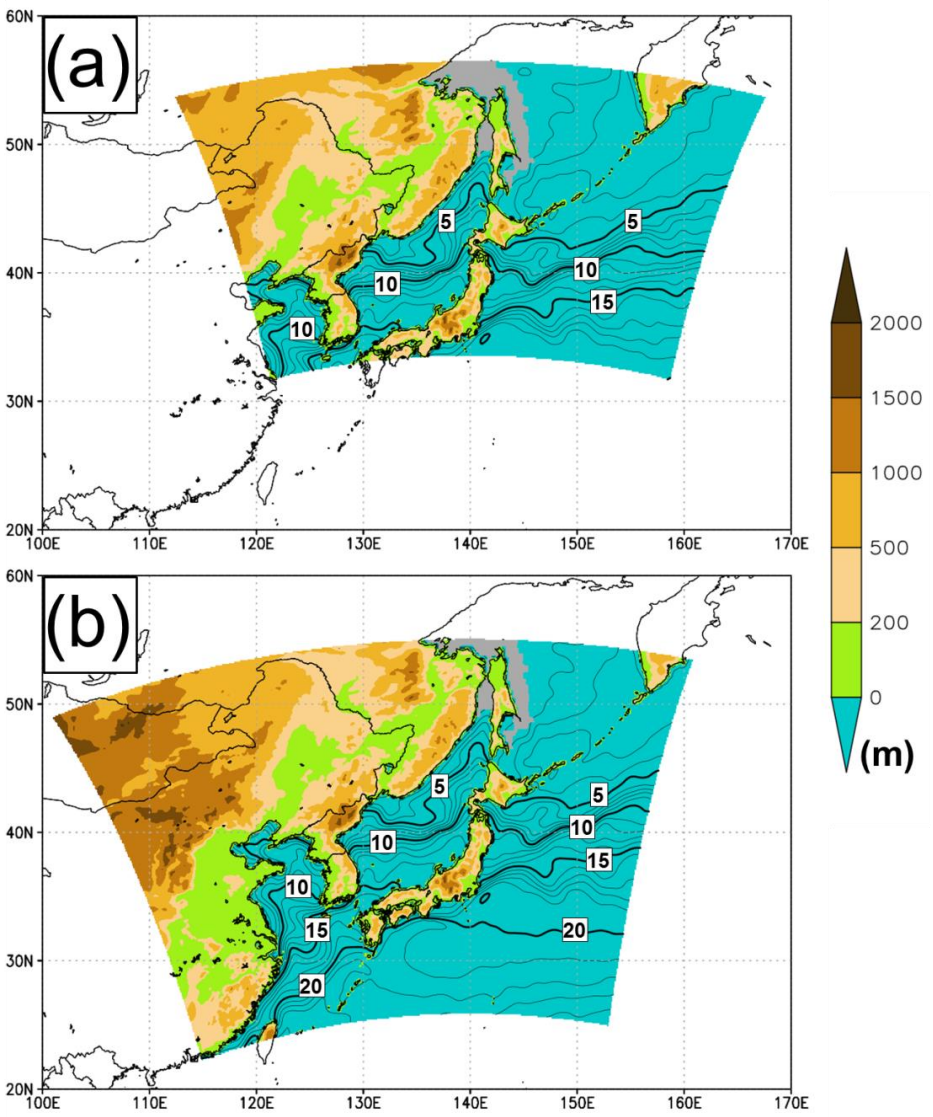

Fig. 5.1 Model domains of the numerical simulations for the MVs in (a) NE area and in (b) NW and SW area. The topography (color; m) and SST (contour; the contour interval is 1 °C) used for the numerical simulations are drawn. The distribution of the sea ice is drawn by gray shade.

An explicit three-ice bulk scheme (Ikawa et al. 1991), which predicts mixing ratios of water vapor, cloud water, rain, cloud ice, snow, and graupel, and the number density of cloud ice, is used for microphysics modeling. The Kain–Fritsch convective parameterization scheme (Kain and Fritsch 1990; Kain 2004) and the Mellor–Yamada–Nakanishi–Niino Level-3 boundary layer parameterization scheme (Nakanishi and Niino 2006) are used.

The GANAL composite is used for the initial and boundary conditions. Because of the coarse resolution of GANAL, mesoscale structures are almost smoothed out in the initial field. The simulation is started at −48 hour and is continued until + 24 hour. An average of OISST data between December and January for six winters is used for the SST and the distribution sea ice (Fig. 5.1).

5.3 Overview of the results

We have performed the numerical simulations for the NE_s, NEI_s, NE_e, NW_se, NW_e, and SW_W. Figure 5.2 shows the result of the numerical simulation for each group. In NE_s (Fig.5.2a-b), an MV appears at around 141°E, 46°N at −18 hour. It initially moves south-southwestward, then changes its moving direction to south-southeastward, and finally lands on the northern part of Honshu Island (Fig. 5.2a). The MV is accompanied by a comma-shaped “cloud” (hereafter vertically-integrated condensed water content is referred to as cloud) with a horizontal scale of about 400 km (Fig. 5.2b). In NEI_s (Fig. 5.2c-d), an MV appears off the west of northern part of the Hokkaido Island at 0 hour. It moves south-southeastward and lands on Hokkaido Island but slightly north of the Ishikari Bay (Fig. 5.2c). The MV is accompanied by a comma-shaped cloud with horizontal scale of about 200 km (Fig. 5.2d), which is

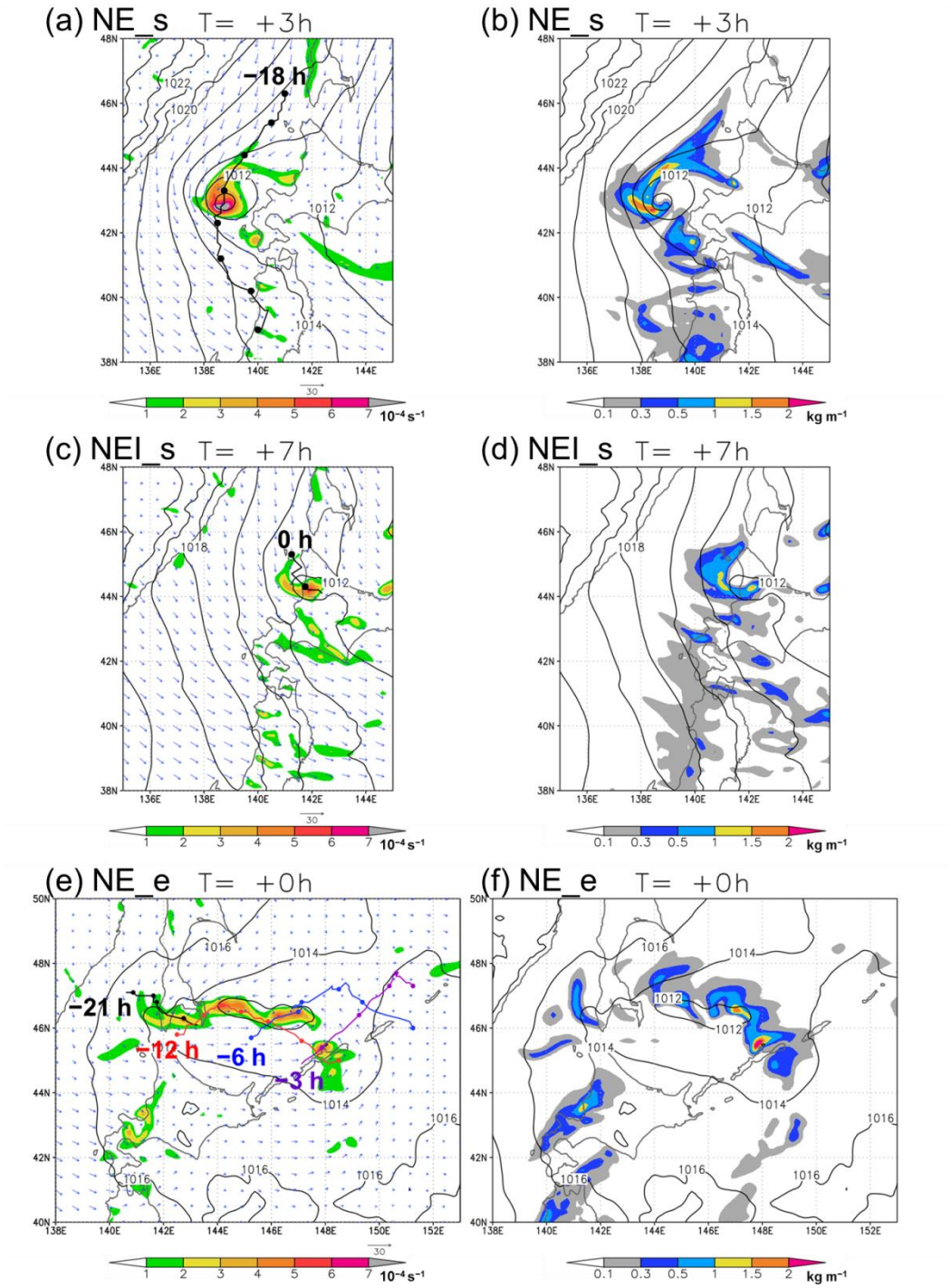

Fig. 5.2 SLP (contour; the contour interval is 2 hPa), vorticity (color; 10^{-4} s^{-1}) and horizontal wind (vector; m s^{-1}) at 950 hPa (left column) and vertically-integrated condensed water content (color; kg m^{-1}) (right column). The tracks of the MVs are drawn with the genesis time of the MVs. The dots in the tracks are plotted in every 6 hour. (a), (b) NE_s at +3 hour, (c), (d) NEI_s at +7 hour, (e), (f) NE_e at 0 hour, (g), (h) NW_se at +8 hour, (i), (j) NW_e at +2 hour, and (k), (l) SW_W at +3 hour.

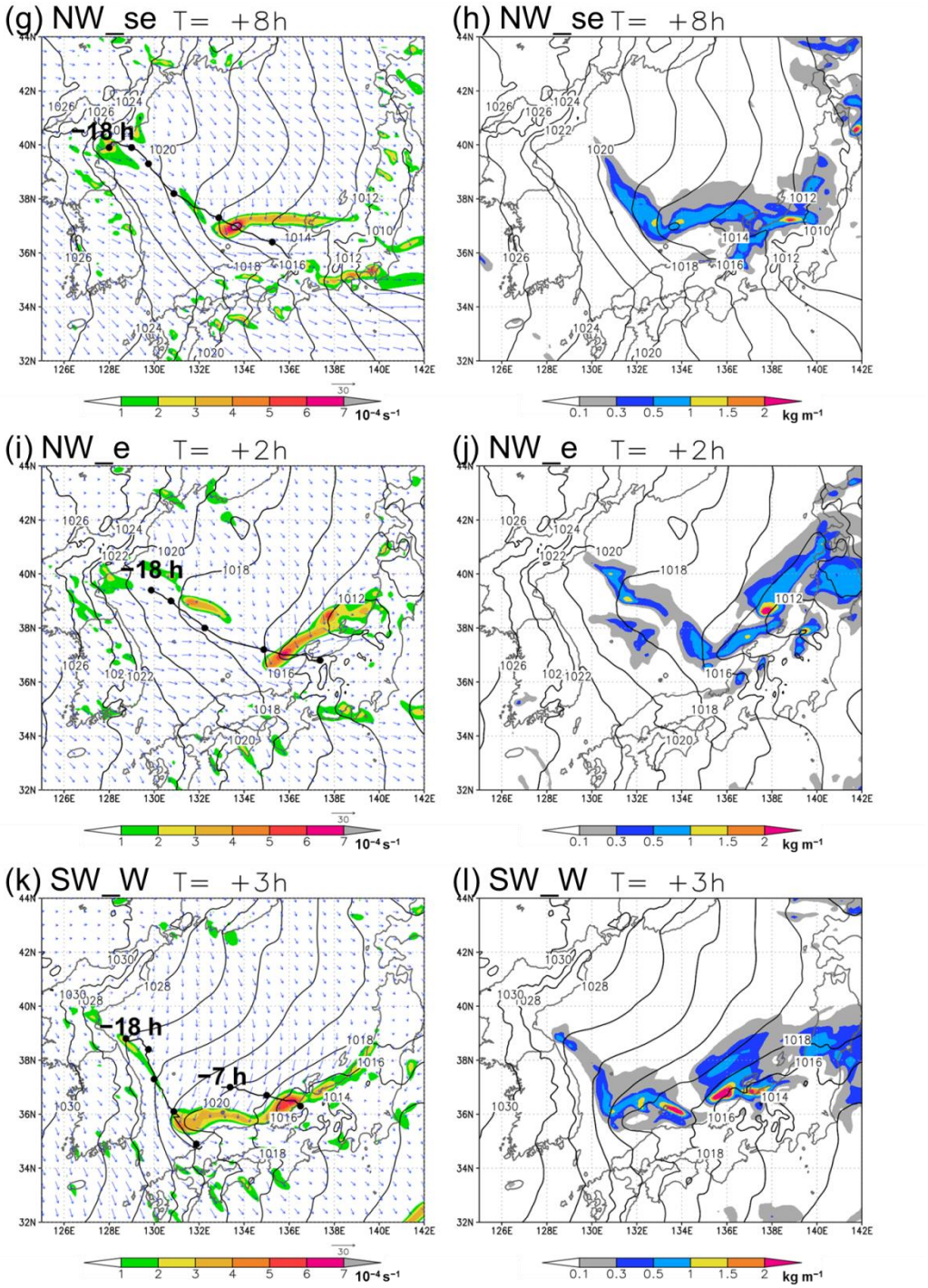

Fig. 5.2 Continued.

smaller than that of NE_s.

In NE_e (Fig. 5.2e-f), four MVs appears in a meso-α-scale low pressure area (Fig. 5.2e). The MV that appears first among the four is generated over the Sea of Japan and moves east-southeastward, whereas the other three MVs are generated over the Sea of Okhotsk, move northeastward initially and change their moving direction southeastward. Each MV is accompanied by a meso-β-scale comma-shaped cloud (Fig. 5.2f). Eventually the easternmost MV (purple line in Fig. 5.2e) develops to have horizontal scale of about 600 km (not shown).

In NW_se (Fig. 5.2g-h) and NW_e (Fig. 5.2i-j), MVs are generated at the northwestern corner of the Sea of Japan at −18 hour. The MV in NW_se moves southeastward and finally lands on the central part of Honshu Island (Fig. 5.2g). On the other hand, the MV in NW_e initially moves southeastward as in NW_se, whereas it gradually changes its moving direction to the east. Both MVs are located at a bending point of the cloud band associated with the JPCZ (Fig. 5.2h and 5.2j).

In SW_W (Fig. 5.2k-l), two MVs exist at + 3 hour (Fig. 5.2k). One MV appears at around 129°E, 39°N at −18 hour and moves south-southeastward. The other MV is generated at around 133.5°E, 37°N at −7 hour and moves east-southeastward. The latter corresponds to the MV in SW_W, although it is generated slightly east compared with typical MVs in SW_W. Both MVs are accompanied by cloud and precipitation on their northern side and their centers are collocated with cloud free areas (Fig. 5.2l).

Overall, the numerical simulation successfully reproduces the characteristics of the MVs in each group. This confirms that the environment obtained by the composite analysis contains the important ingredients for generating the corresponding MVs in each group. Since we use GANAL composite, the mesoscale structures are almost

smoothed out from the initial and boundary conditions. Therefore, certain mechanisms which generate the MVs are considered to exist in the large-scale environment. The MV reproduced in the numerical simulation using the composite field is also considered to have general characteristics of the MVs in each group. The generation and development mechanisms of the MVs are examined in the following subsections.

5.4 Factors for the development of the MVs

In this subsection we examine the development mechanisms of the MVs in NE_s, NW_se, NW_e, and SW_W.

5.4.1 The MVs in NE_s

We first examine the structure of the simulated MV in NE_s. Figure 5.3 shows time evolution of the simulated MV for NE_s. A weak synoptic-scale SLP trough embedded in the Aleutian Low moves southward before −24 hour (not shown). When the western end of the SLP trough comes into the Strait of Tartary (Mamiya Strait), an area of large vorticity appears in the trough (Fig. 5.3 a-b). At the early stage of the MV, a narrow area of large vorticity associated with the MV (Fig. 5.3b-d) is collocated with strong updraft associated with cumulus heating (not shown). Therefore, the MV is generated through the stretching of the surrounding vorticity associated with the SLP trough. Then the MV develops to have closed SLP contours (Fig. 5.3e-g). The SLP of the center of the MV at + 6 hour drops more than 4 hPa compared with surroundings (Fig. 5.3f). At this stage the MV is surrounded with a comma-shaped cloud (Fig. 5.4a). After this time, the MV gradually becomes rather circular shape (Fig. 5.3h) and the cloud structure changes into spiralform with a cloud free eye (Fig. 5.4b).

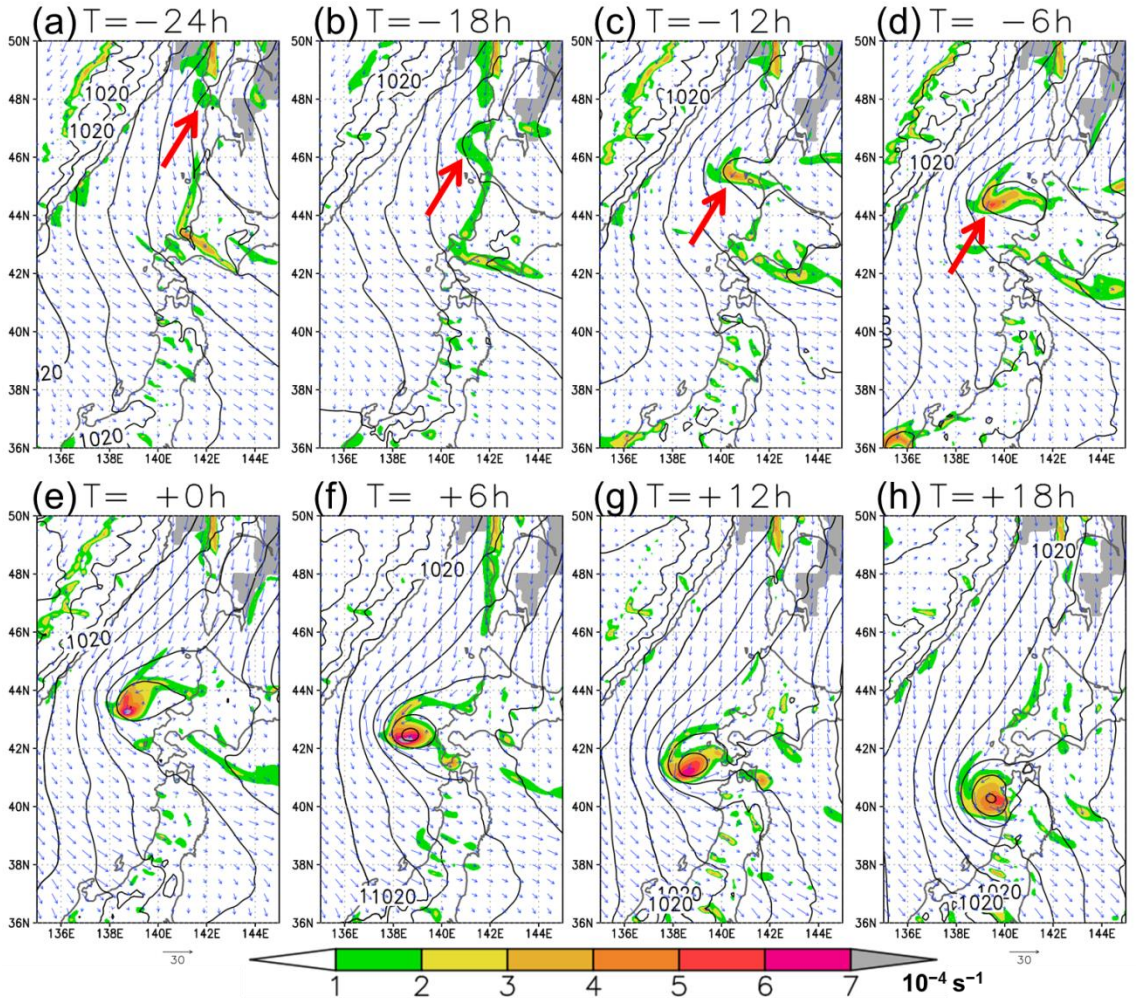

Fig. 5.3 SLP (contour; the contour interval is 2 hPa), vorticity (color; 10^{-4} s^{-1}) and horizontal wind (vector; m s^{-1}) at 950 hPa for NE_s. The distribution of the sea ice is drawn by gray shade.

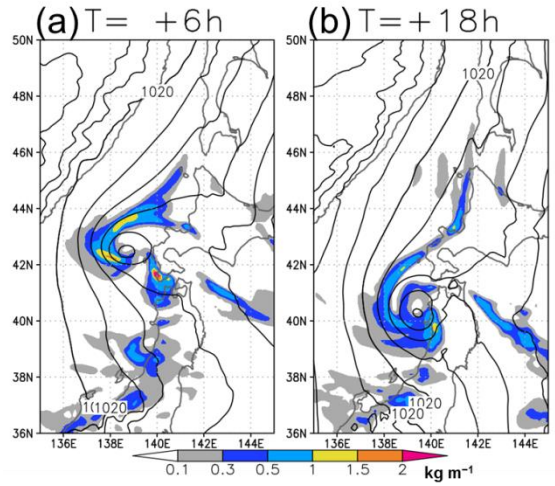

Fig. 5.4 SLP (contour; the contour interval is 2 hPa) and vertically integrated condensed water content (color; kg m^{-1}) for NE_s.

Figure 5.5 shows temperature field at 850 hPa. At +6 hour (Fig. 5.5a), a warm area collocated with the SLP minimum, whereas cold air intrudes eastward to the south of the warm area, which is similar to the composite field (Fig. 4.7b). At this time a positive PV anomaly also intrudes into 600 hPa to the south of the MV (not shown). This temperature structure and the upper-level PV anomaly imply a baroclinic development of the MV. On the other hand, the intrusion of the cold air becomes indistinct and the baroclinicity around the MV becomes weaker at +18 hour (Fig. 5.5b). This results in the circular shape of the MV with spiralform cloud, which appears in less baroclinic environment (Yanase and Niino 2007). Note that Shimada et al. (2014) reported that a PL having a similar track had a comma-shaped cloud initially but finally the cloud pattern changed into spiralform.

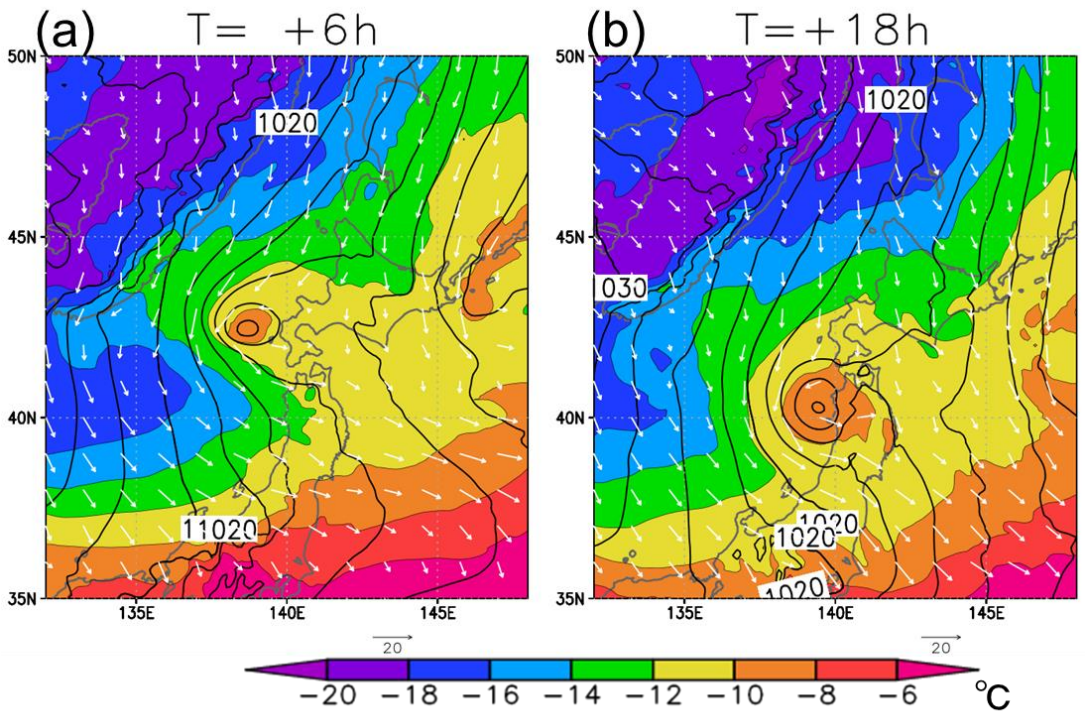

Fig. 5.5 SLP (contour; the contour interval is 2 hPa), temperature (color; °C) and horizontal wind (vector; m s^{-1}) at 850 hPa for NE_s.

A notable feature of the MV is the warm area around the center of the MV. To examine the formation processes of the warm area, we have conducted a backward trajectory analysis. A total of 98 parcels were distributed around the center of the warm area having temperature > −10 °C at 850 hPa at +6 hour (see Fig. 5.5a), and their backward trajectories are obtained for a period of 30 hours. The forth-order Runge–Kutta method with a time step of 30 seconds is adopted to calculate the movement of the parcel. The velocity components at each point on the trajectory are calculated every 30 seconds by linearly interpolating the model outputs stored every 1 hour spatially and temporally. The potential temperature, mixing ratio of water vapor, and equivalent potential temperature of the parcels are also calculated using the same interpolation method.

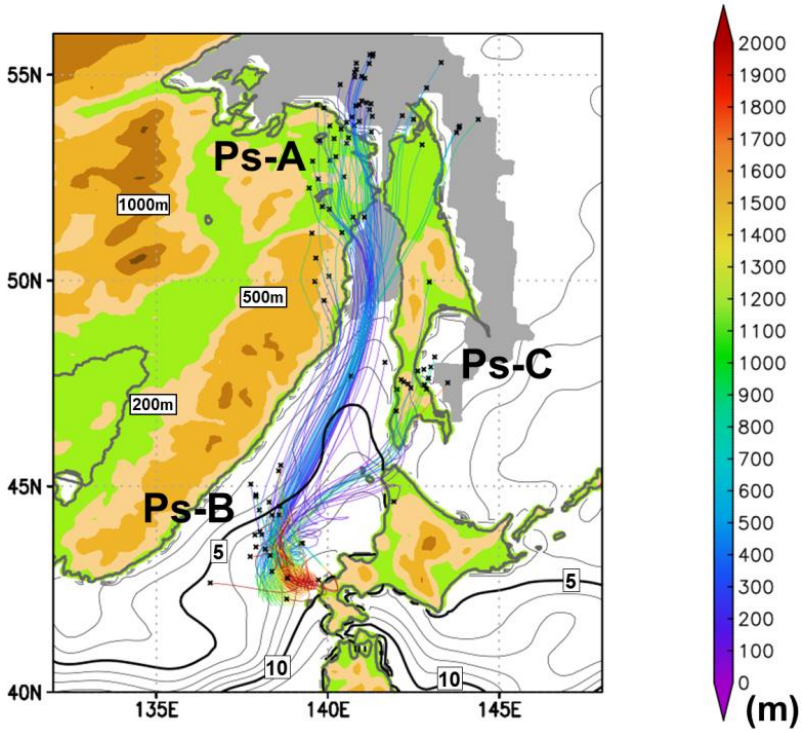

Fig. 5.6 Trajectories of the parcels between −24 hour and + 6 hour. Colors on each trajectory indicate parcel height. The black dots indicate the location of the parcels at −24 hour. The SST and topography are also drawn. The distribution of the sea ice is drawn by gray shade.

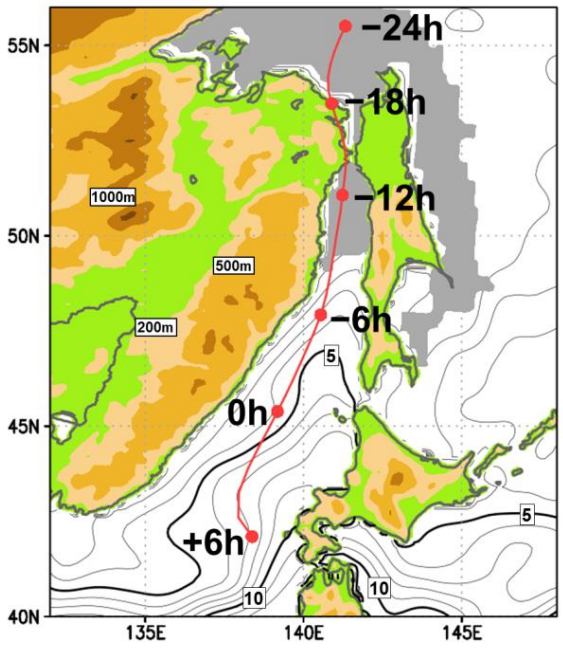

Fig. 5.7 A trajectory of a parcel of Ps-A between −24 hour and + 6 hour.

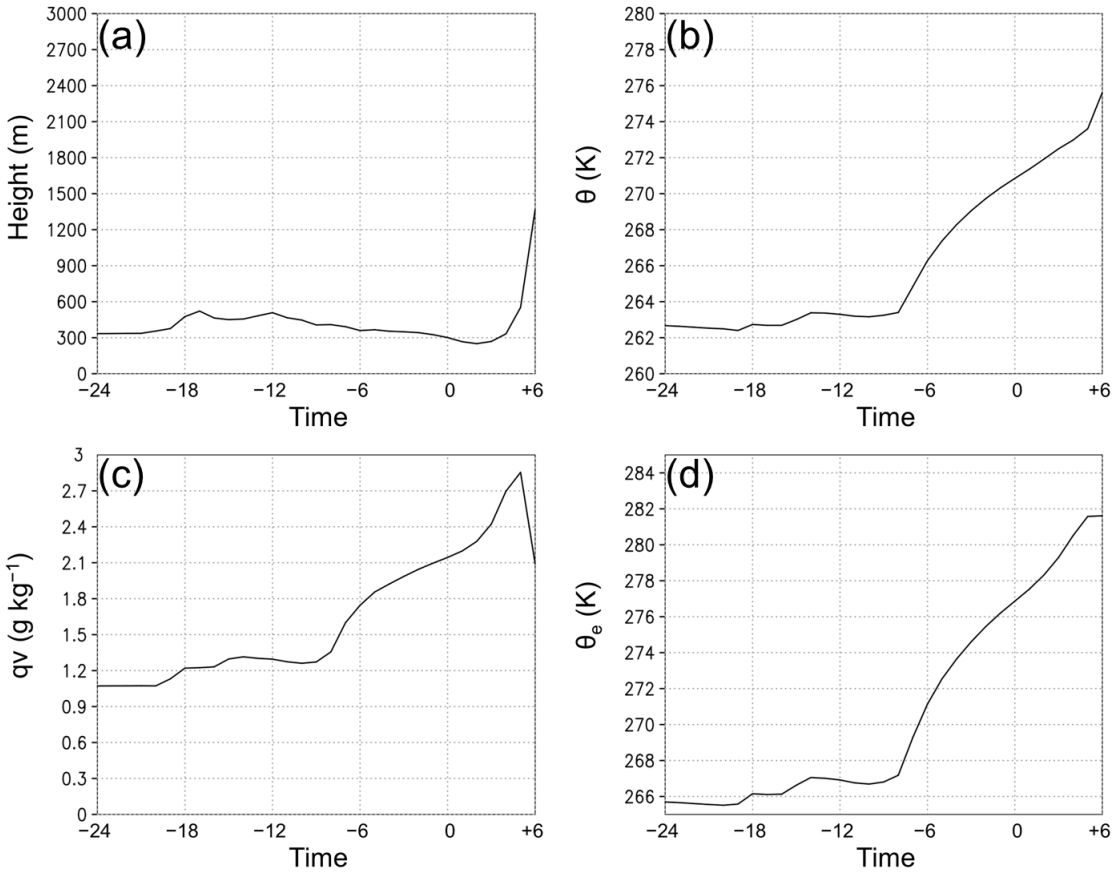

Fig. 5.8 Time series of (a) height, (b) potential temperature, (c) mixing ratio, and (d) equivalent potential temperature of the parcel shown in Fig. 5.7.

Figure 5.6 shows the trajectory of the parcels. More than a half of parcels coming into the warm area are found to pass through the low-level over the Strait of Tartary (Ps-A), where the SST is relatively high. About a quarter of the parcels is originally located to the west of Hokkaido Island and moves with the MV (Ps-B), while the other parcels comes from the southern part of Sakhalin (Ps-C). It should be noted that no parcel directly comes from over the Asian Continent. This is due to the blocking of cold air by the mountains along the coast of the continent, which is higher than 1000 m.

Since the Ps-A make largest contribution to formation of the warm area, they are examined in more detail. Figure 5.7 shows a trajectory of a typical parcel of Ps-A. It is located over the sea ice in the Okhotsk Sea at −24 hour and moves over the sea ice in the Strait of Tartary until −8 hour. Then it goes over the open ocean having high SST. The parcel remains below 600 m through this period except the last two hours when it is elevated by the updraft associated with cumulus convection (Fig. 5.8a). The potential temperature and mixing ratio of water vapor of the parcel scarcely increase when it is above the sea ice. Once it comes over the open ocean, they increase gradually due to sensible and latent heat fluxes from the sea surface (Fig. 5.8b-c). The potential temperature and mixing ratio of water vapor of the parcel rise 10 K and 1.5 g kg^{-1}, respectively, during 12 hours. This corresponds to 15 K increase of equivalent potential temperature (Fig. 5.8d). Thus, the flux from relatively warm sea surface in the Strait of Tartary seems important or the formation of the warm area and development of the MV.

In order to examine the contribution of the factors such as condensational heating, warm SST and topography, we have performed a set of sensitivity experiments. The control experiment is the numerical simulation for NE_s (CNTL). The setting of the sensitivity experiments are summarized in Table 5.1: To examine the contribution of

condensational heating at initial and mature stages of the MV, we design two DRY experiments (DRY_T−24 and DRY_T0). In these two experiments, calculations are started with full physics at −48 hour, but the effect of moisture is switched off after −24 hour and 0 hour in DRY_T−24 and DRY_T0, respectively. To evaluate the sensitivity to the warm SST in the Strait of Tartary, SST and/or distribution of sea ice are changed (SST−5, ICE, and SST−5_ICE). In the SST−5 experiment, the SST of the Sea of Japan for latitude > 42°N is decreased by 5 °C (Fig. 5.9a). In the ICE experiment, the Strait of Tartary for the latitude > 46°N is covered by sea ice (Fig. 5.9b). In the SST−5_ICE experiment, both the SST and the distribution of the sea ice are changed (Fig. 5.9c). To evaluate the effect of the mountains along the eastern coast of Asian Continent, an experiment without the mountains is performed (No_Mt). In the No_Mt, the elevation of the mountain where the elevation is higher than 100 m is reduced to 100 m (Fig. 5.9d). To evaluate the development of the MV, an average vorticity within 150 km radius from the center of the MV between 950 and 850 hPa is calculated for each experiment (Fig. 5.10).

Table 5.1 Configuration of the sensitivity experiments for NE_s

Experiment	Configuration
CNTL	Control simulation including all the physical processes.
DRY_T−24	No moisture after −24 hour
DRY_T0	No moisture after 0 hour
SST−5	The SST of the Sea of Japan for latitude > 42°N is decreased by 5 °C
ICE	The Strait of Tartary for the latitude > 46°N is covered by the sea ice
SST−5_ICE	The combination of SST−5 and ICE
No_Mt	No mountains along the eastern coast of the Asian continent

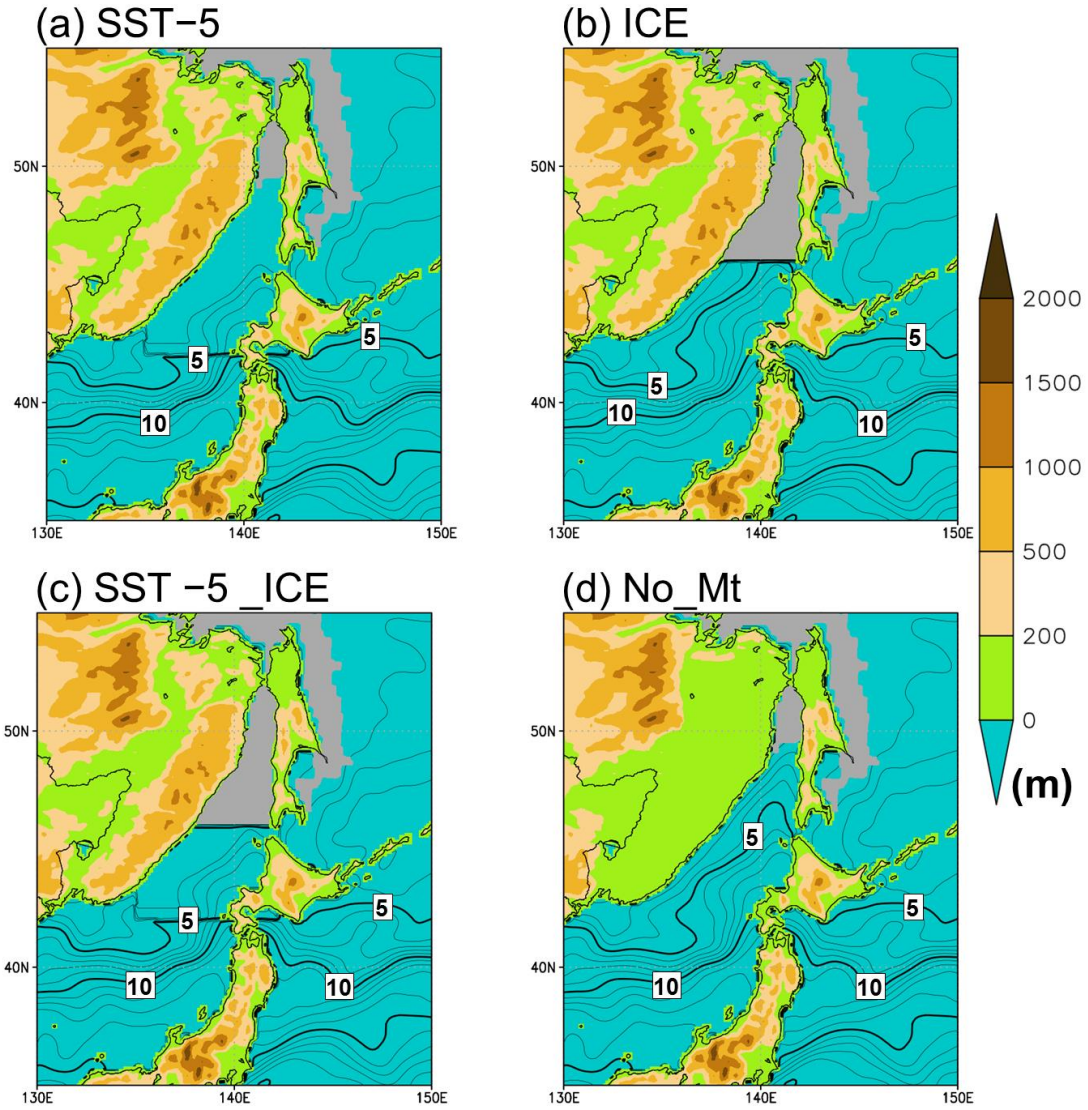

Fig. 5.9 Topography (color; m), SST (contour; the contour interval is 1 ℃) and distribution of Sea ice (gray shade) used in the sensitivity experiments: (a) SST−5, (b) ICE, (c) SST−5_ICE, and (d) No_Mt.

In DRY_T−24 (Fig. 5.11a), although the surface trough exists, the MV does not develop at all. In DRY_T0, the MV weakens within 6 hours after condensational heating is switched off (Fig. 5.10 and Fig. 5.11b). These two experiments demonstrate that the condensational heating is crucial for both the generation and development of the MV. Without the condensational heating, the stretching of vorticity associated with cumulus convection does not occur and consequently the MV cannot form. In the

development stage, the condensational heating sustains the strong circulation of the MV. Moreover, the condensational heating destabilizes the atmosphere, which increases the effect of the upper-level PV anomaly at the low-level. Therefore, the baroclinic development also becomes less significant without the condensational heating.

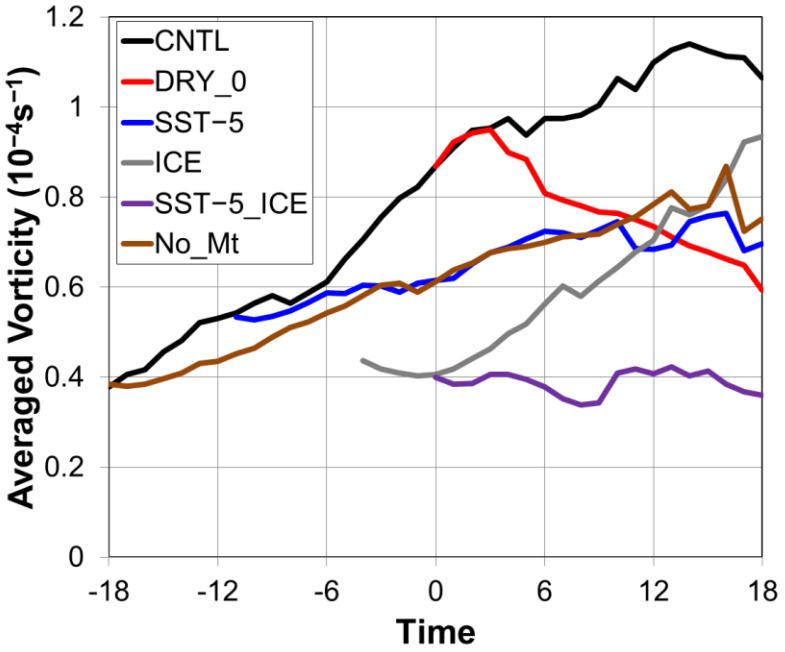

Fig. 5.10 Time series of average vorticity within 150 km radius from the center of the MV between 950 and 850 hPa for each experiment. The plot is started when the maximum vorticity of the MV exceeds 2.0×10^{-4} s^{-1}.

In the experiments in which SST and/or the distribution of sea ice are altered, the time of the generation of the MV is delayed and its location becomes more southward than CNTL (Fig. 5.11c-e). The surface temperature of the ocean is low in the order of SST−5_ICE, ICE, and SST−5. The initiation of the MV becomes late in this order. Since the surface fluxes in these three experiments are less than in CNTL, the atmosphere is more stable and cumulus convection is suppressed. Therefore the initiation of the MVs shifts later and further south.

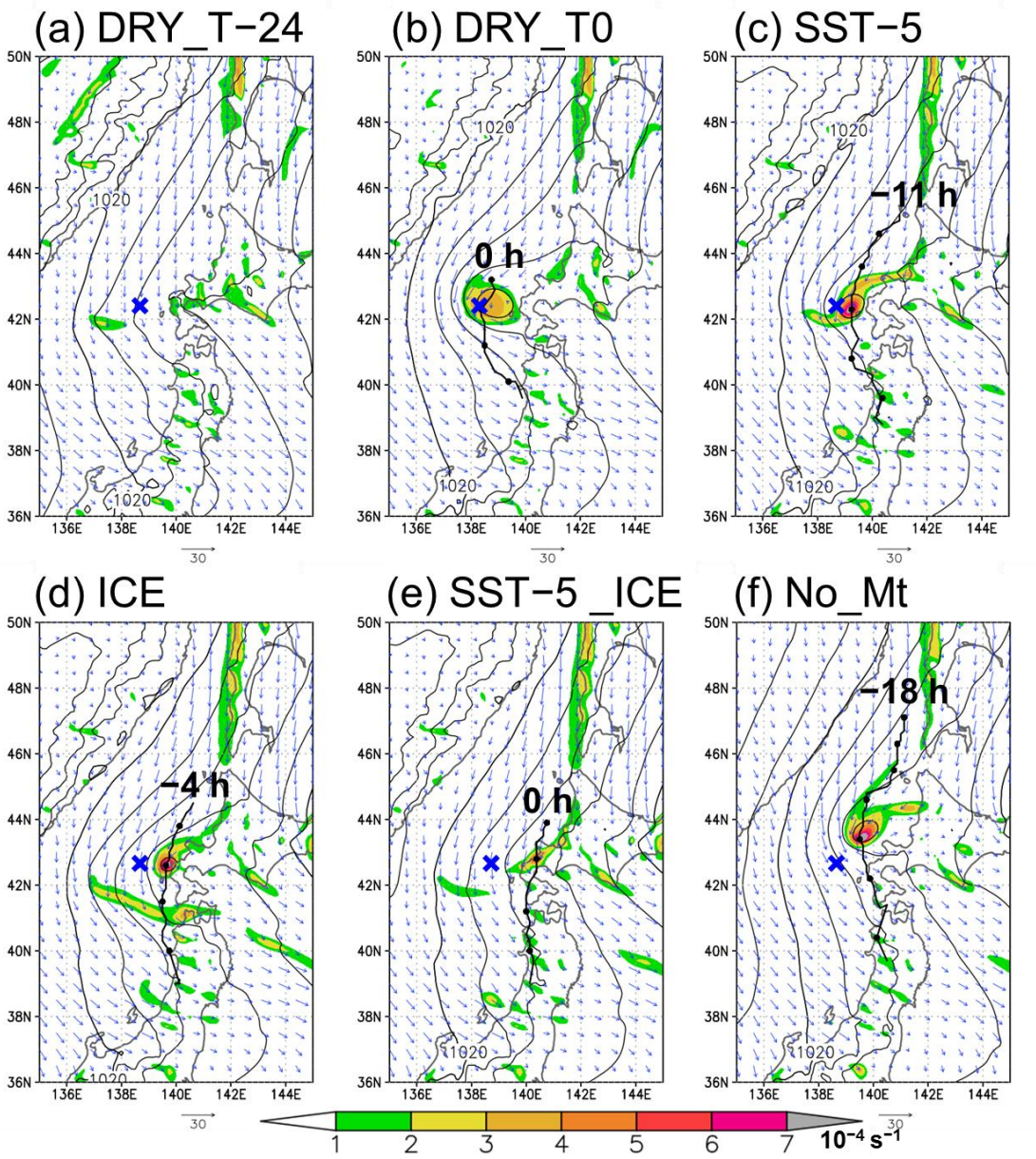

Fig. 5.11 SLP (contour; the contour interval is 2 hPa), vorticity (color; 10^{-4} s^{-1}) and horizontal wind (vector; m s^{-1}) at 950 hPa at + 6 hour in the sensitivity experiments. The tracks of the MVs are drawn with the time of the genesis of the MVs. The dots in the tracks are plotted in every 6 hour. The blue crosses indicate the location of the MV at + 6 hour in CNTL. (a) DRY_T− 24, (b) DRY_T0, (c) SST−5,, (d) ICE, (e) SST−5_ICE, and (f) No_Mt.

The MV in SST−5, the development of the MV is moderate compared with CNTL (Fig. 5.10). Although the formation of the MV in ICE occurs considerably later than in SST−5, its development is faster than in SST−5 due to warm SST of the Sea of Japan to

the west of Hokkaido Island. The MV in SST−5_ICE is quite weak and hardly develops. The warm area associated with the MV in these experiments is also weaker (not shown). The backward trajectories of the parcels coming into the warm areas of the MVs are also calculated for these experiments. Although the most of the parcels come from north as in CNTL, the potential temperature and mixing ratio does not increase as much as in CNTL (not shown). These findings suggest that the warm SST of the Sea of Japan to the west of Hokkaido Island as well as the Strat of Tartary makes favorable condition for the development of MV to the west of Hokkaido Island. It is noteworthy that the track of the MV shifts eastward as the MV becomes weaker. Since the convection is more active in the west side of the MV (Fig. 5.4a), the MV tends to move westward as the convection becomes stronger.

The MV in No_Mt is weaker than CNTL at + 6 hour (Fig. 5.11 f). Although the MV is generated at almost similar timing to CNTL, the development of the MV is moderate compared with CNTL (Fig. 5.10). The backward trajectory analysis shows that some parcels at the low-level around the center of the MV are originated from the low-level over the Asian Continent (not shown). Although such parcels also receive fluxes from the sea surface, they are somewhat colder and less humid than the parcels passing over the Strat of Tartary (not shown). Therefore, the atmosphere is more stable than in CNTL and cumulus convection is less active than in CNTL (not shown). Thus, the mountains along the eastern coast of the Asian Continent also make favorable conditions for the development of the MV to the west of Hokkaido Island. Note that the weaker convection and stronger low-level westerly from Asian Continent shift the track of the MV in No_Mt eastward from that of CNTL.

5.4.2 The MVs in NW_se and NW_e

The simulation for NW_se reproduces both an eastward moving MV (MV-e) and a southeastward moving MV (MV-se) (Fig. 5.12). Therefore, we analyze MVs in NW_se and NW_e using this simulation. A shear zone appears between northeasterly and west-southwesterly winds in the northwestern part of the Sea of Japan at −24 hour (Fig. 5.12a). The shear zone undulates and its eastern part becomes a meso-α-scale low pressure area (hereafter referred to as MAL) (Fig. 5.12b). The MV-e is generated at the western edge of a trough which extends from the MAL (Fig. 5.12 c-d). Subsequently to the MV-e, the MV-se forms within a strong horizontal shear at the northwestern corner of the Sea of Japan at −12 hour (Fig. 5.12c). A distinct shear zone extends toward east from the MV-se, whereas a weak shear zone also forms to the northwest of the MV-se (Fig. 5.12e-g). Thus, the MV-e and MV-se are closely related to the shear zone. This shear zone corresponds to the JPCZ.

Figure 5.13 shows temperature and geopotential height field at 850 hPa. The MV-e is located at the confluence of two streams from north and west (Fig. 5.13a). The direction of isohypse changes around the MV-e from east-southeastward to east-northeastward. The shear zone is almost parallel to the isohypse, although its eastern side is somewhat more tilted. The MV-se is also collocated with the confluence of the two streams where the isotherm bends almost 90-degree (Fig. 5.13b). The isohypse also curves from southeastward to east-southeastward. The shear zone around the MV-se is also parallel to the isohypse. Note that the horizontal warm advection is collocated with the MAL (Fig. 5.13a).

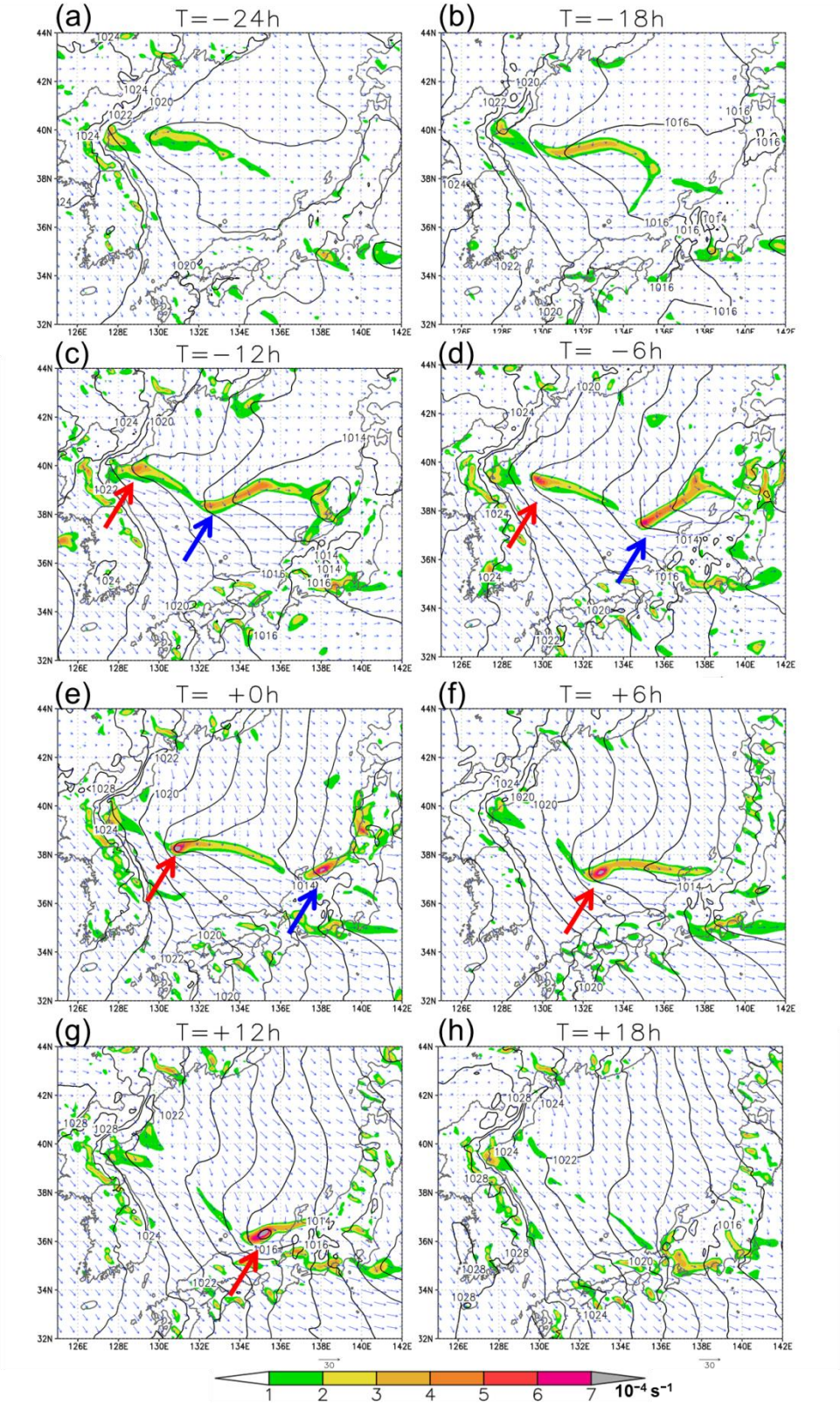

Fig. 5.12 As in Fig. 5.3 except for the NW_se. The MV-e and MV-se are indicated by red and blue arrows, respectively.

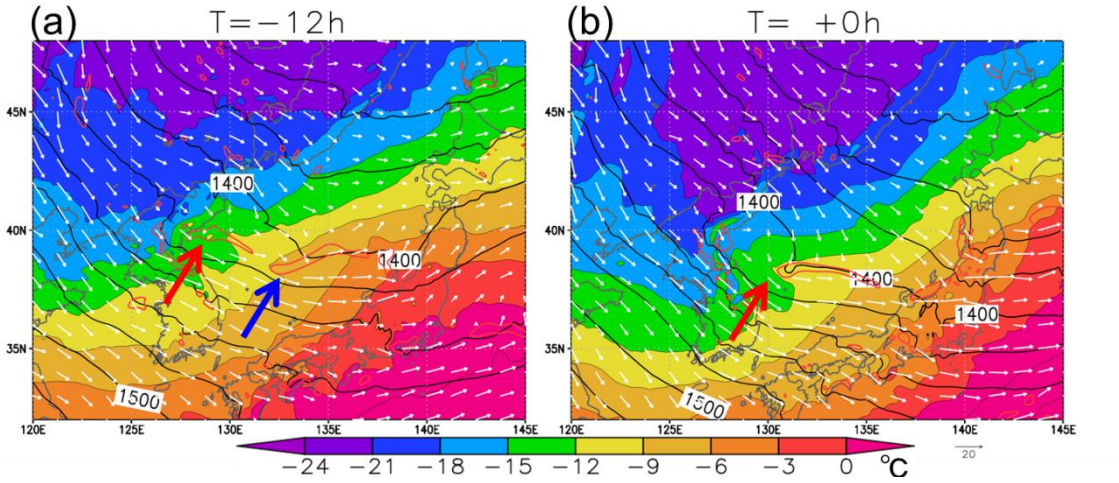

Fig. 5.13 Geopotential height (contour; the contour interval is 20 m), temperature (color; ℃) and horizontal wind (vector; m s^{-1}) at 850 hPa for NW_se. The contour of vorticity with 2.0×10^{-4} s^{-1} is drawn by red lines. The MV-e and MV-se are indicated by red and blue arrows, respectively.

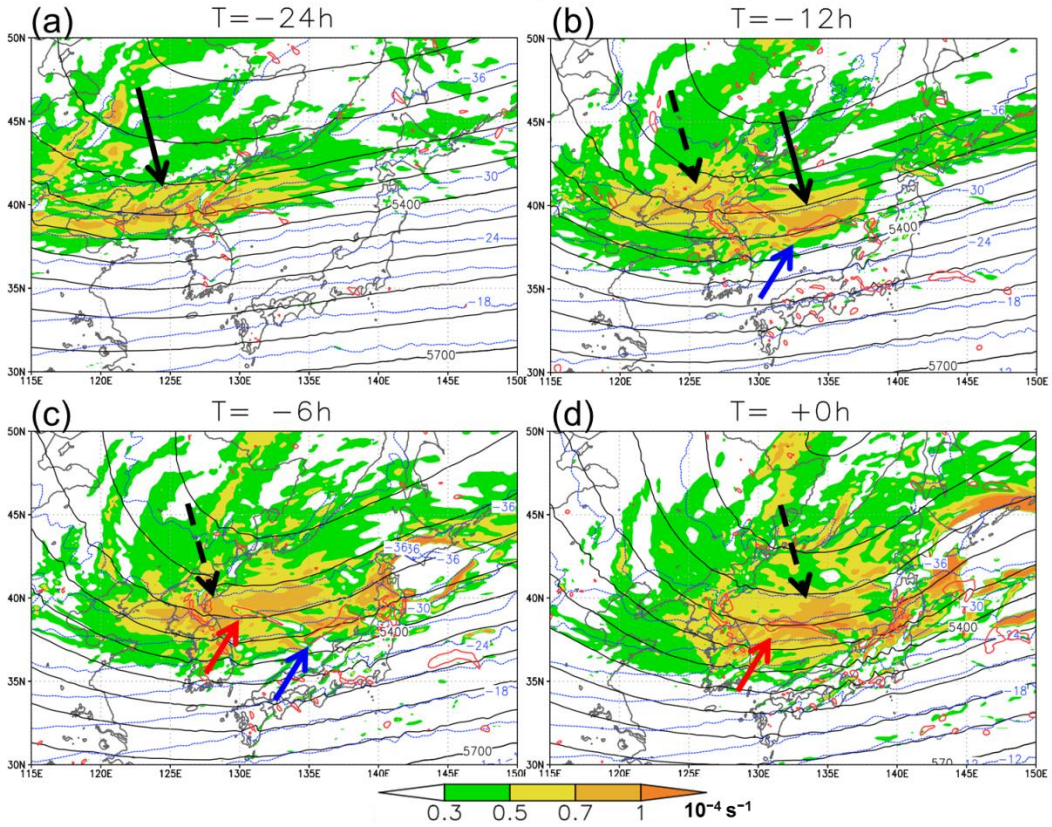

Fig. 5.14, Vorticity (color; 10^{-4} s^{-1}), geopotential height (black contour; the contour interval is 60 m), and temperature (blue contour; the contour interval is 3℃) at 500 hPa for NW_se. The contour of vorticity with 2.0×10^{-4} s^{-1} is drawn by red lines. The bold and broken arrows indicate the upper-level positive vorticity anomalies. The MV-e and MV-se are indicated by red and blue arrows, respectively.

To examine the relationship between the MVs and upper-level structure, Fig. 5.14 shows vorticity, temperature and geopotential height field at 500 hPa. The MV-e and the MAL are generated when a positive vorticity anomaly (indicated by bold arrows in Fig. 5.14) approaches the shear zone (Fig. 5.14a). Although the MAL is located to the east of the vorticity anomaly, which is favorable for the baroclinic development, the MV-e is located slightly south of the vorticity anomaly (Fig. 5.14b-c). The MV-se is also generated when another peak of positive vorticity anomaly (indicated by broken arrows in Fig. 5.14) approaches the shear zone (Fig. 5.14b). At 0 hour, however, it is almost right below the upper-level vorticity anomaly and is located under the colder air than MV-e (Fig. 5.14d), which is favorable for cumulus convection.

As shown in the above, the MVs are closely associated with the shear zone (JPCZ). By the sensitivity experiments, Nagata et al. (1986) and Nagata (1991) showed that the JPCZ is formed due to both the blocking by the mountains at the north of the Korean Peninsula (hereafter referred to as Mt-P) and thermal contrast between the Korean Peninsula and the Sea of Japan. We have performed similar sensitivity experiments for the effect of the Mt-P and Korean Peninsula as well as sensitivity experiments for the condensational heating.

The control experiment is the numerical simulation for NW_se (CNTL). The setting of the sensitivity experiments are summarized in Table 5.2: To evaluate the effect of the Mt-P, experiments with modified topography are performed (Mt500, and Mt1000). In these experiments, the elevation of the Mt-P where the elevation is higher than 500 (1000) m is reduced to 500 (1000) m (Fig. 5.15 a-b). To evaluate the effect of the Korean Peninsula, an experiment in which the Korean Peninsula is changed to ocean is conducted (No_K) (Fig. 5.15c). To examine the contribution of condensational heating

for both MV_e and MV_se, we design two DRY experiments (DRY_T−24 and DRY_T−12). In these two experiments, calculations are started with full physics at −48 hour, but the effect of moisture is switched off after −24 hour and −12 hour in DRY_T−24 and DRY_T−12, respectively. These timings correspond to the generation of MV-e and MV-se, respectively.

Table 5.2. Configuration of the sensitivity experiments for NW_se

Experiment	Configuration
CNTL	Control simulation including all the physical processes.
DRY_T−24	No moisture after −24 hour
DRY_T−12	No moisture after −12 hour
Mt500	The elevation of Mt-P is reduced to 500 m.
Mt1000	The elevation of Mt-P is reduced to 1000 m.
No_K	The Korean Peninsula is changed to ocean.

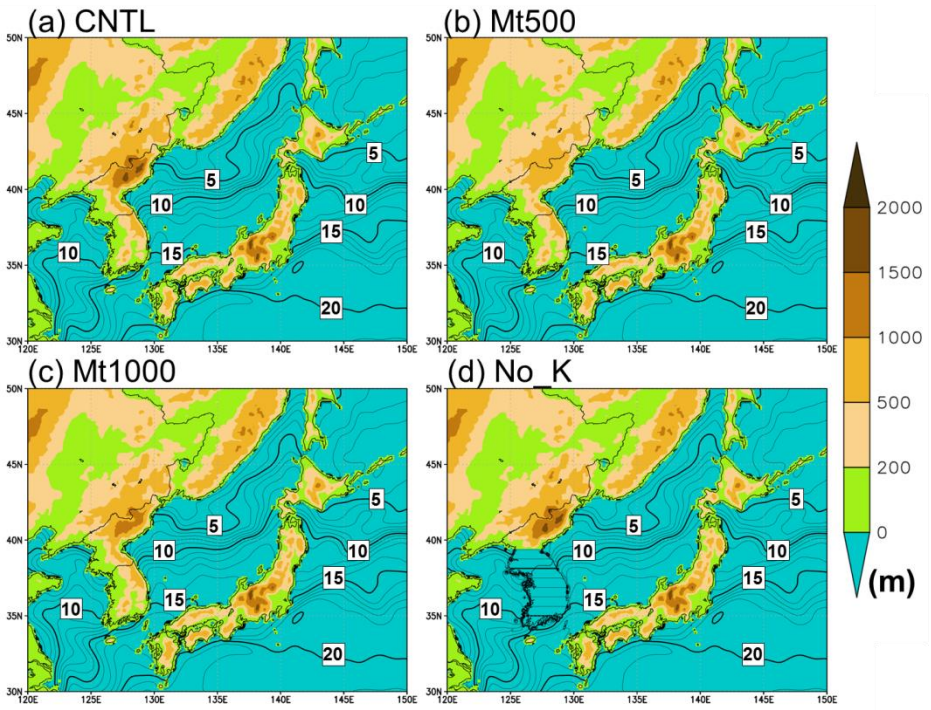

Fig. 5.15 Topography (color; m) and SST (contour; the contour interval is 1 °C) used in the sensitivity experiments: (a) CNTL, (b) Mt500, (c) Mt1000, and (d) No_K.

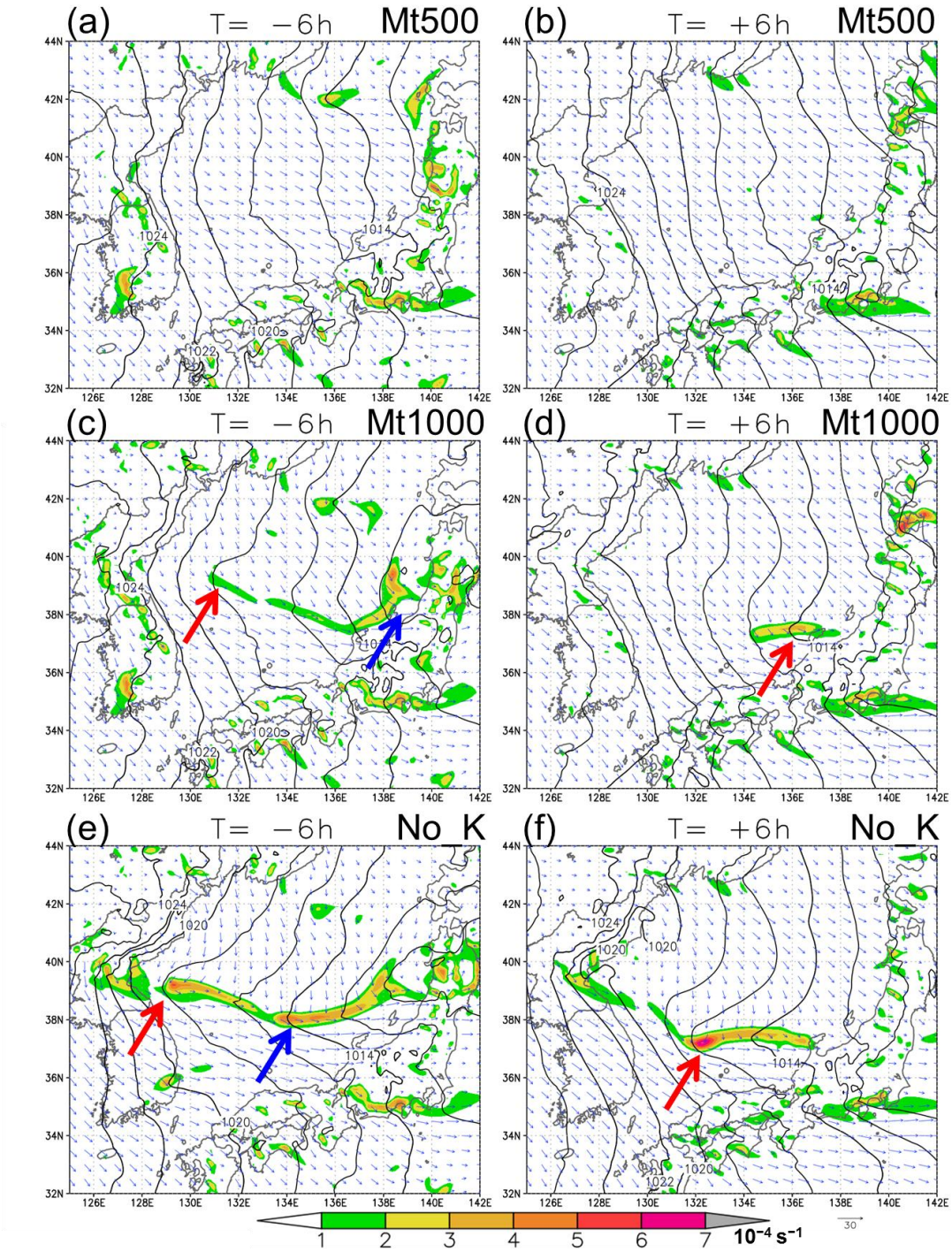

Fig. 5.16 As in Fig. 5.3 except for the sensitivity experiment at −6 and + 6 hour: (a), (b) Mt500, (c), (d) Mt1000, and (e), (f) No_K. The MV-e and MV-se are indicated by red and blue arrows.

In the Mt500, neither MV_e nor MV_se is generated (Fig. 5.16a-b). The shear zone and the MAL do not form, either. On the other hand, in the Mt1000, the MV-e and MV-se are generated as well as the shear zone although they are quite weak (Fig. 5.16c-d). To examine the difference between these two experiments, we calculate the Froude number ($Fr=U/NH$) at the upstream side of the mountains (averaged in 122°E-126°E and 43°N-46°N). Here U is velocity averaged between 950 and 850 hPa, N is Brunt-Vaisala frequency between 950 and 850 hPa, and H is the height of the mountain. If the Fr is larger than 1, the flow can climb over the mountain (Smolarkiewicz and Rotunno 1989, 1990). The time-averaged Fr for H = 500m 1000m through the numerical simulation is 0.66 and 1.32. Therefore cold air climbs over the mountains in Mt500, while it goes around the mountain in Mt1000. These findings indicate that the role of the high mountains at the north of the Korean Peninsula is crucial for the formation of the JPCZ and MVs by separating the cold air flow.

To examine the behavior of the shear zone, Fig. 5.17 shows the difference of SLP (SLP_{diff}) between CNTL and Mt500 (CNTL-Mt500) together with streamline of horizontal wind averaged between 950 and 800 hPa in Mt500. The negative value of SLP_{diff} roughly corresponds to the position of the shear zone. At −24 hour, the low-level wind in Mt500 is westerly and the negative SLP_{diff} starts to extend eastward (Fig. 5.17a). As time elapse, the direction of the low-level wind in Mt500 over the Sea of Japan rotates anticyclonically (Fig. 5.17b-d). The area of negative SLP_{diff} follows the change of the wind direction. This suggests that the direction of the shear zone, which is closely related to the movement of the MVs, primarily corresponds to the large-scale wind at the low-level, which hits the mountains at the north of the Korean Peninsula.

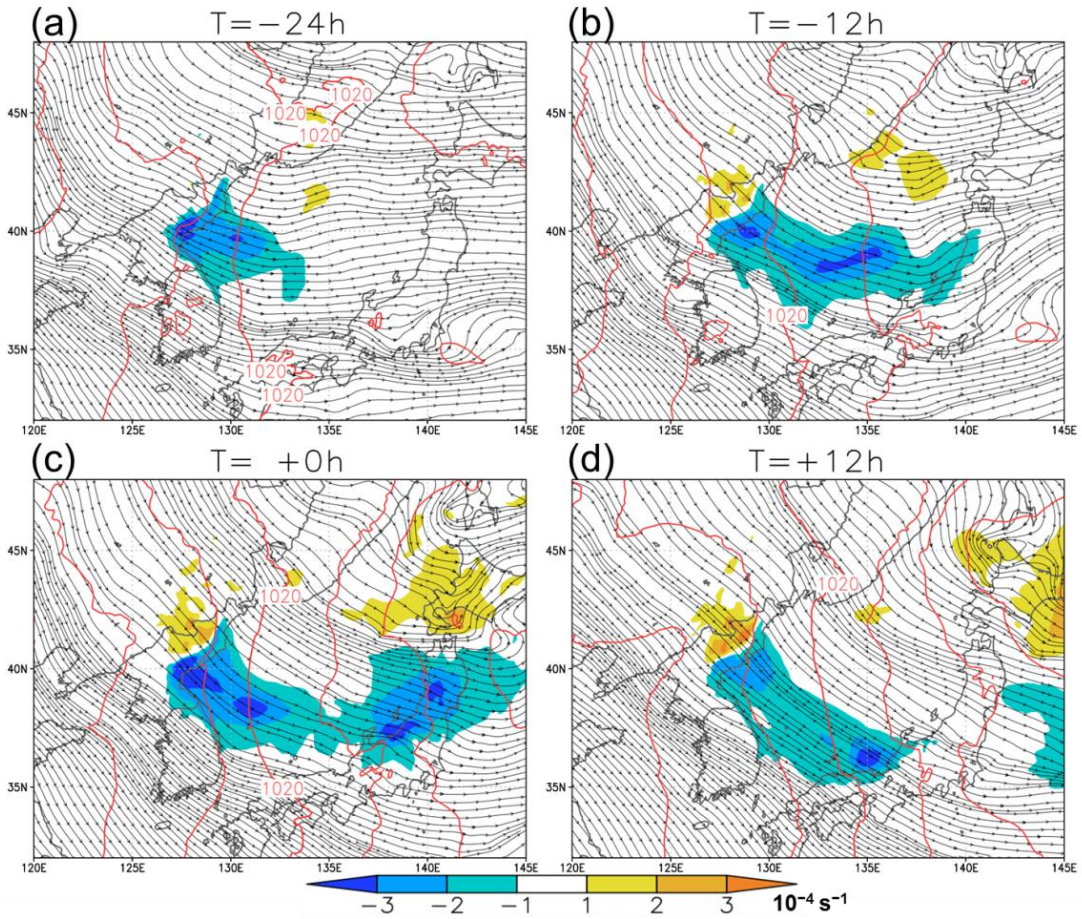

Fig. 5.17 The difference of SLP between CNTL and Mt500 (CNTL−Mt500) (color; hPa), streamline of horizontal wind averaged between 950 and 800 hPa in Mt500 (black line), and SLP in Mt500 (red contour; the contour interval is 2 hPa).

In the No_K, the MVs and shear zone are almost similar to the CNTL (Fig. 5.15e-f). Although the SLP_{diff} between CNTL and No_K is seen over the Korean Peninsula and over the western part of the Sea of Japan, it is not collocated with the shear zone (not shown). Thus, the thermal contrast between the Korean Peninsula and the Sea of Japan hardly contribute to the formation of the JPCZ, while the MVs and the mountains at the north of the Korean Peninsula are crucial. This result is different from Nagata et al. (1986) and Nagata (1991). This is likely to be due to coarse resolution of topography in their model, in which the elevation of the Mt-P is less than 1000 m. Therefore, the effect of the Mt-P is likely to be underestimated in their study.

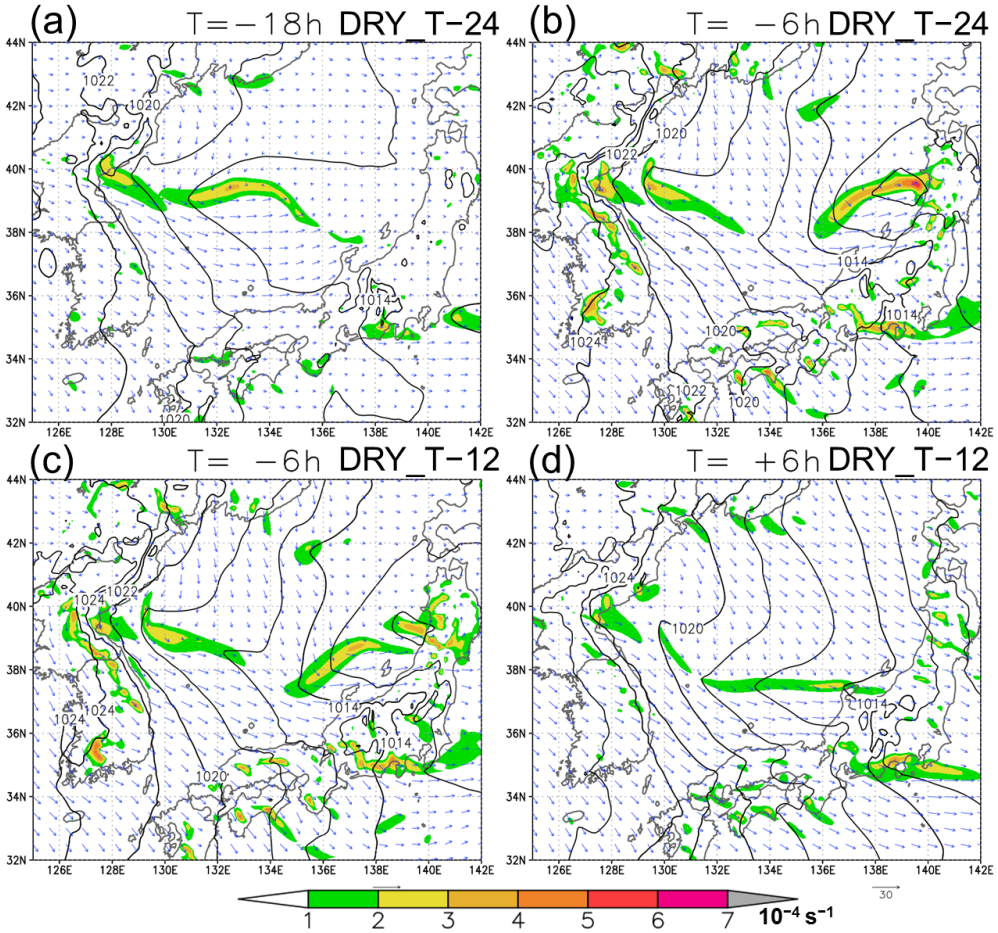

Fig. 5.18 As in Fig. 5.3 except for the dry sensitivity experiment: (a), (b) DRY_T−24, and (c), (d) DRY_T−12.

In DRY_ T−24, an undulation of the shear zone is seen at −12 hour (Fig. 5.18a). It then develops into a MAL (Fig. 5.18b). The behavior of the MAL is almost similar to the CNTL. The warm advection around the MAL also exists in DRY_ T−24 (not shown). Therefore, once the MAL forms, it can develop baroclinically without condensational heating. In DRY_T-24, however, the MV-e does not intensify, although the trough extends westward from the MAL (Fig. 5.18b). In DRY_ T−12, a bend of the shear zone is seen, but it does not develop into MV-se (Fig. 5.18c-d). These findings indicates that the initial disturbances of the MVs is dynamically generated in the strong horizontal shear associated the Mt-P, though the condensational heating is crucial to their development.

5.4.3 The MVs in SW_W

The simulation for SW_W reproduces two MVs moving south-southeastward (MV-sse) and east-southeastward (MV-ese) (Fig. 5.19). At −24 hour, a SLP trough extends from the northwestern corner of the Sea of Japan to the western part of Honshu Island (Fig. 5.19a). A weak horizontal shear is seen in the SLP trough at −18 hour (Fig.5.19b). The MV-sse appears in the SLP trough at around 129°E, 39°N (Fig. 5.19a-b). It moves south-southeastward as developing and finally lands on western part of Honshu Island (Fig. 5.19b-f). A weak shear zone extends north-northwestward from the MV-sse (Fig. 5.19e-f). At −12 hour, several peaks of vorticity appear within a shear zone which is collocated with the SLP trough (Fig. 5.19c). One of the vorticity peaks develops into the MV-ese (Fig. 5.19d). It moves east-southeast ward and finally lands on central part of Honshu Island (Fig. 5.19e-f). The MV-ese belongs to SW_W although its track is slightly different from typical MVs in SW_W.

The cold air outbreak is intense over the Yellow Sea and the Korean Peninsula, while it is weak over the Sea of Japan (Fig. 5.20). Therefore, the temperature over the Sea of Japan is relatively warm. The isohypses extend in more meridional direction around the Mt-P than those for NW_se. The SLP trough is collocated with the warm area and is almost parallel to the isotypes (Fig. 5.19). MVs form and develop in the warm area and the SLP trough.

In the upper-level, a positive vorticity anomaly passes over the Sea of Japan (Fig. 5.21). The positive vorticity anomaly exists over the Yellow Sea at −24 hour (Fig. 5.21a). The MV-sse forms at the front side of the positive vorticity anomaly at −18 hour (not shown). The vorticity anomaly comes into the Sea of Japan at −12 hour and the MV-ese forms slightly eastward of the vorticity anomaly (Fig. 5.21b-c). At 0 hour, the

MV-ese is located under the vorticity anomaly (Fig. 5.21d). Thus, the forcing of upper-level vorticity anomaly on the low-level shear associated with the SLP trough is significant for the development of MVs.

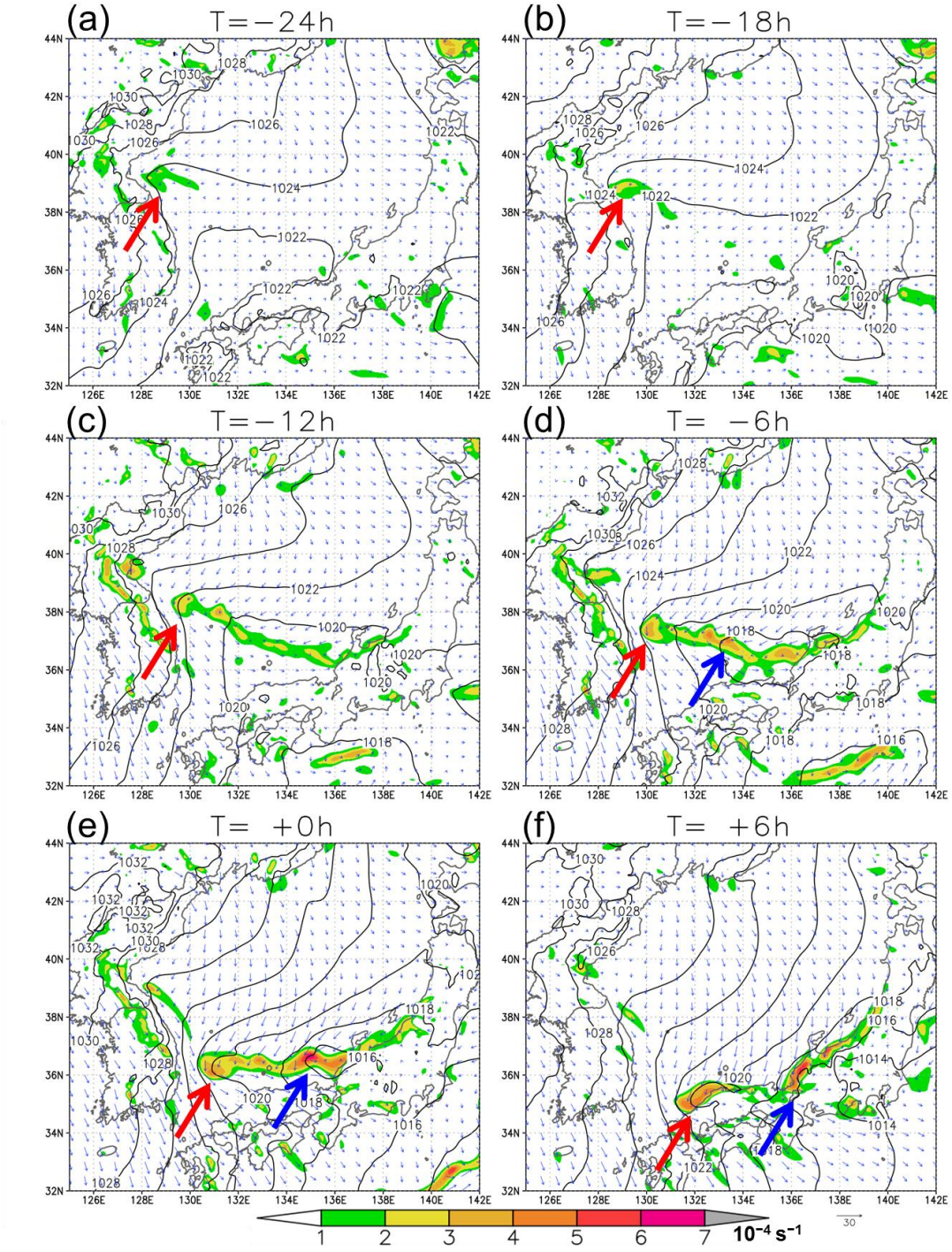

Fig. 5.19 As in Fig. 5.3 except for the SW_W. The MV-sse and MV-ese are indicated by red and blue arrows, respectively.

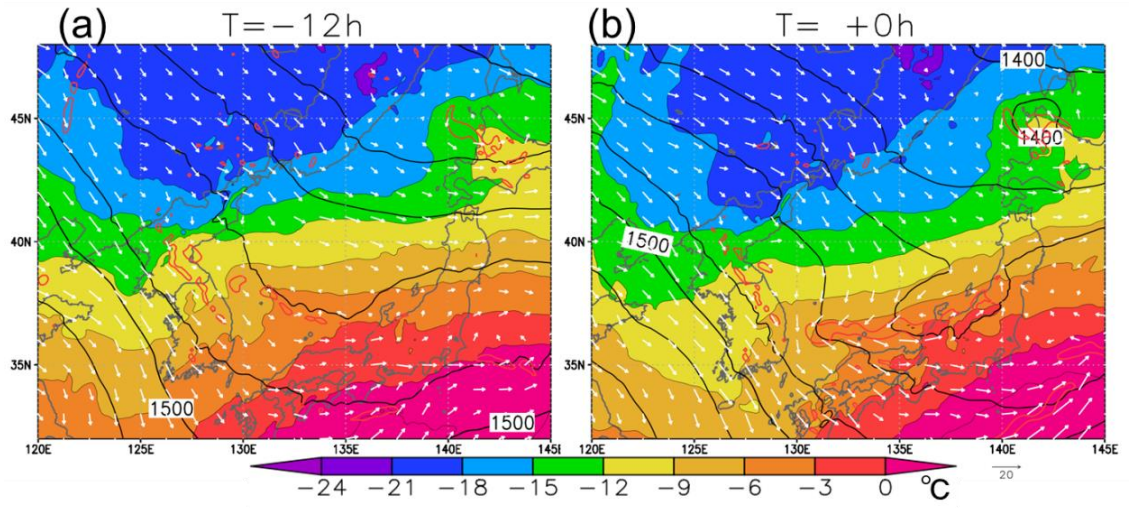

Fig. 5.20 As in Fig. 5.13 except for SW_W.

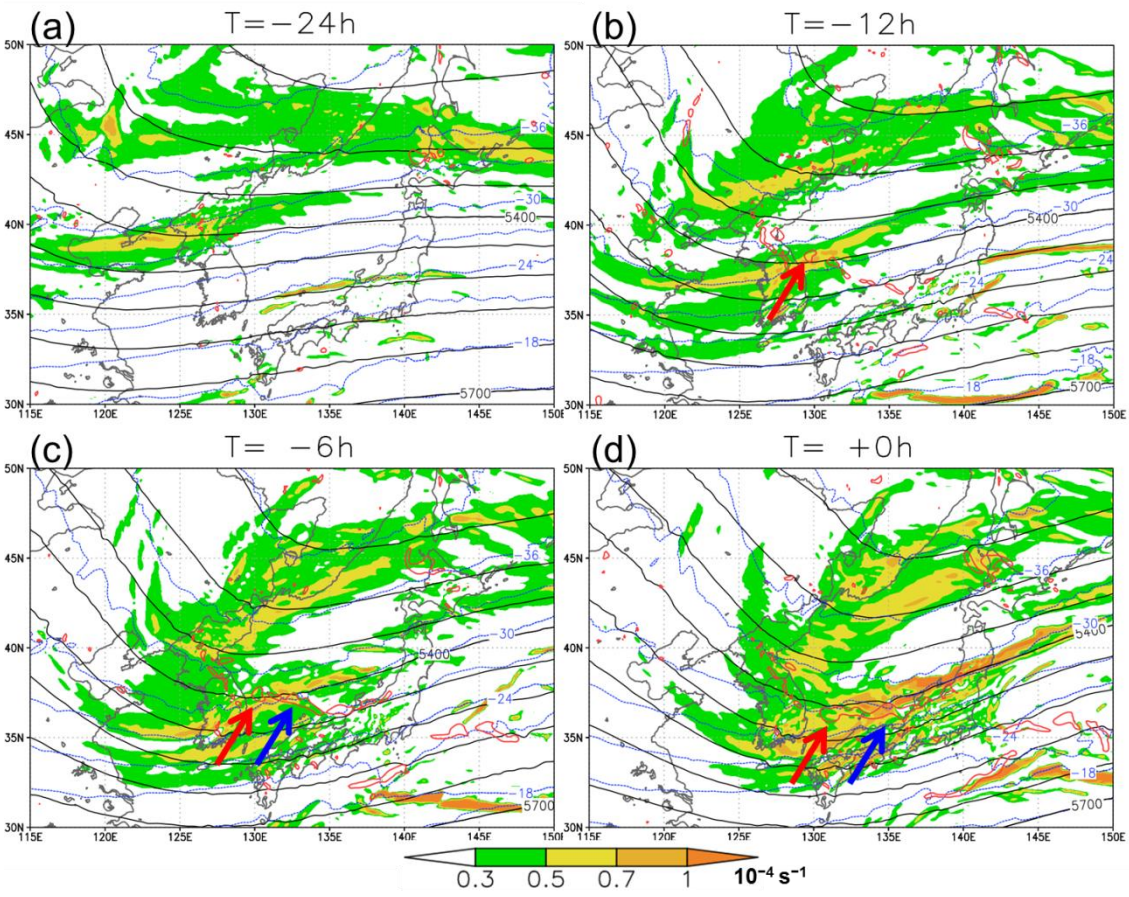

Fig. 5.21, As in Fig. 5.14 except for SW_W. The MV-sse and MV-ese are indicated by red and blue arrows, respectively.

In the composite field, the center of positive vorticity anomaly at the upper-level moves almost zonally over the southern part of the Korean Peninsula (see Fig. 4.39). On the other hand, the positive vorticity anomaly in the simulation moves southeastward over the Korean Peninsula. This might be due to smoothed upper-level structure in the initial field (see Fig. 4.39a) or due to forecasting error for the path of the upper-level trough. The different path of the upper-level vorticity shifts the tracks of the simulated MVs from those of typical MVs in SW_W.

To evaluate the factor that contributes to the development of the MVs, we have performed sensitivity experiments as in NW_se. In addition to the control simulation (CNTL), Mt500 and DRY_T−24 are conducted. The settings of these experiments are the same as those for NW_se.

In Mt500 (Fig. 5.22), the MV-sse does not form. However, the MV-ese weaker than in CNTL is generated near Honshu Island (Fig. 5.22c). A close look at isobars shows that the SLP trough disappears gradually from northwest to southeast. The MV-sse is not generated since the SLP trough disappears around the point of the genesis of the MV-sse before the upper-level vorticity anomaly approaches. On the other hand, the SLP trough remains around the location of the genesis of the MV-ese until the vorticity anomaly approaches. Therefore the MV-ese forms. These results confirm that the forcing of upper-level vorticity anomaly on the low-level shear associated with the SLP trough is important for the generation of MVs. The SLP_{diff} between CNTL and Mt500 reveals that the direction of SLP trough is parallel to the low-level wind direction around the Mt-P as in NW_se (not shown). In SW_W, the low-level wind direction is more meridional than that in NW_se, resulting in the shear zone extending in more meridional direction.

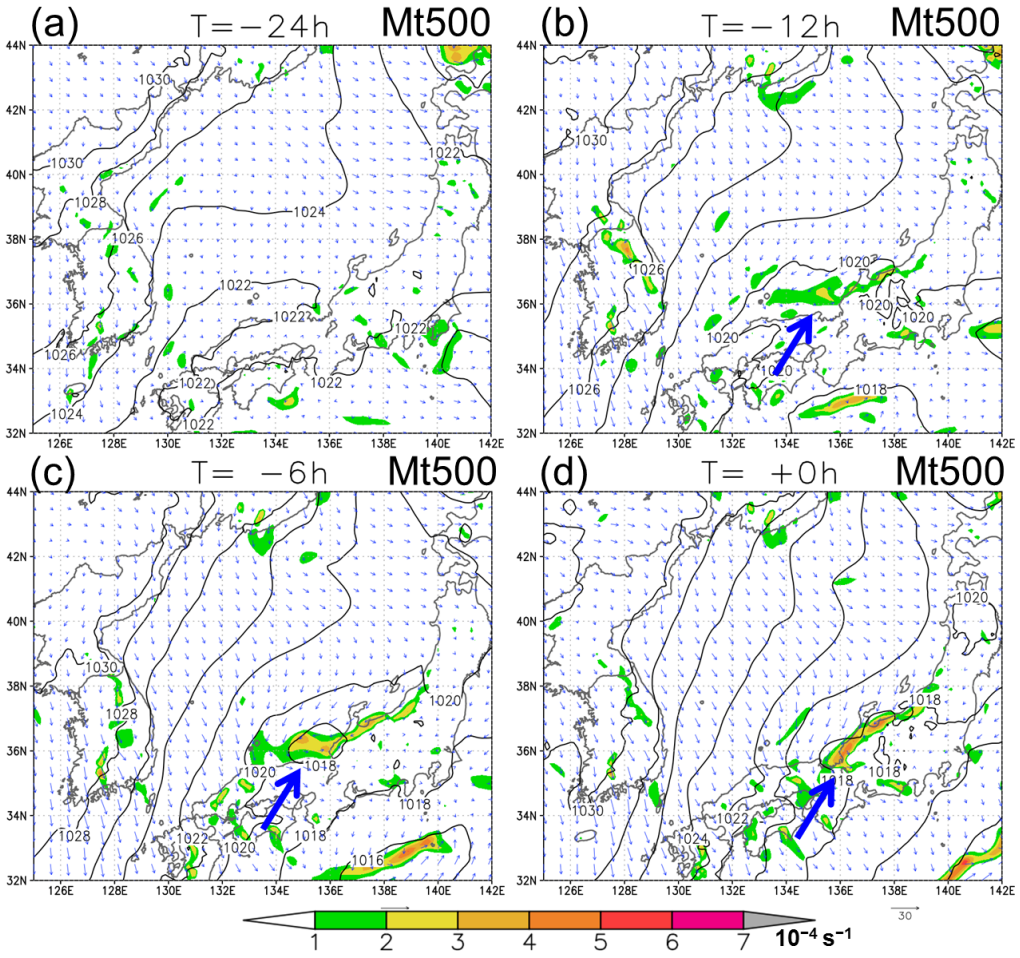

Fig. 5.22 As in Fig. 5.3 except for Mt500 for SW_W: The MV-sse is indicated by blue arrow.

In DRY_T−24 (Fig. 5.23), both MV-sse and MV-ese form. However, the MV-sse does not develop at all, while the MV-ese slightly develops. Since the upper-level vorticity anomaly is located right above the MV-sse at −12 hour (Fig. 5.21b), the baroclinic development of the MV-sse would be less significant after −12 hour. Therefore the MV-sse hardly develops after −12 hour. On the other hand, the MV-ese is located ahead of the upper-level vorticity anomaly. Therefore the MV-ese develops through baroclinic process. However, the MV-ese is quite weak compared with that in CNTL, which indicate that condensational heating is also important for the development of the MV-ese. Thus, both baroclinic process and condensational heating contribute to the development of the MVs in SW_W.

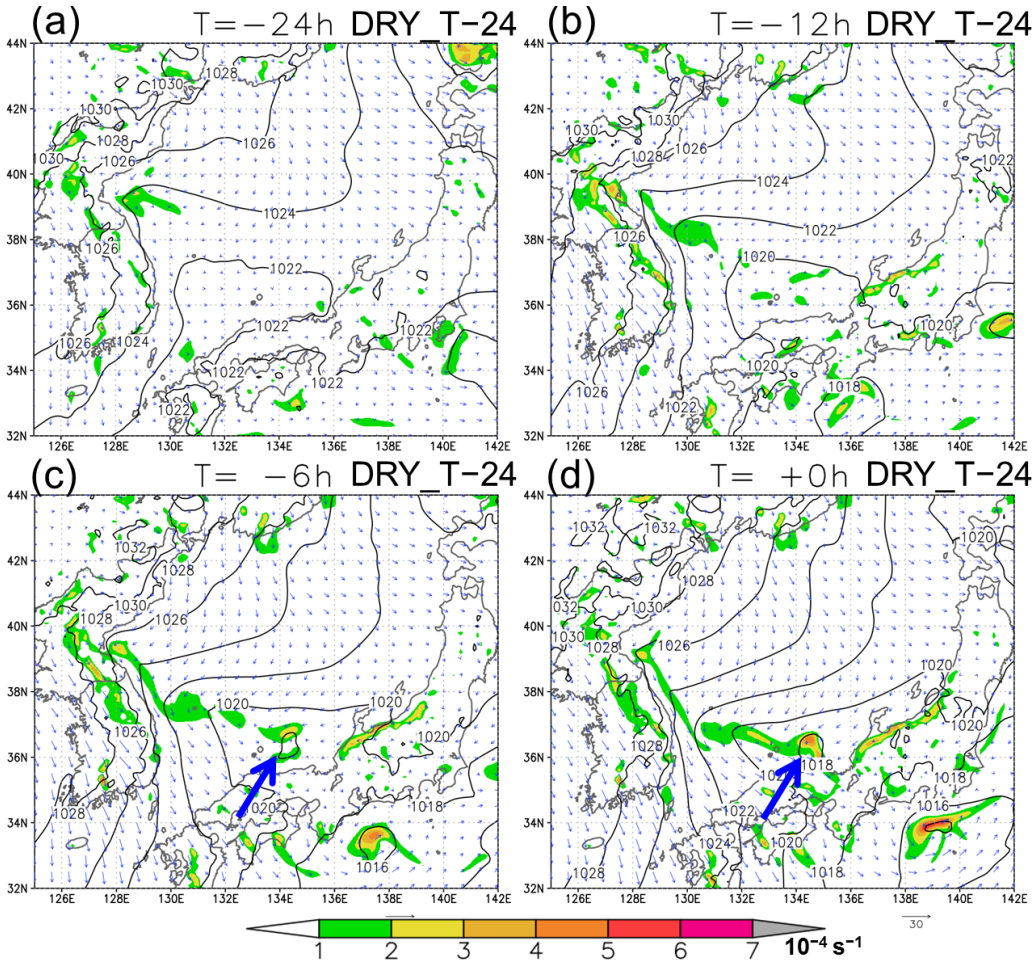

Fig. 5.23 As in Fig. 5.3 except for DRY_T−24 for SW_W: The MV-sse is indicated by blue arrow.

5.5 Discussion

5.5.1 The MVs in NE_s

In subsection 5.4.1, we have demonstrated that warm SST and blocking of cold air by the mountains at the eastern coast of the Asian Continent provide favorable condition for a MV to develop to the west of Hokkaido Island. The MV develops when a weak trough at the low-level comes into this area. The stretching of surrounding vorticity associated with this weak trough is significant for the generation of the MV. However, we have not clarified the formation mechanism of this trough. Here we consider the formation mechanism of the trough from a viewpoint of large-scale environment.

The notable features in the synoptic-scale environment for NE_s are the upper-level trough and the low-level warm and cold anomaly (see Fig. 4.5 and Fig. 4.6). To examine the effects of these structures, we have conducted a piecewise PV inversion (PPVI) analysis (Davis and Emanuel 1991). It enables us to evaluate geopotential height and temperature anomaly fields associated with specific PV anomalies (the inversion technique is described in detail in Davis and Emanuel 1991). In order to make a PPVI, one needs to define the mean and anomaly fields. In this study, they are calculated from the GANAL composite. In what follows, we evaluate the effects of the PV anomaly above 500 hPa (UL), which is associated with the upper-level trough, the PV anomaly between 925 hPa and 600 hPa (IL), which corresponds to inner-level PV anomaly, and the potential temperature anomaly at the surface (SFPT), which is associated with cold and warm air at the low-level.

Figure 5.24 shows the anomaly of geopotential height associated with each PV anomaly and the sum of all PV anomalies at −24 hour. The mean fields and the sum of the mean and anomaly of the geopotential height are also shown in Fig. 5.24. The distribution of the geopotential height anomaly for the sum of all PV anomalies well agrees with that of GANAL composite (not shown). The low-level trough to the west of Hokkaido Island is not seen in the mean field (black contours in Fig. 5.24). A negative height anomaly associated with UL is seen over the Sea of Japan (Fig. 5.24a). The sum of the anomaly and mean fields shows that a trough extends over the northeastern part of the Sea of Japan toward this negative height anomaly from the Aleutian Low. Although the positive anomaly associated with low-level cold air over the Asian Continent (Fig. 5.24c) weakens the negative height anomaly, the sum of all the PV anomalies causes the trough to the west of Hokkaido Island (Fig. 5.24d). The effect of

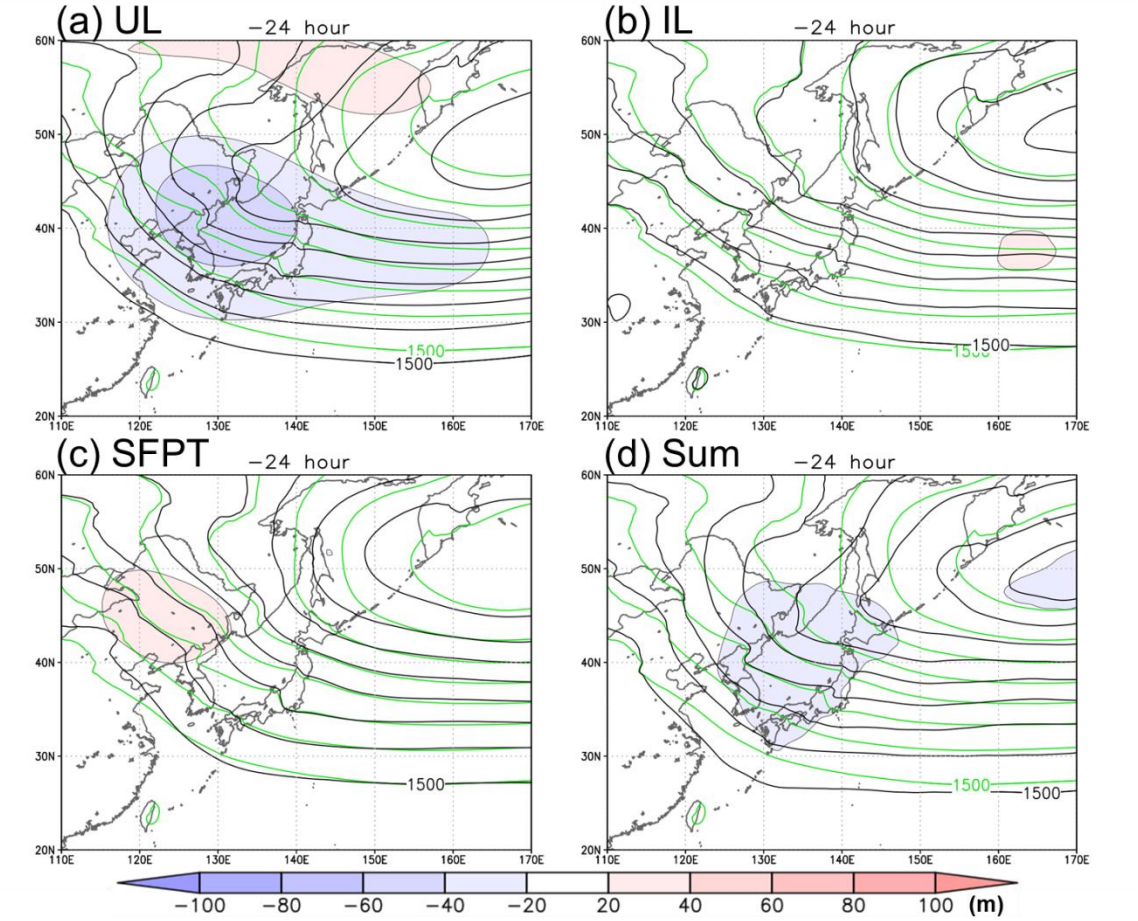

Fig. 5.24 Geopotential height anomalies (color; m), geopotential height of the mean field (black contour; the contour interval is 30 m), and the sum of the anomaly and the mean field (green contour; the contour interval is 30 m) at 850 hPa at −24 hour for NE_s. (a) UL (b) IL, (c) SFPT, and (d) sum of UL, IL, and SFPT.

IL gives only a minor contribution (Fig. 5.24b). Thus, the low-level trough that causes the genesis of the MV is mainly formed due to the approach of the upper-level trough.

5.5.2 The MVs in NW_se, NW_e, and SW_W

The MVs in NW_se, NW_e, and SW_W are closely related to the shear zone (JPCZ). The direction of the shear zone and movement of the MVs follow large-scale wind direction. Here we consider how the wind direction is determined by large-scale structures using a PPVI analysis.

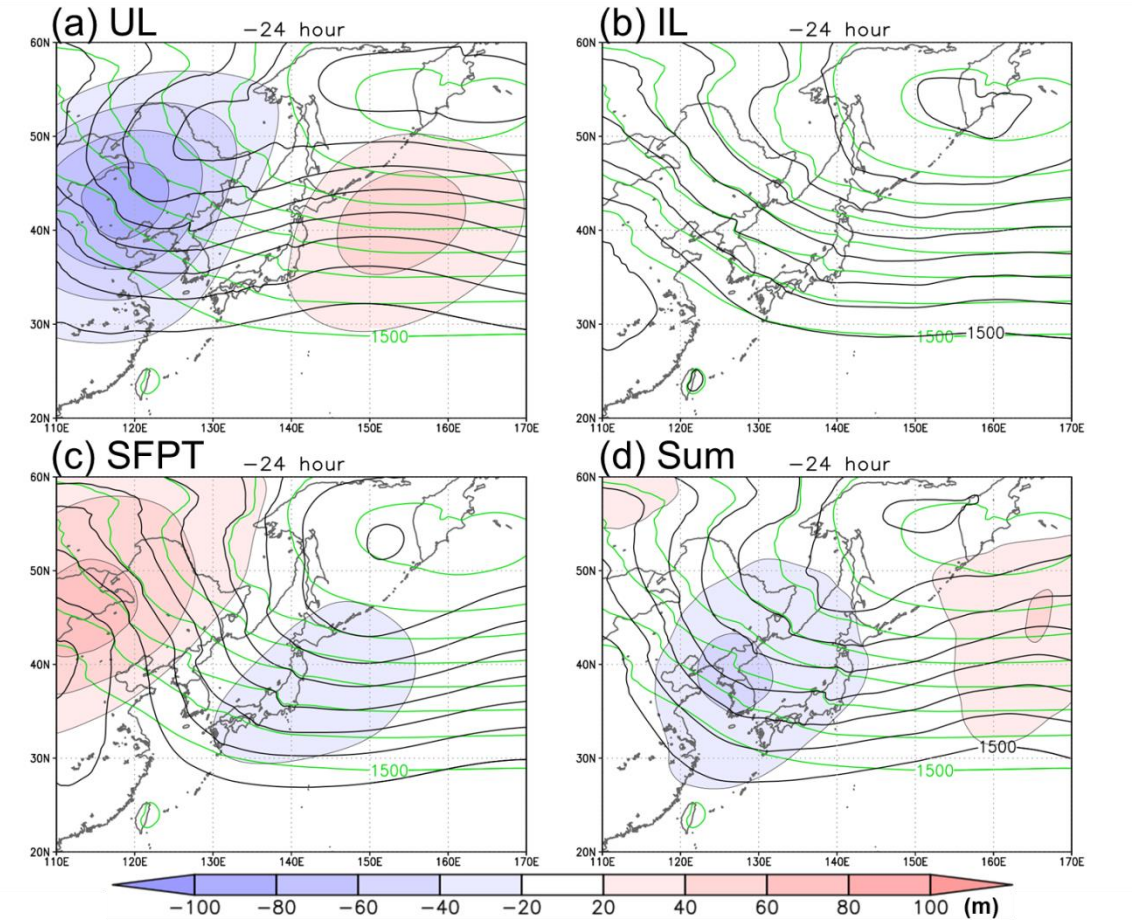

Fig. 5.25 As in Fig. 5.24 except for NW_se at −24 hour.

The negative height anomaly associated UL exists over the Asian Continent at −24 hour in NW_se, which causes the cyclonic rotation of isobars of the mean field over the Sea of Japan (Fig. 5.25a). The positive height anomaly of SFPT associated with low-level cold air over the Asian continent has an opposite effect to the UL (Fig. 5.25c). Since the anomaly due to UL is slightly larger than that due to SFPT, the isobars over the Sea of Japan rotate slightly cyclonically (Fig. 5.25d), which result in westerly over the Sea of Japan. Therefore the shear zone initially extends eastward (Fig. 5. 12a-b).

As time elapse, the negative height anomaly associated with UL moves into the Sea of Japan at 0 hour (Fig. 5.26a), which causes a deep trough over the Sea of Japan. The

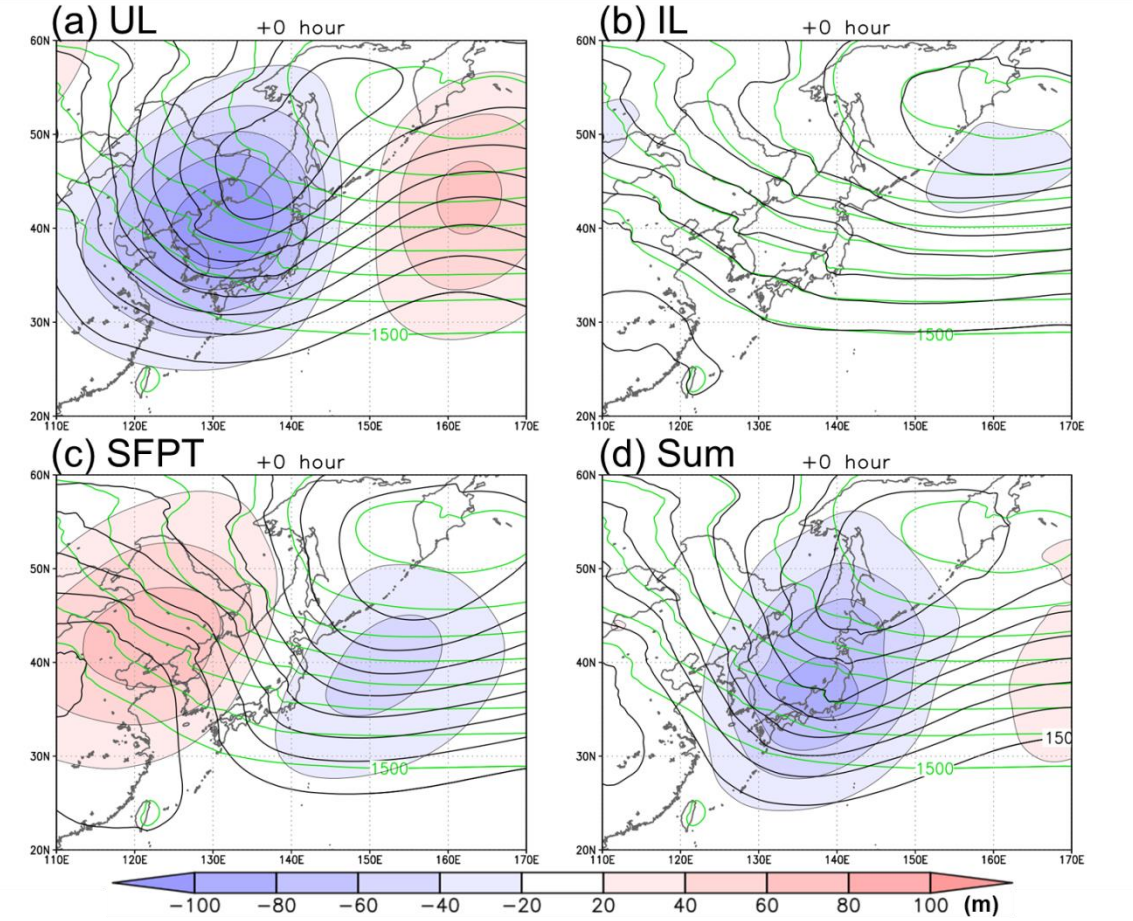

Fig. 5.26 As in Fig. 5.24 except for NW_se at 0 hour.

positive anomaly associated with SFPT remains over the Asian Continent at 0 hour (Fig. 5.26c). The sum of UL and SFPT cause negative height anomaly over Honshu Island (Fig. 5.26d). The isobars over the Sea of Japan extend in more meridional direction than those in the mean field. Therefore the shear zone also extends in the northwest-southeast direction and the MV in NW_se moves to the similar direction.

In contrast to NW_se, the negative height anomaly associated with UL passes over the Korean Peninsula in SW_W (Fig. 5.27a). Though the positive height anomaly associated with SFPT is located over the Asian Continent (Fig. 5.27c), their sum result in negative height anomaly to the south of Korean Peninsula (Fig. 5.27d). If this

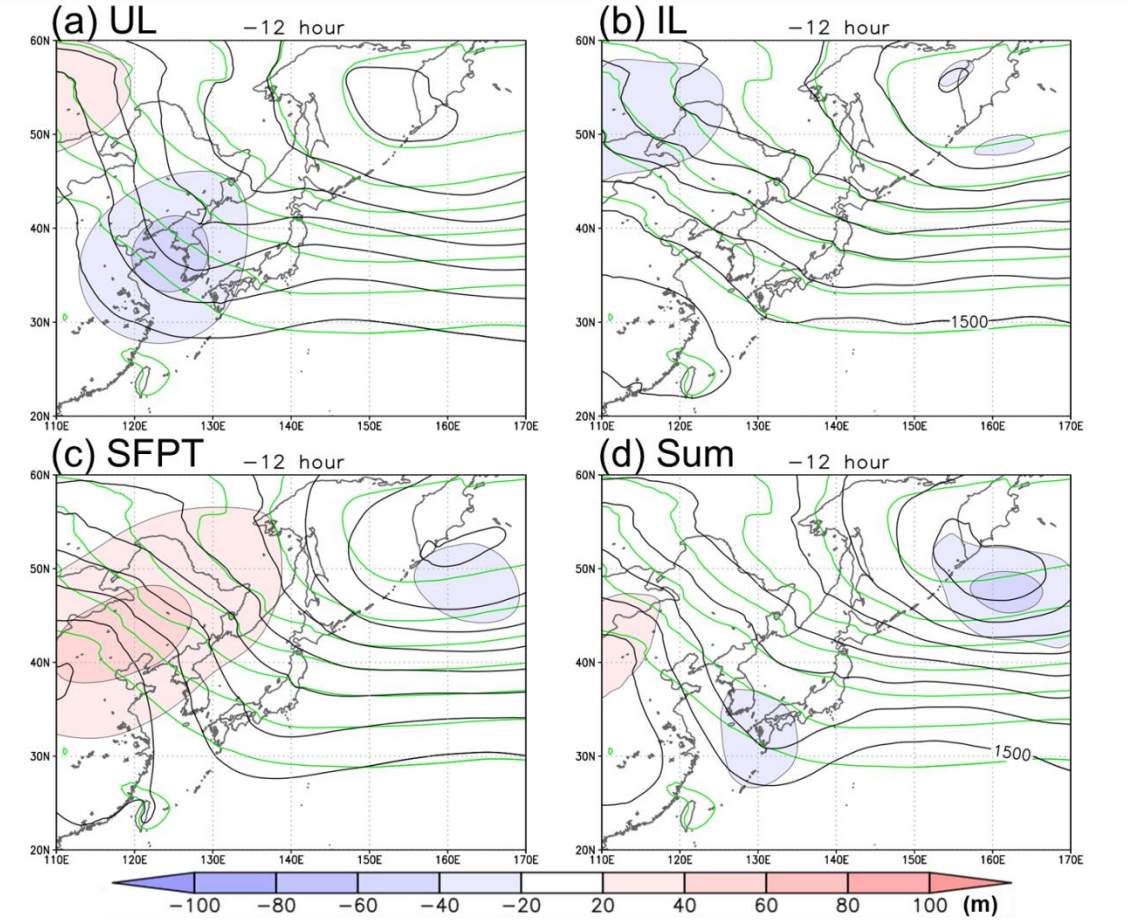

Fig. 5.27 As in Fig. 5.24 except for SW_W at −12 hour.

negative height anomaly is superposed on the mean field, a deep trough forms to the south of Korean Peninsula, which results in meridional isobars around the Mt-P. Therefore the shear zone extends in meridional direction (Fig. 5.19). When the upper-level vorticity anomaly, which passes over the Korean Peninsula, approaches this low-level shear zone, the MV is generated over the southwestern part of the Sea of Japan.

5.6 Conclusions

In this chapter, we have performed numerical simulations in which the GANAL composite fields are used for initial and boundary conditions. The numerical simulations have successfully reproduced MVs and their characteristics in each group. These results confirm that each composite field has the essential factors of the environment for the generating an MV in the corresponding group. Since mesoscale features are almost smoothed out in the initial and boundary fields of the GANAL composite, these results also suggest that there are certain mechanisms through which the corresponding MVs are generated in the prescribed large-scale environments. The reproduced MVs are considered to have general characteristics of the MVs in corresponding groups. Therefore, we have analyzed the development mechanism for the MVs in NE_s, NW_e, NW_se, and SW_W in more detail.

The MVs in NE_s appears within a weak large-scale SLP trough extending westward from in the Aleutian Low. The SLP trough is caused by the upper-level positive vorticity anomaly. The MV is initially generated through stretching of surrounding vorticity by strong updraft associated with cumulus heating. Then, it develops through baroclinic process associated with the zonal temperature gradient and interaction with the upper-level positive vorticity anomaly. At this stage, the MV is accompanied by comma-shaped cloud. It becomes to have a more circular shape and is eventually accompanied by spiralform cloud environmental baroclinicity is reduced. DRY sensitivity experiments show that the condensational heating is crucial for both the generation and development of the MV.

The sensitivity experiments in which SST, the distribution of sea ice and topography are changed show that the warm SST in the Strat of Tartary and the Sea of

Japan to the west of Hokkaido Island forms less stable atmosphere over the northeastern part of the Sea of Japan, which is favorable for cumulus convection. Thus, the MVs tend to develop to the west of Hokkaido Island. The blocking of cold air by the mountains along the eastern coast of the Asian Continent also contributes to forming favorable condition for the development of the MVs to the west of Hokkaido Island.

The numerical simulation for NW_se has reproduced both MVs in NW_e and NW_se. The eastward moving MV appears in a trough extending from a MAL located to the east, while the southeastward moving MV appears at a bending point of the shear zone. Both of them are generated within a region with strong horizontal shear of the JPCZ. DRY sensitivity experiment shows that the initial disturbances of these MVs are generated without condensational heating. However, the condensational heating plays a crucial role in the development of the MVs.

The sensitivity experiments with modified topography have been performed. Unlike Nagata (1991), the mountains at the north of Korean Peninsula play a primary role for the formation of the JPCZ and the MVs, while the thermal contrast between the Korean Peninsula and the Sea of Japan contribute little to the formation of the JPCZ. The direction of the JPCZ, which is closely related to the movement of the MVs, is determined by the large-scale wind at the low-level. The PPVI shows that the large-scale wind direction at the low-level is determined by the path and movement of the upper-level positive vorticity anomaly and the low-level cold air over the Asian Continent.

The MV in SW_W is generated through interaction between low-level shear associated with JPCZ and the upper-level positive vorticity anomaly. Both baroclinic process associated with upper-level vorticity anomaly and condensational heating is

significant for the development of the MV. The upper-level trough that passes relatively southward causes low-level winds having more meridional component around the mountains at the north of Korean Peninsula, which results in the JPCZ extending in a meridional direction. When the trough taking a southern course interacts with the JPCZ, the MV occurs at the southwestern part of the Sea of Japan.

6. General conclusions and future perspectives

In this thesis, we have investigated the general characteristics of the mesoscale vortices (MVs) observed over the Sea of Japan in winter. Since the characteristics of MVs varies from case to case, a statistical study for the MVs is necessary to acquire comprehensive understanding of the characteristics of MVs. One of the useful methods for the statistical analysis is an objective tracking of MVs. Recent high-resolution operational mesoscale model has a potential to reproduce meso-β-scale MVs. Consequently, an objective tracking of MVs including meso-β-scale vortices, which have been difficult due to coarse resolution of datasets, becomes practicable. Therefore, we have developed a new objective tracking method for MVs and performed statistical analyses and numerical simulations for MVs.

First, we have developed a new objective tracking method for MVs using Meso-Scale Analysis (MANAL) data provided by Japan Meteorological Agency. By using MANAL having horizontal resolution of 5 km, our new method can detect and track meso-β-scale MVs including those embedded in a larger disturbance, which have been difficult for the previous objective tracking methods. Another novel point of our method is that it can discriminate MVs and synoptic-scale disturbances based of the size and shape of the vortices without referring to the environmental conditions such as thermal stratification (e.g. Yanase et al. 2015). Thus, it enables to examine the environmental conditions of MVs independently.

Using the new objective tracking method, we have analyzed climatology of the MVs over the Sea of Japan. The tracks of the MVs are concentrated in the western part of the Sea of Japan and to the west of Hokkaido Island. This result agrees well with previous studies based on satellite images during a relatively short period (Asai 1988).

The MVs are classified according to the region where they attained their maximum intensity. MVs in each region have different characteristics with regard to their direction of movement, size, and intensity.

To reveal the general characteristics of the MVs, the MVs are classified according to their locations and moving directions, and the environment and structure of the MVs in each group are examined by composite analyses of Global Analysis (GANAL) and MANAL data.

One of the common features of the environment of the MVs in various groups is a cold air outbreak in the low-level. The MVs appears at the edge of the low-level cold air where two different airmasses are adjacent and consequently both large baroclinicity and horizontal shear exist. Another common feature is an upper-level trough accompanied by cold air, which provides a less stable stratification and dynamic forcing to the MVs. However, the configuration of these large-scale features for the MVs as well as mesoscale structure of the MVs varies among groups of the MVs. In the northeastern part of the Sea of Japan, both the MVs moving southward (NE_s and NEI_s) and eastward (NE_e) are found. The former is associated with zonal temperature gradient, while the latter develops in the meridional temperature gradient. The MVs in the northwestern part of the Sea of Japan (NW_e and NW_se) and southwestern part of the Sea of Japan (SW_W) are associated with a convergence zone (JPCZ) which is formed in the lee side of the mountain at the north of the Korean Peninsula. However, the behavior of the JPCZ and its relationship with the MVs vary according to the location and the direction of movement of the MVs.

We have performed numerical simulations using the composite fields of GANAL for the initial and boundary conditions. The numerical simulations successfully

reproduce the characteristics of the MV in each group, although the composite fields of GANAL are so smooth that they do not contain an initial disturbance for an MV. This result confirms that the composite fields represent general characteristics of the environment for the corresponding MVs. We have analyzed the development mechanism for the MVs in NE_s, NW_se, NW_e, and SW_W using the results of the simulations and several sensitivity experiments. The summary of these analyses is shown in Fig. 6.1.

As for the MV in NE_s, cumulus convection turns out to be crucial for its generation and development, while it also exhibits characteristics of baroclinic development. The warm SST in the Strait of Tartary and the Sea of Japan, and the blocking of cold air by the mountains along the eastern coast of the Asian Continent gives a favorable environment for the development of the MV to the west of Hokkaido Island.

The MVs in NW_se, NW_e and SW_W form within the JPCZ. Both the interaction between the upper-level trough and the low-level JPCZ, and condensational heating play important roles for the genesis and development of the MVs. The sensitivity experiments reveal that blocking of the cold air by the mountains at the north of the Korean Peninsula is essential for the formation of the JPCZ and the MVs. The extending direction of the JPCZ and the motion of the MVs are determined by the large-scale wind direction, which, in turn, is determined by the upper-level trough and the low-level cold air over the Asian Continent. The location of the genesis of the MV is also determined by the path of the upper-level trough.

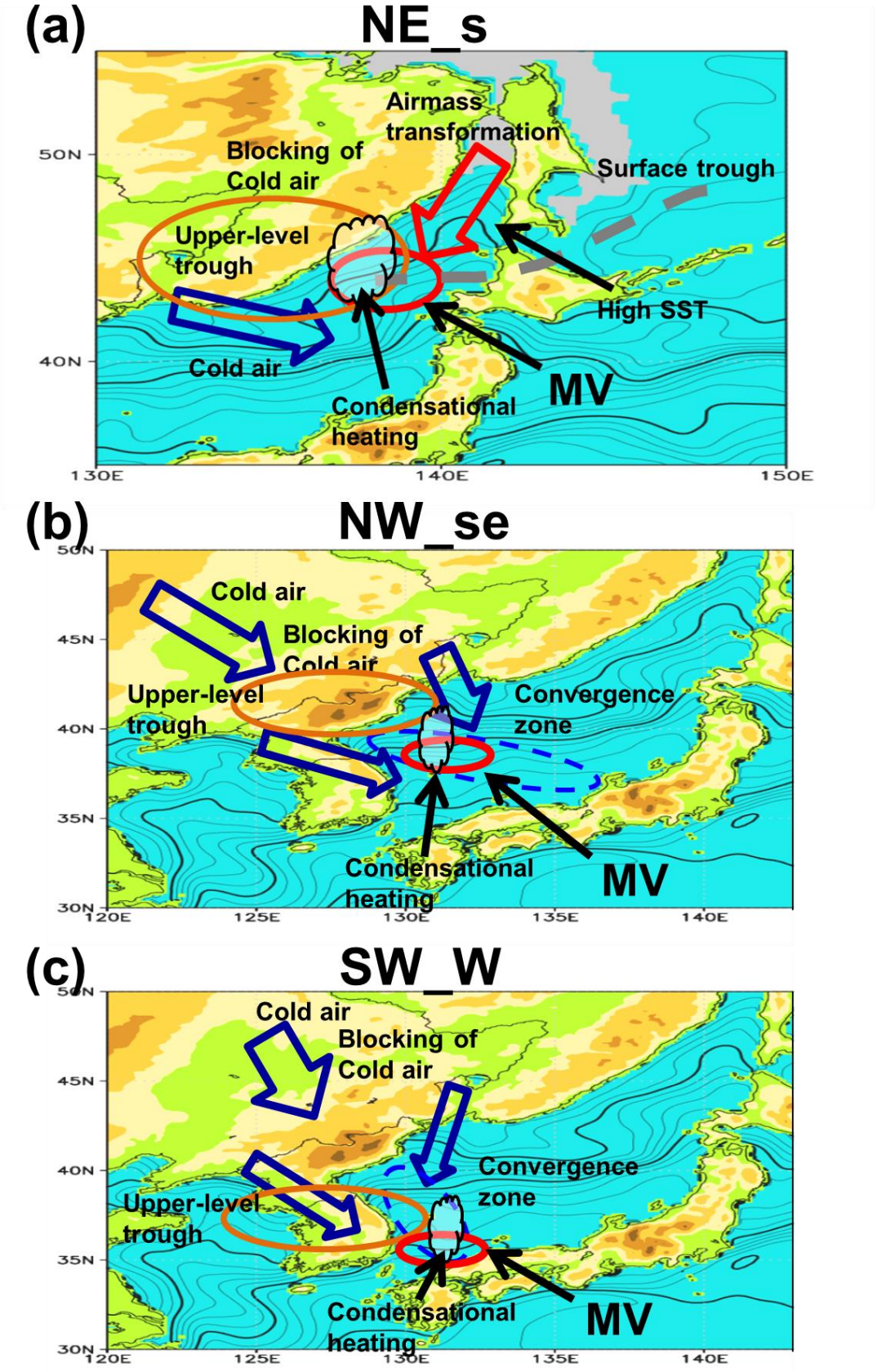

Fig. 6.1 Schematic illustration of (a) NW_e, (b) NW_se, and (c) SW_W.

This is the first research into the objective tracking of MVs that includes meso-β-scale MVs. Our method enables us to perform a statistical analysis of meso-β-scale MVs as well as meso-α-scale MVs. The meso-β-scale MVs are also observed over the northeastern Atlantic (Harold et al. 1999; Condron et al. 2006; Blechschmidt 2008) and the Great Lakes (Hjelmfelt 1990; Laird et al. 2001). However, little is known about their climatology. We can apply our new tracking method to other regions where MVs frequently form, and study similarities and differences of their characteristics among different regions around the world. The difference and similarity between meso-α- and meso-β-scale MVs also need to be clarified.

The present study reveals the relationship between the MVs and synoptic-scale structures including a cold air outbreak and an upper-level trough. Since the synoptic-scale structures are related to the phenomena having larger spatial scale and low frequency such as Arctic Oscillation (Thompson and Wallace 1998) and SST, the climatology of the MVs is also likely to depend on them. Several studies on polar lows over the North Atlantic suggest a certain relationship between polar lows and low frequency atmospheric circulations (e.g. Mallet et al. 2013; Rojo et al. 2015). Since our analysis is restricted within 6 winters due to inhomogeneity of dataset, however, it is difficult to discuss a long-term variation. The long-term variation of the MVs needs to be clarified in the future.

The MVs are reproduced in the numerical simulation using the composite fields of GANAL for the initial and boundary conditions. This result implies that the behavior of MVs can be estimated from synoptic-scale fields. Therefore we are able to estimate the statistical characteristics of MVs using re-analysis datasets or climate prediction datasets, in which MVs are not explicitly resolved.

Acknowledgement

I would like to sincerely thank Prof. Hiroshi Niino for his supervision. I appreciate the examiners, Prof. Masaki Satoh, Prof. Yukari Takayabu, Prof. Hiroyasu Hasumi, and Hiroaki Miura. I particularly thank to Dr. Wataru Yanase for his fruitful advices and suggestions. Special thanks to Prof Keita Iga, Dr. Junshi Ito, and Dr. Eigo Tochimoto for their useful comments. I am grateful to Dr. Kozo Ninomiya, Mr. Udai Shimada, Mr. Yasutaka Hirokawa, and Thomas Spengler for their constructive advices. I appreciate Prof. C. Davis for providing the program for the piecewise PV inversion technique. I also thanks to various support by staffs and students at the Dynamic Marine Meteorology Group, Atmosphere and Ocean Research Institute, The University of Tokyo.

MANAL and GANAL data are provided by Japan Meteorological Agency (JMA) and are collected and distributed by the Research Institute for Sustainable Humanosphere, Kyoto University. MTSAT-2 IR images are provided by Kochi University. The OISST dataset is provided by NOAA. The JMA nonhydrostatic model is obtained from JMA numerical weather prediction platform. The computation was carried out using the computer facilities at the Information Technology Center, The University of Tokyo.

I am deeply thanks to my parents for allowing me to go on to the doctoral course and every supports. I also thank to my family for their warm encouragement. Finally I would like to thank all people and things supporting me.

References

Asai, T. 1988. Meso-scale features of heavy snowfalls in Japan Sea coastal regions of Japan (in Japanese). *Tenki* **35**, 156-161.

Asai, T. and Miura, Y. 1981. An Analytical Study of Meso-Scale Vortex-Like Disturbances Observed around Wakasa Bay Area. *J. Meteor. Soc. Japan* **59**, 832-843.

Blechschmidt, A. 2008. A 2-year climatology of polar low events over the Nordic Seas from satellite remote sensing. *Geophys. Res. Lett.* **35**, L09815.

Businger, S. 1987. The synoptic climatology of polar-low outbreaks over the Gulf of Alaska and the Bering Sea. *Tellus A* **39**, 307-325.

Carleton, A. M., and D. A. Carpenter, 1990. Satellite climatology of polar lows and broadscale climatic associations for the southern hemisphere. *Int. J. Climatol.*, **10**, 219-246

Chen, F. and von Storch, H. 2013. Trends and Variability of North Pacific Polar Lows. *Adv. in Meteor.*, **2013**, 1–11.

Condron, A., Bigg, G. and Renfrew, I. 2006. Polar mesoscale cyclones in the northeast Atlantic: Comparing climatologies from ERA-40 and satellite imagery. *Mon. Wea. Rev.* **134**, 1518-1533.

Davis, C. A. and Emanuel, K. A. 1991. Potential vorticity diagnostics of cyclogenesis. *Mon. Wea. Rev.* **119**, 1929-1953.

Fu, G., Niino, H., Kimura, R. and Kato, T. 2004. A polar low over the Japan Sea on 21 January 1997. Part I: Observational analysis. *Mon. Wea. Rev.* **132**, 1537-1551.

Fu, G., Niino, H., Kimura, R. and Kato, T. 2004. Multiple polar mesocyclones over the Japan Sea on 11 February 1997. *Mon. Wea. Rev.* **132**, 793-814.

Harold, J., Bigg, G. and Turner, J. 1999. Mesocyclone activity over the North-East Atlantic. Part 1: Vortex distribution and variability. *Int. J. Climatol.* **19**, 1187-1204.

Hjelmfelt, M. R. 1990. Numerical study of the influence of environmental conditions on lake-effect snowstorms over Lake Michigan. *Mon. Wea. Rev.* **118**, 138-150.

Honda, Y., Nishijima, M., Koizumi, K., Ohta, Y., Tamiya, K., Kawabata, T. *et al.* 2005. A pre-operational variational data assimilation system for a non-hydrostatic model at the Japan Meteorological Agency: Formulation and preliminary results. *Quart. J. Roy. Meteor. Soc.* **131**, 3465-3475.

Ikawa, M., Mizuno, H., Matsuo, T., Murakami, M., Yamada, Y. and Saito, K. 1991. Numerical modeling of the convective snow cloud over the Sea of Japan. Precipitation mechanism and sensitivity to ice crystal nucleation rates. *J. Meteor. Soc. Japan* **69**, 641-667.

Iwasaki, T., Shoji, T., Kanno, Y., Sawada, M., Ujiie, M. and Takaya, K. 2014. Isentropic Analysis of Polar Cold Airmass Streams in the Northern Hemispheric Winter. *J. Atmos. Sci.* **71**, 2230-2243.

Japan Meteorological Agency, 2013: Outline of the operational numerical weather prediction at the Japan Meteorological Agency (March 2013; available online at http://www.jma.go.jp/jma/jma-eng/jma-center/nwp/outline2013-nwp/index.htm)

Kain, J. 2004. The Kain-Fritsch convective parameterization: An update. *J. Appl. Meteor.***43**, 170-181.

Kain, J. S. and Fritsch, J. M. 1990. A one-dimensional entraining/detraining plume model and its application in convective parameterization. *J. Atmos. Sci.* **47**, 2784-2802.

Kato, T. 2005. Momentum energy budget analysis on a vortex disturbance developing along the Japan-Sea Polar-Airmass Convergence Zone (in Japanese). *Meteor. Res. Note* **208**, 277-284.

Kobayashi, S., Ota, Y., Harada, Y., Ebita, A., Moriya, M., Onoda, H. *et al.* 2015. The JRA-55 Reanalysis: General Specifications and Basic Characteristics. *J. Meteor. Soc. Japan.* **93**, 5-48.

Kolstad, E. W. 2006. A new climatology of favourable conditions for reverse‐shear polar lows. *Tellus A* **58**, 344-354.

Kolstad, E. W. 2011. A global climatology of favourable conditions for polar lows. *Quart. J. Roy. Meteor. Soc.* **137**, 1749-1761.

Kuroda, Y. 1992. The convergent cloud band and the shipwreck in the Japan Sea (in Japanese). *Umi to sora* **67**, 261-279.

Laffineur, T., Claud, C., Chaboureau, J.-P. and Noer, G. 2014. Polar lows over the Nordic Seas: Improved representation in ERA-Interim compared to ERA-40 and the impact on downscaled simulations. *Mon. Wea. Rev.* **142**, 2271-2289.

Laird, N., Miller, L. and Kristovich, D. 2001. Synthetic dual-Doppler analysis of a winter mesoscale vortex. *Mon. Wea. Rev.* **129**, 312-331.

Lee, T.-Y., Park, Y.-Y. and Lin, Y.-L. 1998. A numerical modeling study of mesoscale cyclogenesis to the east of the Korean Peninsula. *Mon. Wea. Rev.* **126**, 2305.2229.

Maejima, Y. and Iga, K. 2012. The Time Evolution of Meso-scale Disturbances in the Atmosphere Caused by Frontal Instability. *Theoretical and Applied Mechanics Japan* **60**, 183-191.

Mallet, P. E., Claud, C., Cassou, C., Noer, G. and Kodera, K. 2013. Polar lows over the Nordic and Labrador Seas: Synoptic circulation patterns and associations with North Atlantic‐Europe wintertime weather regimes. *J. Geophys. Res.*: *Atmos.* **118**, 2455.2372.

Miyazawa, S. 1967. On vortical meso scale disturbances observed during the period of heavy snow or rain in the Hokuriku district. *J. Meteor. Soc. Japan* **45**, 166-176.

Nagata, M. 1991. Further numerical study on the formation of the convergent cloud band over the Japan Sea in winter. *J. Meteor. Soc. Japan* **69**, 419-428.

Nagata, M. 1993. Meso-beta-scale vortices developing along the japan-sea polar-airmass convergence zone (JPCZ) cloud band - Numerical-simulation. *J. Meteor. Soc. Japan* **71**, 43-57.

Nagata, M., Ikawa, M., Yoshizumi, S. and Yoshida, T. 1986. On the formation of a convergent cloud band over the Japan Sea in winter; numerical experiments. *J. Meteor. Soc. Japan* **64**, 841-855.

Nakanishi, M. and Niino, H. 2006. An improved Mellor-Yamada level-3 model: Its numerical stability and application to a regional prediction of advection fog. *Bound-Layer Meteor.* **119**, 397-407.

Ninomiya, K. 1989. Polar Comma-Cloud Lows over the Japan Sea and the Northwestern Pacific in Winter. *J. Meteor. Soc. Japan* **67**, 83-97.

Ninomiya, K. 1994. A meso-scale low family formed over the northeastern Japan Sea in the northwestern part of a parent Polar low. *J. Meteor. Soc. Japan* **72**, 589-603.

Ninomiya, K. and Hoshino, K. 1990. Evolution process and multi-scale structure of a polar low developed over the Japan Sea on 11-12 December 1985. Part II, Meso-β-scale low in meso-α-scale polar low. *J. Meteor. Soc. Japan* **68**, 307-317.

Ninomiya, K., Hoshino, K. and Kurihara, K. 1990. Evolution process and multi-scale structure of a polar low developed over the Japan Sea on 11-12 December 1989. Part I: Evolution process and meso-α-scale structure. *J. Meteor. Soc. Japan* **68**, 293-306.

Okabayashi, T. and Satomi, M. 1971. A study on the snowfall and its original clouds by the meteorological radar and satellite (Part I) (in Japanese). *Tenki* **18**, 573-581.

Ookubo, A. 1995. Two types of vortical disturbances over the Hokuriku district in winter (in Japanese). *Tenki* **42**, 705-714.

Orlanski, I. 1975. A rational subdivision of scales for atmospheric processes. *Bull. Amer. Meteor. Soc.* **56**, 5.26-530.

Rasmussen, E., and J. Turner, 2003: *Polar Lows.* Cambridge University Press, 612 pp.

Reynolds, R., Smith, T., Liu, C., Chelton, D., Casey, K. and Schlax, M. 2007. Daily high-resolution-blended analyses for sea surface temperature. *J. Climate* **20**, 5473-5496.

Rojo, M., Claud, C., Mallet, P., Noer, G., Carleton, A. and Vicomte, M. 2015. Polar low tracks over the Nordic Seas: a 14-winter climatic analysis. *Tellus A* **67**.

Saito, K., Fujita, T., Yamada, Y., Ishida, J., Kumagai, Y., Aranami, K. *et al.* 2006. The operational JMA nonhydrostatic mesoscale model. *Mon. Wea. Rev.* **134**, 1266-1298.

Shimada, U., Wada, A., Yamazaki, K. and Kitabatake, N. 2014. Roles of an upper-level cold vortex and low-level baroclinicity in the development of polar lows over the Sea of Japan. *Tellus A* **66**.

Shimizu, N. and Uchida, A. 1974. An Observational Study of Organized Snow Echo over the Japan Sea. *J. Meteor. Soc. Japan.* **5.21**89-299.

Shimizu, S. and Uyeda, H. 2012. Algorithm for the Identification and Tracking of Convective Cells Based on Constant and Adaptive Threshold Methods Using a New Cell-Merging and -Splitting Scheme. *J. Meteor. Soc. Japan* **90**, 869-889.

Smolarkiewicz, P. K. and Rotunno, R. 1989. Low Froude number flow past three-dimensional obstacles. Part I: Baroclinically generated lee vortices. *J. Atmos. Sci.* **46**, 1154-1164.

Smolarkiewicz, P. K. and Rotunno, R. 1990. Low Froude number flow past three-dimensional obstacles. Part II: Upwind flow reversal zone. *J. Atmos. Sci.* **47**, 1498-1511.

Terpstra, A. 2014. Dynamical Perspectives on the Formation and Intensification of Polar Lows. Ph.D. thesis, University of Bergen, 117 pp.

Thompson, D. W. J. and Wallace, J. M. 1998. The Arctic Oscillation signature in the wintertime geopotential height and temperature fields. *Geophys. Res. Lett.* **25**, 1297-1300.

Tsuboki, K., and G. Wakahama, 1992: Mesoscale cyclogenesis in winter monsoon air streams - quasi-geostrophic baroclinic instability as a mechanism of the cyclogenesis off the west coast of Hokkaido Island, Japan. *J. Meteor. Soc. Japan*, **70**, 77–93.

Tsuboki, K. and Asai, T. 2004. The multi-scale structure and development mechanism of mesoscale cyclones over the sea of Japan in winter. *J. Meteor. Soc. Japan* **82**, 597-621.

Watanabe, S. and Niino, H. 2014. Genesis and Development Mechanisms of a Polar Mesocyclone over the Japan Sea. *Mon. Wea. Rev.* **142**, 2248-2270.

Wilhelmsen, K. 1985. Climatological study of gale-producing polar lows near Norway. *Tellus A* **37**, 451-459.

Wu, L., Martin, J. and Petty, G. 2011. Piecewise potential vorticity diagnosis of the development of a polar low over the Sea of Japan. *Tellus A* **63**, 198-211.

Xia, L., Zahn, M., Hodges, K., Feser, F. and Von Storch, H. 2012. A comparison of two identification and tracking methods for polar lows. *Tellus A* **64**, 1-11.

Yagi, S. 1986. " Convergent band cloud" and" Cu-Cb line" over the Japan Sea affected by topographic features in the coast of the Asian Continent (in Japanese). *Tenki* **33**, 453-465.

Yamagishi, Y., Doi, M., Kitabatake, N. and Kamiguchi, H. 1992. A polar low which accompanied strong gust (in Japanese). *Tenki* **39**, 27-36.

Yanase, W., Fu, G., Niino, H. and Kato, T. 2004. A polar low over the Japan Sea on 21 January 1997. Part II: A numerical study. *Mon. Wea. Rev.* **132**, 155.20574.

Yanase, W. and Niino, H. 2007. Dependence of polar low development on baroclinicity and physical processes: An idealized high-resolution numerical experiment. *J. Atmos. Sci.* **64**, 3044-3067.

Yanase, W., Niino, H., Watanabe, S.-i. I., Hodges, K., Zahn, M., Spengler, T. *et al.* 2015. Climatology of polar lows over the Sea of Japan using the JRA-55 reanalysis. *J. Climate*.

Yarnal, B. and Henderson, K. G. 1989. A climatology of polar low cyclogenetic regions over the North Pacific Ocean. *J. Climate* **2**, 1476-1491.

Zahn, M. and von Storch, H. 2008. Tracking Polar Lows in CLM. *Meteorol. Zeitschrift* **17**, 445-453.

Zappa, G., Shaffrey, L. and Hodges, K. 2014. Can Polar Lows be Objectively Identified and Tracked in the ECMWF Operational Analysis and the ERA-Interim Reanalysis? *Mon. Wea. Rev.* **142**, 2596-2608.